



HAL
open science

Emerging DSP techniques for multi-core fiber transmission systems

Akram Abouseif

► **To cite this version:**

Akram Abouseif. Emerging DSP techniques for multi-core fiber transmission systems. Networking and Internet Architecture [cs.NI]. Institut Polytechnique de Paris, 2020. English. NNT : 2020IPPAT013 . tel-03101838

HAL Id: tel-03101838

<https://theses.hal.science/tel-03101838>

Submitted on 7 Jan 2021

HAL is a multi-disciplinary open access archive for the deposit and dissemination of scientific research documents, whether they are published or not. The documents may come from teaching and research institutions in France or abroad, or from public or private research centers.

L'archive ouverte pluridisciplinaire **HAL**, est destinée au dépôt et à la diffusion de documents scientifiques de niveau recherche, publiés ou non, émanant des établissements d'enseignement et de recherche français ou étrangers, des laboratoires publics ou privés.

Emerging DSP Techniques for Multi-Core Fiber Transmission Systems

Thèse de doctorat de l'Institut Polytechnique de Paris
préparée à Télécom Paris

École doctorale n°626 Institut Polytechnique de Paris (ED IP Paris)
Spécialité de doctorat : Information, communications, électronique

Thèse présentée et soutenue à Palaiseau, le 25 Juin, 2020, par

AKRAM ABOUSEIF

Composition du Jury :

Pr. Catherine LEPERS Télécom SudParis, France	Président
Dr. Chigo OKONKWO Eindhoven University of Technology, Netherlands	Rapporteur
Pr. Christophe PEUCHERET Université de Rennes I, ENSSAT, France	Rapporteur
Pr. Oussama DAMEN University of Waterloo, Canada	Examineur
Dr. Jean-Christophe ANTONA Alcatel Submarine Networks, France	Examineur
Pr. Ghaya Rekaya-Ben Othman Télécom Paris, France	Directeur de thèse
Pr. Yves Jaouën Télécom Paris, France	Co-directeur de thèse

-To-
My Parents
Ahmed Abouseif & Ola Hamed

Acknowledgements

I want first to express all my gratitude to every person who was part of my great experience during these years.

Thanks go out to my supervisors Pr. Ghaya Rekaya-Ben Othman and Pr. Yves Jouën for giving me the opportunity to start my PhD thesis and the great support and helpful discussion during my work. I had the chance to learn a lot from you in both professional and personal aspects.

I would like to thank the jury members for accepting to be part of my thesis evaluation. It is an honor that Dr. Chigo OKONKWO and Pr. Christophe PEUCHERET accepted to review my thesis. I would also like to thank each of Pr. Oussama DAMEN, Pr. Catherine LEPERS, and Dr. Jean-Christophe ANTONA to be part of the examiners.

Not forgotten my friends, it was a pleasure knowing you and have the opportunity to share beautiful moments, thank you for your support and kindness to me. I would like to thank my dear friend Homa Nikbakht, I was being blessed by your support and friendship over the years.

Lastly, I would like to thank my family, my sisters: Nermeen, Yosra, Yara and my brother Mohammed. I am forever indebted to my Mother and Father, for the continuous support they have given me throughout these years; I could not have done it without them.

Abstract

Optical communication systems have gone through several phases over the last few decades. Optical degrees of freedom, such as amplitude, phase, wavelength and polarization, have already been deployed in existing optical networks. It is foreseeable that optical systems, as we know, will reach their theoretical limits of non-linear capability. At present, space is the last degree of freedom to be implemented to continue to meet future capacity demands for the next few years. Therefore, intensive research is being conducted to explore all aspects of the deployment of space-division multiplexing (SDM). However, SDM systems face several impairments due to the interaction of spatial channels, which impacts system performance. To this end, in this thesis, we focus on multicore fibers (MCFs) as the most promising approach for the first representative of the SDM system. We present different digital and optical solutions to mitigate the non-unitary effect known as Core Dependent Loss (CDL) that degrades system performance.

The first part of the thesis presents all the design techniques of MCFs and their limits. Then, we study the transmission performance of MCFs, taking into account the propagation impairments that affect MCF systems. Afterward, we propose a theoretical channel model that allows the identification of the MCF system. We have shown that optical and wireless communications have different performances.

The second part is devoted to the optical enhancement technique. The solution is taken up in the form of core scrambling which allows to average the losses. A theoretical channel model is proposed with optimal performances. We also derive an upper bound of the error probability showing the advantage brought by core scrambling.

In the following section, we present a digital solution for further improvement. The proposed solution is the zero forcing pre-compensation with the help of the MCF channel model to allocate the power in each core. The second technique is the use of space-time (ST) coding for further mitigation of the CDL. All simulation results are analytically validated by deriving the upper bounds of the error probability.

The last part is devoted to MCF systems, including few-mode fiber (FMF-MCF). We explain the physical impairments faced by transmission systems. Then, we propose a channel model of the transmission system. This chapter aims to provide the knowledge and tools needed to evaluate FMF-MCF systems for future work.

Keywords: Optical Fiber Communications, Space Division Multiplexing, Core Dependent Loss, Fiber Design, Multiple-Input-Multiple-Output, Space-Time Coding.

Contents

Glossary	xi
Notations & Symbols	xiii
List of Figures	xv
List of Tables	xix
General Introduction	1
1 The Road to Space Division Multiplexing	5
1.1 From Single Mode Fiber to Space Division Multiplexing	5
1.1.1 Principle of Single Mode Fiber (SMF)	6
1.1.2 Polarization Division Multiplexing (PDM)	15
1.1.3 Wavelength Division Multiplexing (WDM)	18
1.2 Space Division Multiplexing (SDM)	19
1.2.1 State-of-the-Art	19
1.2.2 SDM Fiber Approaches	21
2 Multi-Core Fiber Structures and Limitations	25
2.1 Multi-Core Fiber Design Techniques	26
2.1.1 Crosstalk Estimation	26
2.1.2 CPT expressions for MCF Designs	29
2.2 Multi-Core Fiber Layouts	34
2.2.1 Experimental Achievements in MCF	34
2.2.2 Multi-Core Fiber Layouts under Evaluations	34
2.3 Propagation in Multi-Core Fiber	36
2.3.1 Linear Crosstalk	37
2.3.2 Misalignment Loss	39
2.3.3 Differential mode group delay	40
2.3.4 Core Dependent Loss	41

3	Performance of Multi-Core Fiber Systems Impaired by CDL	43
3.1	MCF Transmission System Model	44
3.1.1	Core Crosstalk and Misalignment Loss Channel Matrix	44
3.1.2	MCF Channel Model	45
3.1.3	MIMO-MCF Transmission Performance	48
3.2	Theoretical Analysis of MCF Channel	50
3.2.1	Analytical Derivation	50
3.2.2	Theoretical Channel Model Validation	53
3.3	Analytical Study of Multi-Core Fiber Performance	55
3.3.1	Error probability upper bound of MCF optical system with ML decoder	56
3.3.2	Error probability upper bound of MCF Optical System with ZF Decoder	59
4	Core Scrambling Techniques for Multi-Core Fiber	63
4.1	Performance Enhancement of MCF using Core Scrambling	64
4.1.1	MCF Transmission Channel Model Including Core Scrambling	64
4.1.2	Core Scrambling Strategies	64
4.2	Theoretical Analysis of MCF Channel with Scrambling	69
4.2.1	Analytical Derivation including the Scrambling	69
4.2.2	Number of Optimal Core Scrambling	71
4.3	Analytical Study of Multi-Core Fiber Performance with Core Scrambling	72
4.3.1	Error Probability Upper Bound of MCF System with Core Scrambling	73
5	Pre-Compensation Technique for Multi-Core Fiber	77
5.1	Capacity and Power Allocation in Wireless Communication	78
5.1.1	Capacity of Communication Systems	78
5.1.2	Open/Closed Loop Systems	80
5.2	Zero-Forcing Precoding System	81
5.2.1	ZF Precoding Challenges in Optical Systems	82
5.3	ZF Pre-compensation for MCF Transmission System	84
6	Space-Time Coding for Multi-Core Fiber	89
6.1	ST coding for wireless MIMO channels	90
6.1.1	ST coded for Rayleigh fading channels	90
6.1.2	Space-Time Block Codes	91
6.2	ST coding for MCF system impaired by CDL	95
6.2.1	Error probability of ST coded over MCF optical system	95

6.2.2	Combination of TAST code and core scrambling	100
7	Introduction to Massive SDM Transmission Systems	105
7.1	The Future of Massive SDM	105
7.1.1	Massive SDM Achievements	106
7.1.2	Massive SDM impairment	107
7.2	Massive SDM Channel Model	108
7.2.1	Future Validations	110
	Conclusions & Outlook	113
A	Matrix and Distribution Operations	117
A.1	QR Decomposition	117
A.2	The PDF of the maximum and minimum of normal distribution	118
A.3	SVD decomposition	118
	Bibliography	119
	Publications	129

Glossary

AWGN Additive White Gaussian Noise	Hetero-MCF Heterogeneous Multi-core Fiber
BER Bit Error Rate	Hetero-TA-MCF Heterogeneous Trench Assisted Multi-core Fiber
BPSK Binary-phase Shift Keying	Homo-MCF Homogeneous Multi-core Fiber
CCDF Complementary Cumulative Distribution Function	Homo-TA-MCF Homogeneous Trench Assisted Multi-core Fiber
CD Chromatic Dispersion	IC-XT Inter Core Crosstalk
CDF Cumulative Distribution Function	IM-XT Inter More Crosstalk
CMT Coupled Mode Theory	ISI Inter-symbol Interference
CP Cyclic Prefix	LD Laser Diode
CPT Coupled Power Theory	LO Local Oscillator
CS Core Scrambler	LP Linearly Polarized
CSI Channel State Information	MCF Multi-core Fiber
CU Channel Use	MDL Mode Dependent Loss
DD Direct Detection	MDM Mode-Division Multiplexing
DEMUX De-multiplexer	MIMO Multiple-Input Multiple-output
DMGD Differential Mode Group Delay	ML Maximum Likelihood
DoF Degrees of Freedom	MMF Multi-mode Fiber
DPSK Differential Phase Shift Keying	MSDM Massive Space Division Multiplexing
DSP Digital Signal Processing	MUX Multiplexer
DWDM Dense Wavelength-Division Multiplexing	MZM Mach-Zender Modulator
EAM Electro-Absorption Modulator	NRZ Non Return To Zero
EDFA Erbium Doped Fiber Amplifier	OFDM Orthogonal-Frequency Division Multiplexing
FDE Frequency Domain Equalization	OOK On-Off Keying
FEC Forward Error Correction	ODF Orthogonal Defect Factor
FMF Few-mode fiber	PBC Polarization Beam Combiner
FFT Fast Fourier Transform	PBS Polarization Beam Splitter
FWM Four wave Mixing	PDF Probability Density Function
GVD Group Velocity Dispersion	

Glossary

PDL Polarization Dependent Loss	SPM Self Phase Modulation
PDM Polarization-Division Multiplexing	ST Space-Time
PMD Polarization Mode Dispersion	STBC Space Time Block Code
QAM Quadrature Amplitude Modulation	SVD Singular Value Decomposition
QPSK Quadrature-Phase Shift Keying	TAST Threaded Algebraic Space Time
RZ Return to Zero	TDE Time Domain Equalization
SD Sphere Decoder	WDM Wavelength-Division Multiplexing
SDL Spatial Dependent Loss	WF Waterfilling
SDM Space-division multiplexing	XPM Cross Phase Modulation
SMF Single-mode Fiber	ZF Zero Forcing
SNR Signal to Noise Ratio	

Notations & Symbols

Notation	Definition	unit
x	scalar	
\mathbf{x}	vector	
\mathbf{X}	matrix	
$\ \cdot\ $	norm	
$(\cdot)^T$	transpose	
$(\cdot)^*$	conjugate	
$(\cdot)^\dagger$	transpose conjugate	
$\mathbb{E}[\cdot]$	Expectation	
i	imaginary unit, $i^2 = -1$	
$\Im(\cdot)$	Imaginary part of a complex number	
$\Pr\{\cdot\}$	Probability	
$\Pr\{\cdot \cdot\}$	Conditional probability	
$\Re(\cdot)$	Real part of a complex number	
α	Fiber loss coefficient	dB/km
A_{eff}	Fiber effective area	m^2
$\beta(\omega)$	Fiber propagation constant	rad/km
β_1	Fiber group velocity inverse	ps/km
β_2	Fiber group velocity dispersion	ps^2/km
c	light velocity in vacuum	m/s
C	Channel capacity	bit/s/Hz
C	Number of cores in SDM system	
$\Delta\tau$	Differential group delay	ps
d	correlation length	m
d_{min}	minimal distance of a code or a constellation	
D	Dispersion coefficient	ps/nm/km
E_b	Energy per information bit	J
E_s	Energy per modulated symbol	J
γ_{NL}	Non-linearity coefficient	$\text{km}^{-1}\text{W}^{-1}$
Γ_{dB}	Polarization dependent loss	dB
I_Q, I_I	quadrature and in-phase currents	
λ_c	Laser wavelength	m
L	Fiber length	m
L_{eff}	Effective length of the fiber	m
q	number of states in a constellation	
M	number of modes in SDM system	
$\mathbf{n}(\omega)$	Fiber refractive index	
N_0	Noise spectral density per real dimension	W/Hz

Notations & Symbols

ω	Pulsation (angular frequency)	rad/s
Φ	Phase	rad
τ	Photodiode responsivity	A/W
r_{FEC}	FEC rate	
r_{ST}	STBC rate	
R_{pk}	bending radius	mm
R_s	Symbol rate	Baud
t	time	s
T_s	Symbol duration	s
V_π	MZ extinction voltage	V
ε	Core dependent loss	
δ	Orthogonal defect factor	
γ	Signal to noise ratio	

List of Figures

1.1	Optical fiber technologies and physical dimensions	7
1.2	Optical modulation techniques: (a) Direct modulation and (b) External modulation	8
1.3	Mach-Zehnder modulation principle	8
1.4	Binary optical modulation: (a) OOK and (b) BPSK	9
1.5	Quadrature constellations of 4-QAM and 16-QAM	10
1.6	Direct detection: (a) NRZ-OOK scheme and (b) DPSK scheme	10
1.7	Coherent receiver scheme	11
1.8	Single mode fiber design	12
1.9	Chromatic dispersion in fiber propagation	14
1.10	Polarization division multiplexing: (a) transmitting scheme and (b) receiver scheme.	16
1.11	Polarization mode dispersion effect	17
1.12	Polarization dependent loss effect	18
1.13	Wave division multiplexing transmission scheme	18
1.14	The evolution of the optical transmission capacity over the years [1]	20
1.15	Spatial multiplexing and demultiplexing scheme	21
1.16	Amplification schemes: (a) core pumping and (b) cladding pumping	21
1.17	SDM approaches:(a) Fiber bundles, (b) FMF, (c) MMF, (d) MCF and (e) Massive SDM (MCF and FMF)	23
2.1	Schematics of (a) bent multi-core fiber and (b) fiber cross-section [2]	26
2.2	Random phase-offsets applied to all cores at every segment [2]	27
2.3	Schematic diagram explaining stochastic behaviors and statistical parameters of XT in MCF [2]	28
2.4	Core index profile: (a) Step-index profile and (b) Trench assisted profile.	29
2.5	The total crosstalk versus core pitch for different MCF core design	30

LIST OF FIGURES

2.6	Schematic of the dependence of bending diameter of the heterogeneous and homogeneous MCF	33
2.7	MCF structures, the cladding diameter $CD_1 = 125\mu_m$, $CD_2 = 210\mu_m$ and $CD_3 = 243\mu_m$, core pitch $\Lambda_1 = 24\mu_m$, $\Lambda_2 = 33\mu_m$, $\Lambda_3 = 40\mu_m$ and $\Lambda_4 = 33\mu_m$, $D_1 < D_2$	36
2.8	MCF under evaluation to organize various the coupling level and the core design	37
2.9	Multi-core Fiber transmission scheme for: (a) uncoupled MCF and (b) coupled MCF. DSP: digital signal processing and MIMO: multiple-input-multiple-output.	38
2.10	Fiber Misalignment Types: (a) Transverse Misalignment, (b) Longitudinal Misalignment and (c) Angular Misalignment	39
3.1	Illustration of MCF channel model	45
3.2	PDF of the CDL distribution for: (a) 7-core Hetero-MCF and (b) 7-core Hetero-TA-MCF with $\sigma_{x,y} = \{3\%,5\%,7\% \}a_1$	46
3.3	PDF of the CDL distribution for: (a) 19-core Hetero-MCF and (b) 19-core Homo-MCF with $\sigma_{x,y} = \{3\%,5\%,7\% \}a_1$	47
3.4	PDF of the CDL distribution for: (a) 12-core Hetero-MCF and (b) 12-core Hetero-TA-MCF with $\sigma_{x,y} = \{3\%,5\%,7\% \}a_1$	48
3.5	MCF transmission system scheme	48
3.6	7-core Hetero-MCF Performance function of the transmission distance, with and without full MIMO and at SNR = 10dB and $\sigma_{x,y} = 7\% a_1$	49
3.7	The average and standard deviation of critical parameters	50
3.8	Comparison between the simulated and the Theoretical PDF distribution, the upper figures are the PDF of the singular value and the bottom figures are the PDF of the CDL	53
3.9	The Singular value and CDL distribution Kullback divergence structures: (A) 7-core Hetero-MCF, (C) 12-core Hetero-MCF, (E) 19-core Hetero-MCF and (F) 19-core Homo-MCF.	54
3.10	Simulation and analytical upper bound of ML detection for 7-core Hetero-MCF	59
3.11	Simulation and analytical upper bound of ZF detection for 7-core Hetero-MCF	61
4.1	Multi-Core Fiber transmission system with random core scramblers	64
4.2	7-core Hetero-MCF with corresponding core parameters	65
4.3	Simulated and theoretical channel model	65

4.4	Core scrambling implementation using DEMUX/MUX	66
4.5	Deterministic scramblers strategies: (a) Snail scrambler, (b) Circular scrambler and (c) Snake scrambler	67
4.6	Comparison between the Snail scramblers and random scramblers with number of section equal to 300	67
4.7	Snail scrambling System performance after applying 5 core scramblers.	67
4.8	Comparison between the Circular scramblers and random scramblers with number of section equal to 300	68
4.9	Circular scrambling System performance after applying 5 core scramblers.	68
4.10	Comparison between the Snake scramblers and random scramblers with number of section equal to 300	69
4.11	Snake scrambling System performance after applying 5 core scramblers.	69
4.12	The CDL function of the number of deterministic scramblers	71
4.13	Simulated and Theoretical PDF of the singular value (λ) with Optimal deterministic scrambling for: (a) 12-core Hetero-MCF, (b) 12-core Hetero-TA-MCF, (c) 7-core Hetero-MCF and (d) 19-core Homo-MCF	72
4.14	Simulation and theoretical upper bound of ML and ZF detection with core scrambling for 7-core Hetero-MCF, $CDL = 1.8\text{dB}$	74
5.1	Communication channel including encoder and decoder	78
5.2	MIMO wireless system	79
5.3	Open Loop System	80
5.4	Closed Loop System	81
5.5	ZF precoding scheme	82
5.6	The average capacity versus the SNR for: the 7-core Hetero-MCF and 19-core Hetero-MCF with $\sigma_{x,y} = \{3\%, 7\%\}a_1$ and $K = 300$	83
5.7	ZF pre-compensation MCF transmission system	85
5.8	$\bar{\mathbf{H}}^{-1}$ eigenvalues of the 7-core Hetero-MCF.	85
5.9	The average and standard deviation of critical parameters	86
6.1	3×3 TAST and 7×7 TAST architecture	93
6.2	Space-Time coded MCF transmission system	96
6.3	7×7 TAST code performance for 7-core Hetero-MCF, misalignment level ($\sigma_{x,y}=7\%r_c$) corresponding to $CDL = 8\text{dB}$	99
6.4	Space-Time coded MCF transmission system including core scrambling	100

LIST OF FIGURES

6.5	BER performance of 7-core Hetero-MCF with 7×7 TAST code and Snail scrambling, with misalignment level $\sigma_{x,y} = 7\%r_c$ corresponding to CDL = 1.8dB	101
6.6	CDF of the ODF for 7×7 TAST with and without core scrambling	101
7.1	Massive SDM fiber with three modes propagating $\{LP_{01}, LP_{11a}$ and $LP_{11b}\}$	106
7.2	Illustration drawing of the crosstalk relation between two cores each propagates two modes $\{LP_{01}$ and $LP_{11a}\}$	107
7.3	IC-XT function of the core pitch after 100 km propagating	108
7.4	Massive space division multiplexing transmission system. MC: mode converter.	109

List of Tables

1.1	System requirements for different region, '*' indicates the requirement level	20
1.2	FMF parameters for 3, 6 and 10 modes, for $\lambda = 1.55\mu m$ and $NA = 0.205$. [3]	22
1.3	Comparison between the FMF/MMF and the MCF	23
2.1	Recently Achievement reported for MCF transmission	35
2.2	Cores parameters	36
6.1	STBC codes	92
6.2	Comparison of the complexities using ML and ZF decoders	100
7.1	Recently Achievement reported for Massive SDM transmission	106

General Introduction

The optical fiber communication has witnessed several evolution phases over the years since the laser invention in 1960 [4]. The development of the optical network can be categorized into three stages. First, the introduction of the optical systems that operate at wavelength $1.55 \mu m$ where the fiber loss is equal to 0.2 dB/km. This generation allows us to reach a 70 km transmission distance with a 10 Gb/s bit rate. The second generation was the implementation of optical amplification without the need for the optical-electrical-optical conversion (O-E-O) devices, which adds more cost to the system deployments. The wideband erbium-doped fiber amplifiers (EDFA) allowed us to operate with the wavelength-division multiplexing (WDM) and deploy optical communication in the long-haul systems. Besides, the WDM systems permit to have access to up to 80 channels separated by 50 GHz; each channel can carry up to 40 Gb/s bit rate. In the third generation, the coherent system that allows the detection of the amplitude and phase, the coherent technology was the primary key to exceed 10 Tbits per second capacity era and continue addressing the internet capacity demands. The coherent detection allows applying higher-order modulation formats and the optical light's two orthogonal polarization, so implementing the polarization-division multiplexing (PDM) systems. These high-speed systems require using digital signal processing algorithms at the receiver side to compensate the different transmission impairments.

The capacity of the deployed optical fibers is reaching the Shannon capacity limit; simultaneously, the degrees of freedoms in the conventional fiber are already exploited. According to the 2019 Cisco Visual Networking Index (VNI) report [5], the report provides forecasts of the 2022 network in comparison to the 2017 network. Annual global internet protocol (IP) traffic will reach 1.2 Petabyte/s by 2022 up from 371 Terabyte/s in 2017. The traffic will be shared between different application trends such as the IP video traffic, the Virtual Reality (VR) and internet video to the TV. The IP video traffic will have the most significant amount by reaching 82 percent of all IP traffic by 2022, four-fold from 2017.

All these upcoming technologies required a quick response in order to keep delivering the capacity demands. Hopefully, space is the remaining degree of freedom to be used to address the next leap in capacity. In fact, the year 2020 will witness launching some projects based on the space-division multiplexing (SDM) systems. During the third quarter of 2020, Google will turn on their private Dunant undersea cable between the USA and France [6]. The cable will break the capacity record by transmitting 250 Terabits of data per second. Dunant will be the first undersea transmission system to use SDM technologies. The second project introduced by Google is Equiano cable that connects Africa with Europe [7]. Equiano will be the first undersea system to deploy optical switching based on the fiber-pair level instead of the wavelength level. Although these projects are based on increasing the fiber pairs approach, using SDM technologies is an indication that the next generation fiber cables are near to be deployed. Still, this system will face a cost-efficiency issue by optimizing the cost per bit and enlarging the system dimension. Therefore, intensive research on the alternative approaches of space multiplexing is carried on to address the main problems in SDM transmission systems.

In General, the SDM systems can be realized by multi-mode fiber (MMF) allowing the propagation of more than one mode or multi-core fiber (MCF) in single cladding, each core carries single mode or multi modes. These new generations of fiber optics are promising solutions to address the required capacity and cost efficiency despite changing the optical network infrastructure. However, several challenges should be addressed in order to provide reliable communication. These challenges are distributed over different fields: the optimal SDM fiber design, the optoelectronic devices to manipulate the spatial paths, and the signal processing technique to mitigate the impairment rising from the SDM systems.

Thesis contribution and Goals

In this thesis, we present modern optical and digital techniques to enhance the transmission performance of the MCFs. The propagating mode in multi-core fiber is impacted by non-unitary effects, causing a degradation in the system capacity; this impairment known as core dependent loss (CDL).

In [3], the authors provided almost a full investigation of the few-mode fiber transmission system. The studies provided well known wireless communication techniques such as space-time coding (ST) to mitigate the mode dependent loss (MDL). The interesting results brought by this thesis proved the potential of the multiple-input multiple-output

(MIMO) wireless technique to contribute in the space division multiplexing (SDM) transmission systems. This initiates a further investigation for the second approach of the SDM system represented in the multi-core fibers.

This thesis carried out at LTCI (Laboratoire de Traitement et communication de l'information) laboratory of Télécom ParisTech since January 2017. It is motivated by the performance evaluation of the multi-core fiber systems considering the core dependent loss (CDL) impairment. We analyzed the CDL effect on the system capacity and proposed optical and digital solutions to enhance the MCF transmission system performance.

Thesis Outline

The thesis is organized in seven chapters, as follows:

- **Chapter 1:** In this chapter, we review the evolution of the optical communication systems over the last three decades. We illustrate the basic principle of the propagation in single mode fiber by explaining the main impairments that affect the transmission performance. Moreover, we present all the degrees of freedom deployed in existing optical fiber networks to cope with the increasing capacity demands. Afterward, we introduce the space division multiplexing as the potential solution to overcome the anticipated capacity crunch. Finally, we introduce the different approaches to realize space division multiplexing.
- **Chapter 2:** This chapter focuses on the multi-core fiber by providing all the details concerning the fiber design. We explain the design techniques applied in the literature. We also illustrate the limitation in the manufacturing processes based on the design techniques and the propagation impairments in a multi-core fiber. We present the most significant experimental demonstration carried out in laboratories for high bit rate transmission systems. In order to facilitate our research, we focus on the most commonly used multi-core fiber structures in the literature. Lastly, we explain all the necessary parameters for each layout.
- **Chapter 3:** We start this chapter by proposing the channel matrix model for the crosstalk and misalignment loss impairments. From that, we represent a physical MCF transmission model based on the core dependent loss impairment. Then, we aim to propose a theoretical channel model to estimate the MCF transmission performance. Finally, based on the channel model, we derive an upper bound on the error probability considering optimal and sub-optimal decoders.

- Chapter 4: This chapter aims to provide an optical solution to reduce the core dependent loss and enhance the transmission performance. We propose random and deterministic core scrambling techniques to reduce the core dependent loss in the system efficiently. Then, we obtain an optimal number of deterministic scrambling depends on the theoretical channel model. Lastly, we introduce a low complex detection solution by applying the Zero Forcing sub-optimal decoder.
- Chapter 5: This chapter is dedicated to the digital approach to mitigate the core dependent loss and enhance system performance. We propose a Zero-Forcing compensation technique inspired by the Zero-Forcing precoding in wireless communication. Finally, we study the decoding complexity and the performance of the Maximum-likelihood decoder and the sub-optimal Zero-Forcing decoder.
- Chapter 6: This chapter is a continuity of the digital solution for enhancing the MCF transmission performance. In this part, we investigate the space-time coding performance over the MCF system, aiming to completely mitigate the core dependent loss. Then, we evaluate the MCF system performance by combing the core scrambling strategy with the space-time coding technique. Finally, we support our results by driving an upper bound error probability for different transmission schemes.
- Chapter 7: This chapter is an introduction to the Massive SDM (combining the MMFs and MCFs). We review some experimental demonstrations of the Massive SDM transmission in the literature. Finally, we propose channel mode for the Massive SDM systems and give some perspective for the future work.

Chapter 1

The Road to Space Division Multiplexing

Optical fibers have been introduced to the telecommunication field due to their low attenuation and wide spectral bandwidth. Since the 1970s, the optical fiber networks had seen several developments and techniques to improve the performance and transmission reach. Starting from applying the simple OOK modulation format, then wave-division multiplexing with the in-line EDFA systems and ending by the deployment of the coherent receiver and the polarization division multiplexing with higher modulation formats. Nowadays, optical fibers have access to all the application regions, from a few meters to thousands of kilometers network. However, the maximum capacity that the conventional fibers can hold reaches their limits while the demand for higher bit rates rises year after year. Therefore, investigations are carried on currently in order to provide the required technical solutions for future capacity demand.

In this chapter, we begin by reviewing the basic principles of the optical fiber systems. We give a brief illustration of the transmission and receiving technologies. Then, we review the propagation in the optical medium and its impairments. Meanwhile, we describe the evolution of the optical technologies which are deployed in the current systems. Finally, we present the space division multiplexing (SDM) as a possible technique to overcome the nonlinear optical limitation. We introduce the different SDM approaches and provide a comparison based on the system design and requirements.

1.1 From Single Mode Fiber to Space Division Multiplexing

The history of the optical transmission capacity is back to the early 1970s. The first generation of optical fiber operates at wavelength $0.8\mu m$ with attenuation loss around 2.5 dB/km caused by the silica absorption and the OH^- ions [4]. After, the use of the

two low-loss regions, the $1.55\mu\text{m}$ and $1.3\mu\text{m}$ minimizes the fiber attenuation for optical communication. Later on, high-speed electronic devices allow implementing the external modulator to reach a bit rate equal to 10 Gbits/s bit rate [8]. Since the 1990s, optical communication has seen a fast development of the capacity brought by introducing the wave division multiplexing (WDM) and the optical amplification [9]. The WDM systems reached nearly 1 Tbits/s by utilizing 80 channels modulated by 10 Gbits/s separated by 50 GHz [10]. In 2010, the implementation of coherent detection allowed access to the phase and the polarization state of the received optical signal. The integration between the WDM and the polarization division multiplexing (PDM) reaches 100 Gbits/s per wavelength. Further, advanced modulation formats were investigated to achieve high spectral efficiency (SE). In [11], an experiment had been reported an achievement capacity of around 100 Tbits/s with 128-QAM for short reach due to the sensitivity to nonlinear effects. The last three decades can be categorized based on the optical fiber systems technologies as shown in Fig. 1.1.

According to global internet communication technology, there will be 8 billion mobile broadband subscriptions worldwide. Thus, it is speculated that the capacity limit of single mode fiber (100 Tbits/s) will be reached by the year 2023. In order to give an idea about the capacity impact, let us take the video as an example of one of the significant consumption sources of the mobile data network. The video demand accounts for 55% of the network traffic, growing each year exponentially. The video streaming could reach 213.6 Tbits/s traffic in some famous events. For that, new optical networks need to be developed in order to accommodate the new capacity requirements. Thus, intensive research is carried out on the space division multiplexing (SDM) as the last degree of freedom (DoF). The SDM can be deployed based on the multi-mode fiber (MMF) or multi-core fiber (MCF), which will be detailed later. The next section provides an overview of the propagation principle on the conventional single mode fiber.

1.1.1 Principle of Single Mode Fiber (SMF)

1.1.1.1 Optical Transmitter

The information bit sequence is converted to an electrical signal that aims to modulate the optical light emitted by the laser diode (LD). The LD generates the optical carrier for specific wavelength and power where the amplitude and phase of the optical signal are determined by the information bit with the modulation device's help. However, this direct modulation technique is not preferable due to frequency variation which will be explained in the following.

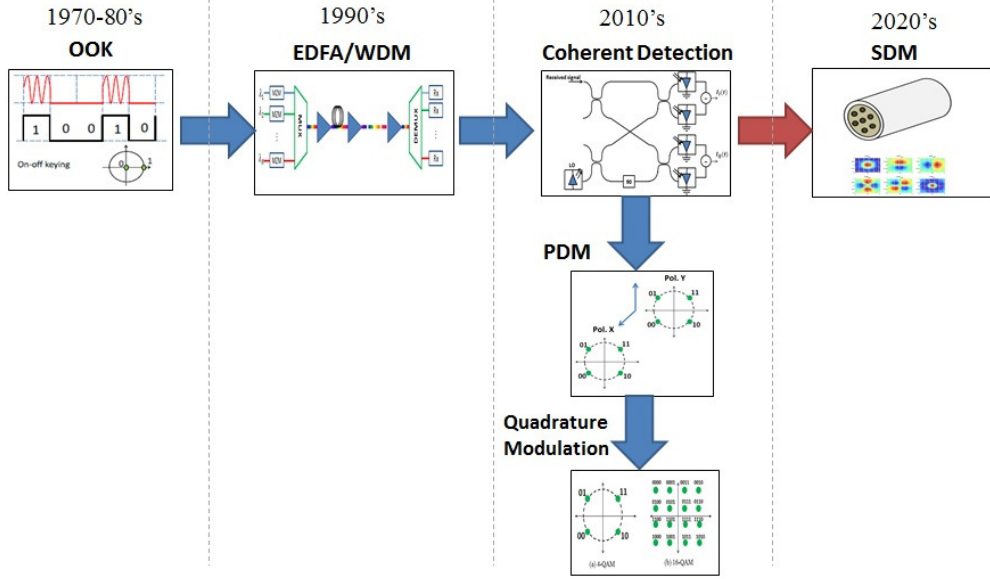


Figure 1.1: Optical fiber technologies and physical dimensions

Optical modulation

The electrical field of the optical signal at the modulator output is given by:

$$E(t) = A(t) \exp(w_0 t \pm \phi t) \tag{1.1}$$

where A and ϕ are the amplitude and phase, respectively. $w_0 = 2\pi f_0$ is the carrier frequency in rad/s and f_0 is the frequency of the signal and is given by $f_0 = \frac{c}{\lambda_0}$, c is the speed of light which is equal to 3×10^8 m/s and λ_0 is the wavelength carrier.

Various technologies of the optical modulation exist as shown in Fig. 1.2 [12]. The easiest method is to use the direct modulation where the power is modulated directly by a modulated electrical signal. However, this method is known for its unwanted variation of the lasing frequency due to the frequency chirp [13]. The second approach uses the external modulator, such as electro-absorption modulator (EAM), phase modulator and Mach-Zehnder modulator (MZM). In the case of an electro-absorption modulator, the modulation is based on the semiconductor material’s absorption coefficient. This family is suitable for access networks of rates up to 40 Gb/s at large bandwidth ~ 40 GHz and low frequency chirping effect.

The MZM is weakly wavelength dependent while having a high cost and power consumption which is unsuitable for access networks. In Fig. 1.3, the MZM is composed of two 3 dB couplers with two arms. At the upper arm, we apply a modulated driving voltage to control the light propagating phase while the lower arm is set as a reference. It creates interference at the MZM output which translates into optical signal amplitude variations.

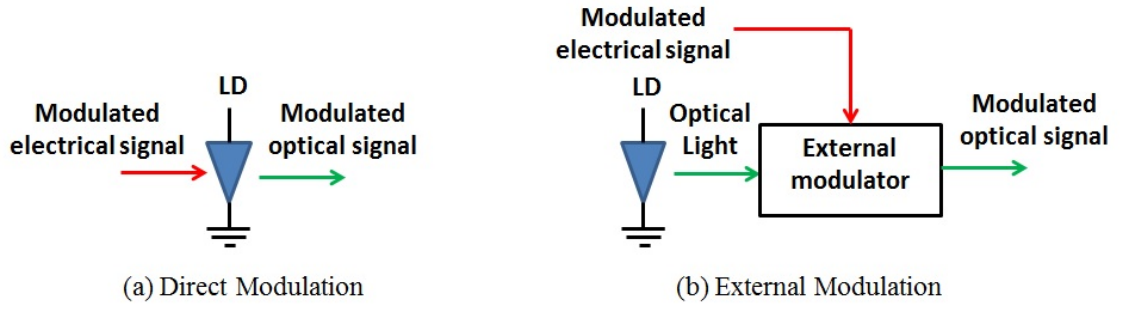


Figure 1.2: Optical modulation techniques: (a) Direct modulation and (b) External modulation

The relation of the incident light E_{in} and the modulated signal E_{out} based on the MZM characterization is given by:

$$E_{out} = E_{in} \cdot \cos\left(\pi \frac{V_{mod}}{2V_{\pi}}\right) \quad (1.2)$$

V_{mod} is the voltage applied on the upper arm, V_{π} is the drive voltage corresponding to phase shift from maximum to minimum (constructive and destructive) interference between the two arms.

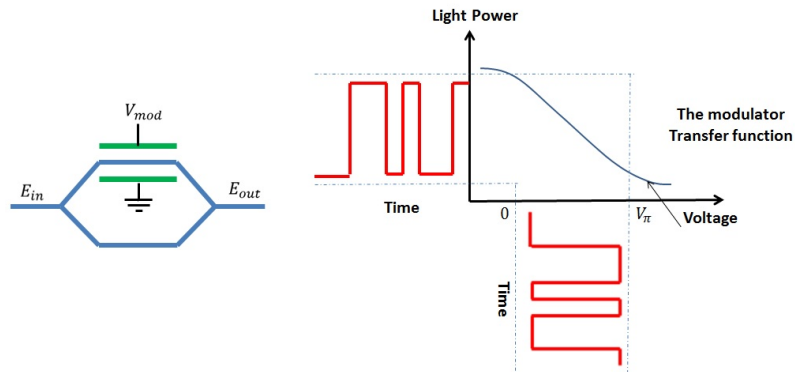


Figure 1.3: Mach-Zehnder modulation principle

Modulation formats

The modulation principle is to modify the signal states to create what is called symbols, the set of all possible symbols from the alphabet of the modulation. The modulation techniques can be classified as:

- **On-off keying (OOK):** in another way, non-return-to-zero (NRZ) where the weak optical power is translated to "0" bit and the high optical power is translated to

"1" bit. The NRZ-OOK is realized by single MZM driven by the peak-to-peak electrical signal amplitude while applying a single photodiode can easily retrieve the transmitted bits followed by decision threshold at the receiver side. The NRZ-OOK is a simple format with low cost which made it the preferred modulation format for optical transmission systems during many years.

- **Binary phase shift keying (BPSK):** in this method, we modulate the phase instead of the amplitude as the OOK. The null phase is referred to "0" bit and the π -phase to "1" bit ($E_{out} = +/ - E_{in}$ corresponds to "1" or "0"). The BPSK can be achieved using the MZM with similar architecture compared to the OOK except that a voltage of twice peak-to-peak amplitude drives the MZM. At the receiver side, we need an optical phase discriminator for phase-amplitude conversion using a balanced photodetector before the electrical conversion. The spectral efficiency (SE) of the BPSK is the same as the OOK (1 bit/symbol) with the same average energy E_s . However, the distance between the two symbols is larger than the one in the OOK (see Fig. 1.4) which provides the BPSK with 3dB noise sensitivity improvement compared to the OOK.

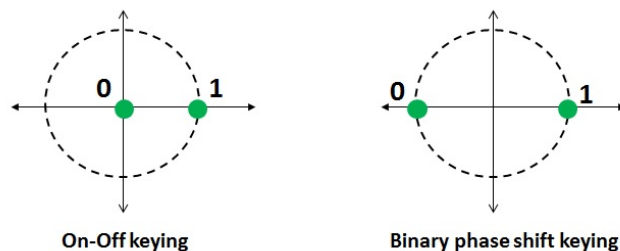


Figure 1.4: Binary optical modulation: (a) OOK and (b) BPSK

- **Quadrature amplitude modulation (QAM):** the multi-level modulation formats were introduced to the optical communications to increase the optical systems' capacity. To construct a QAM transmitter, we need two parallel MZMs with $\pi/2$ phase-shift between their outputs (for the in-phase I and in-quadrature Q modulation). The QAM modulation can ensure spectral efficiency beyond 2 bits/symbol. The alphabet in QAM constellation is constructed by q symbols equal to 2^n where n is the number of bits per symbol, called q -QAM. In order to realize the QAM constellation, we modulate the amplitudes of two copies of the same carrier using the MZM. The difference between the two carriers is $\pi/2$ phase shift, the summation between the two modulations creates the I and Q components of the QAM symbols (constellation). In Fig. 1.5, we give two examples of QAM constellations (4-QAM

1. THE ROAD TO SPACE DIVISION MULTIPLEXING

and 16-QAM). Concerning the receiving side, a coherent receiver is necessary in order to retrieve the signal from the multi-level modulation formats.

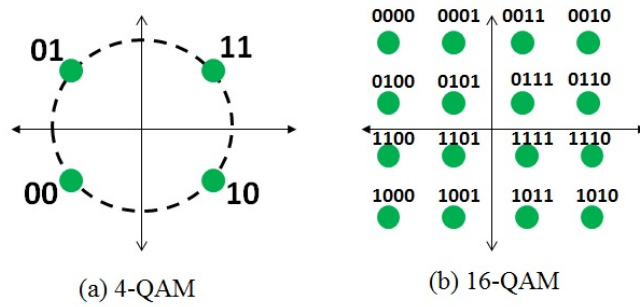


Figure 1.5: Quadrature constellations of 4-QAM and 16-QAM

1.1.1.2 Optical Receivers

The complexity technique in retrieving the signal at the receiver side depends on the modulation methods applied at the transmission side. However, two schemes could be used as follows.

- Direct detection

The direct detection (DD) is mainly deployed for OOK and BPSK modulations to provide an optical capacity of up to 40 Gb/s. In the case of OOK, a simple scheme is deployed by using a single photodiode that detects the intensity of the received optical power and translates it into an electrical current, as shown in Fig. 1.6(a). For BPSK, the phase is modulated which is lost using the same scheme for OOK. Therefore, we apply optical phase discriminator in order to keep the complexity low which can be seen in Fig. 1.6(b). We apply a single symbol delay on one of the duplicated signals before the two photodiodes provide an electrical current proportional to the phase shift between consecutive optical signals.

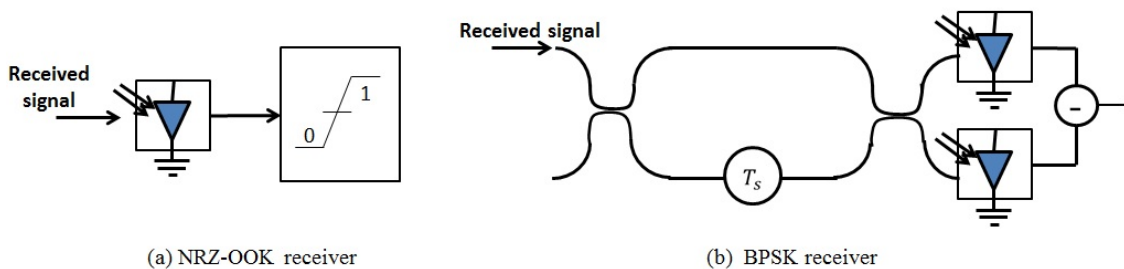


Figure 1.6: Direct detection: (a) NRZ-OOK scheme and (b) DPSK scheme

• **Coherent detection**

The coherent detection was first introduced in the 1980s [14], a local oscillator (LO) laser is added to beat the received signal with almost the same frequency. The goal is to improve the receiver sensitivity at the cost of highly complex equipment for phase shift compensation between the received signal and the LO. In [15][16], it had been shown that the noise sensitivity of coherent detection is better than direct detection and differential detection. However, the introduction of the optical amplification decreases the implementation complexity while keeping similar sensitivity. Since high speed integrated circuits are available, DSP solutions based on coherent detection for phase and polarization recovery have been suggested.

As shown in Fig. 1.7, the electrical signal comprises two components, the in-phase (I) and in-quadrature (Q). We apply a $\frac{\pi}{2}$ -hybrid phase diversity where the LO frequency ω_{LO} is close to the carrier frequency ω_0 . Then, the LO is duplicated into two $\frac{\pi}{2}$ -phase shift copies that interfere with the incident signal which is expressed as [15]:

$$\begin{aligned} I_I(t) &= \tau \sqrt{A_s(t) \cdot A_{LO}(t)} \cdot \cos(\theta_s(t) - \theta_{LO}(t)) \\ I_Q(t) &= \tau \sqrt{A_s(t) \cdot A_{LO}(t)} \cdot \sin(\theta_s(t) - \theta_{LO}(t)) \end{aligned} \quad (1.3)$$

where τ is the photodiode. $A_s(t)$, $A_{LO}(t)$, $\theta_s(t)$ and $\theta_{LO}(t)$ represent the powers and the phases of the received signal and the local oscillator, respectively. As shown in Eq. 1.3, when $\Delta\omega = \omega_s - \omega_{LO} = 0$ means that the frequency offset is perfectly compensated (homodyne detection).

The coherent detection allows having access to the amplitude and the phase of the optical signal. Also, combining the coherent detection with the digital signal processing algorithms opens the way to the digital mitigation of the linear and non-linear impairments of the optical transmission link.

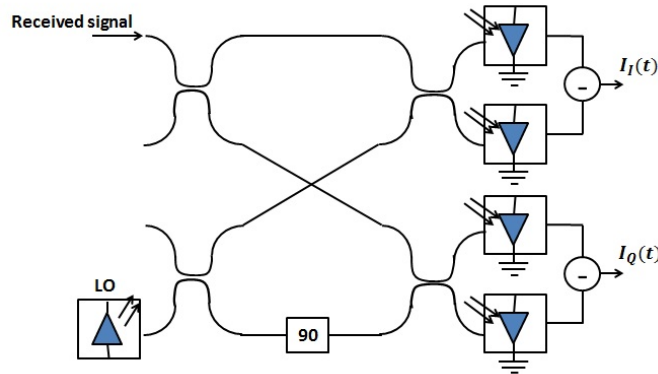


Figure 1.7: Coherent receiver scheme

1.1.1.3 Propagation in single mode fiber (SMF)

The fiber is a cylindrical waveguide where the light propagates through nonlinear medium consists of two reflective indices. The highest reflective index belong to the core medium n_{core} while the lowest belong to the cladding $n_{cladding}$ ($n_{cladding} < n_{core}$) as shown in Fig. 1.8. This construction allows confining the light inside the waveguide while propagating by successive internal reflection at the boundary. Moreover, the fiber is categorizes based on the propagating light rays; also called modes, the fiber with only one propagating mode is referred to single mode fiber (SMF) and multi-mode fiber when it allows more than one mode to propagate.

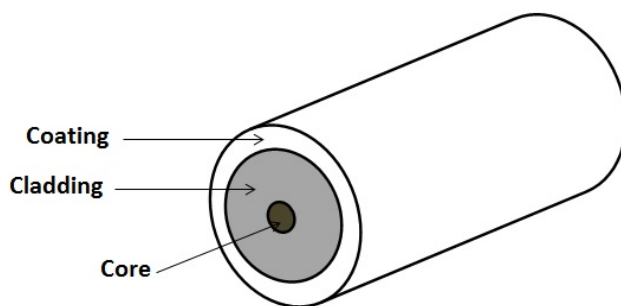


Figure 1.8: Single mode fiber design

The condition controls the number of modes that propagates in the optical fiber is based on the normalized frequency V , which is given as [17]:

$$V = \frac{2\pi r_c}{\lambda_0} \sqrt{n_{core} - n_{cladding}} \quad (1.4)$$

the wavelength of the optical signal is λ_0 while r_c is the core radius. Each mode has its own cut-off frequency as the resulting solution of the wave propagation equation, and the mode propagates when the cut-off frequency is higher than V . However, this is true for all modes except the fundamental mode which always propagates (null cut-off) until reaching $V = 2.405$ where the next modes appear.

In General, the electric field E is expressed in the time domain as [18]:

$$E(x, y, z, t) = F(x, y)A(z, t) \exp(-i(\omega_0 t - \beta z)) \quad (1.5)$$

where z and t are the propagation distance and the time variable, respectively. $A(z, t)$ is the complex envelope of the field and $F(x, y)$ is the normalized spatial distribution of the field in the x-y plane. β is the propagation coefficient approximated by Taylor series that

depends on the angular frequency ω_0 as:

$$\beta_\omega = \beta_0 + \beta_1(\omega - \omega_0) + \beta_2(\omega - \omega_0)^2 + \dots \quad (1.6)$$

where β_i is the i^{th} derivative of β with respect to ω . In Eq. 1.5, A can be found by solving the non-linear Schrodinger equation (NLSE) that describes the propagation in the time domain ([18], Chap.2):

$$\frac{\partial A}{\partial z} = -\frac{\alpha}{2}A + \frac{i}{2}\beta_2\frac{\partial^2 A}{\partial t^2} + i\gamma\|A\|^2A \quad (1.7)$$

α is the attenuation of the fiber. β_2 is the group velocity dependence on the carrier frequency, γ is the non-linear coefficient. Each term in Eq. 1.7 represents physical parameters which we detail in the following.

• Transmission loss

The propagating optical power attenuation depends on the wavelength of the signal. The attenuation can be categorized into Rayleigh scattering and material absorption which affect the optical receiver detection performance that requires a particular power level. Rayleigh scattering in fiber affects more the short wavelengths than the long ones in the region 1200-1715 μm (near-infrared); this degradation can be described as $1/\lambda_0^4$ where λ_0 is the wavelength. Moreover, there is peak absorption at 1.1 μm (i.e. metallic ions) and 1.38 μm (i.e. OH^- ions concentration) which leads to well-known windows in the optical communication (1.3 μm and 1.55 μm). The 1.3 μm window (O band) corresponds to the zero-dispersion window that suits applications with short reach transmission systems. The 1.55 μm window (C band) corresponds to the minimum attenuation window for long-haul transmission. The attenuation after distance L is given by:

$$\alpha = \frac{1}{L} 10 \log_{10} \left(\frac{P_{in}}{P_{out}} \right) \quad (1.8)$$

where P_{in} and P_{out} are the injected power at fiber input and the power after distance L , respectively. Standard single mode fibers (SSMF) are the most known for telecommunication with typical loss coefficient 0.2 dB/km at 1.55 μm as low as 0.15 dB/km for sub-marine fibers.

• Chromatic dispersion

The transmitted optical signal travel at different velocities function of the wavelength that leads to spectral widening of the optical pulse. The effect known as chromatic dispersion

1. THE ROAD TO SPACE DIVISION MULTIPLEXING

(CD) that causes inter-symbol interference (ISI) as shown in Fig. 1.9. The time pulse broadening can be described based on the transmission distance as:

$$\Delta\tau = D.L.\Delta\lambda \quad (1.9)$$

where L is the fiber length and D is the group delay variation per unit length. $\Delta\lambda$ is the wavelength pulse broadening.

From Eq. 1.7, β_2 is related to the group velocity dispersion (GVD) given by:

$$D = -\frac{2\pi c}{\lambda_0^2}\beta_2 \quad (1.10)$$

D is equal to 17 ps/(nm.km) for SSMF fiber at $\lambda_0 = 1.55 \mu m$. Neglecting the losses and the nonlinear effects in Eq. 1.7, we can obtain the transfer function of CD in the frequency domain as:

$$H_{CD}(z, \omega) = \exp\left(-i\frac{D\lambda_0^2 z}{4\pi c}\omega^2\right) \quad (1.11)$$

The CD mitigation is done by applying one of two techniques. Optically, by inserting a dispersion compensating fiber (DCF) which has a negative dispersion coefficient ($D < 0$). Digitally, by applying coherent detection which allows us to compensate the CD in the electrical domain with the digital signal processing (DSP) techniques.

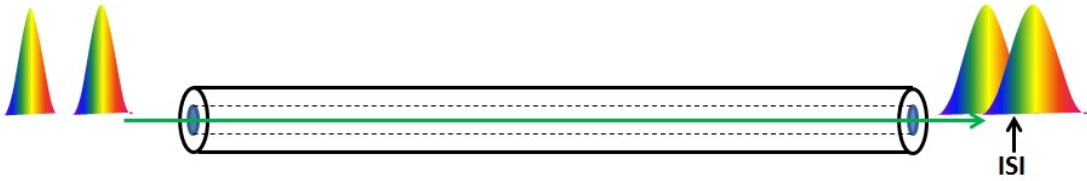


Figure 1.9: Chromatic dispersion in fiber propagation

• Non-linear effects

We can describe the non-linear effects (Kerr effect) as the increment of the refractive index of the fiber while the power of the electric field increases, which is described by:

$$n = n_0 + n_2 \frac{|E|^2}{A_{eff}} \quad (1.12)$$

n_0 is the frequency dependent refractive index and $|E|$ is the power of the incident signal. A_{eff} is the effective core area which varies between [50-100] μm^2 for SMF and

$80\mu m^2$ for SSMF around $1.5\ \mu m$. n_2 is the non-linear refractive index which has value $2 - 3.10^{-20} m^2 W^{-1}$.

The nonlinear term intensity depends on the phase shift in the electrical field; known as self-phase modulation (SPM). Another nonlinear effect called cross phase modulation (XPM) which is induced by the adjacent optical channels. This phenomena is a general case of the SPM in wave division multiplexing (WDM) systems, the XPM is represented as [18]:

$$\phi_{i,NL} = \gamma L_{eff} \left(\left(\sum_{k \neq i} \|E_{k,s}(z=0)\|^2 \right) + 2\|E_{i,s}(z=0)\|^2 \right) \quad (1.13)$$

γ is the non-linear coefficient which is given by:

$$\gamma = a \frac{n_2 \omega_0}{c A_{eff}} \quad (1.14)$$

for SSMF, $a = 1$ for polarization maintaining fibers [19]. L_{eff} represents the effective fiber length where the nonlinear effects are strong [20] which we can approximately define as:

$$L_{eff} \approx \frac{1 - \exp(-\alpha L)}{\alpha} \quad (1.15)$$

where L is the span length. The previous expression shows the nonlinear phase modulation effect on channel i due to the power of other channels and itself. The last nonlinear effect is known as Four-wave mixing (FWM). In this phenomena, we have three channels each carries frequencies $\omega_1, \omega_2, \omega_3$ which creates fourth channel with frequency $\omega_4 = \omega_1 \pm \omega_2 \pm \omega_3$. The impact of the FWM depends on the spacing between the channel and the chromatic dispersion's parameter [20]. In order to reach the best bit error rate (BER), an optimal input power should be injected which is related to the optical transmission architecture that varies with the optical transmission link, the modulation format and the optical components in the link.

1.1.2 Polarization Division Multiplexing (PDM)

The access to the two orthogonal polarizations of the optical signal is available thanks to the coherent receiver. The two polarizations are the decomposition of the electrical field propagating in the transverse plane described based on the state of polarization (SOP) as:

$$\begin{pmatrix} E_x \\ E_y \end{pmatrix} = \begin{pmatrix} \sqrt{P_x} \exp(i\phi_x) \\ \sqrt{P_y} \exp(i\phi_y) \end{pmatrix} \quad (1.16)$$

P_x and P_y are the amplitudes of the polarization E_x and E_y , respectively. ϕ_x and ϕ_y are the phase of the polarization E_x and E_y . In order to realize a polarization division mul-

1. THE ROAD TO SPACE DIVISION MULTIPLEXING

tiplexing (PDM), we modulate the independent orthogonal polarization separately after the polarization beam splitter (PBS) and before combining them by using the polarization beam combiner (PBC) as shown in Fig. 1.10(a). At the receiver side, we split both the signal and the LO into two beams (I and Q) before converting the incident light into intensity current, as shown in Fig. 1.10(b).

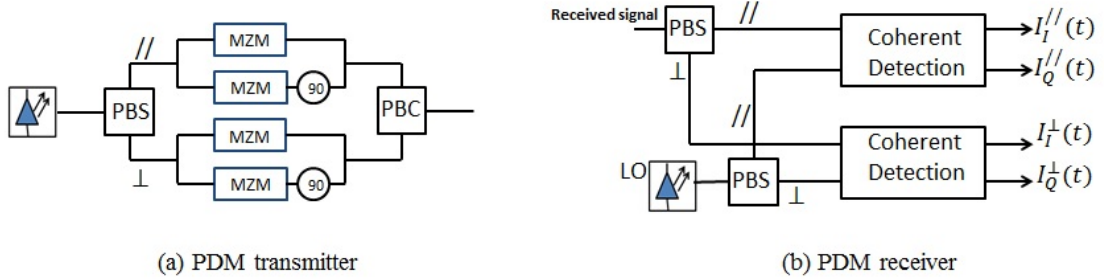


Figure 1.10: Polarization division multiplexing: (a) transmitting scheme and (b) receiver scheme.

Exploring a new degree of freedom to double the capacity of the transmission system introduces new impairment to the system. In addition to the transmission loss and the chromatic dispersion, the PDM suffers from two linear impairments. First, the polarization mode dispersion (PMD), where the two polarizations propagate with different velocities caused by random birefringence. Second, the polarization dependent loss (PDL), where the polarization faces two different attenuation levels.

1.1.2.1 Polarization mode dispersion (PMD)

In ideal fiber with no imperfection (perfect circular fiber), the two polarizations travel with the same velocity and no delay resulting in two parallel channels with no interference. However, the fiber imperfections cannot be avoided due to the manufacturing process and the thermal stress which causes a birefringent waveguide. In this fiber, the two polarizations face two different refractive indices which consequently causes different velocities that induce time delay between the two polarizations (see Fig. 1.11).

The PMD can be modeled as a composite of a concatenation of N independent random oriented birefringent components as:

$$H_{PMD} = \prod_{i=1}^N R_i D_i = \prod_{i=1}^N \begin{pmatrix} \cos(\theta_i) & \sin(\theta_i) \\ -\sin(\theta_i) & \cos(\theta_i) \end{pmatrix} \begin{pmatrix} \exp(-i(\omega\tau_i + \phi_i)/2) & 0 \\ 0 & \exp(+i(\omega\tau_i + \phi_i)/2) \end{pmatrix} \quad (1.17)$$

where R_i is the orientation mismatch of $\theta_i \in [0, \pi]$ between the polarization axes. D_i is the phase shift between the polarization induced by $\phi_i \in [0 : 2\pi]$ as the birefringence effect and

1.1 From Single Mode Fiber to Space Division Multiplexing

$\omega\tau_i$ is frequency dependence of the time delay τ . For long distance links, the accumulated differential group delay $\overline{\Delta\tau}$ is proportional to the square root of fiber length L as [21]:

$$\overline{\Delta\tau} = PMD\sqrt{L} \quad (1.18)$$

where PMD is the fiber PMD coefficient (in $\text{ps}/\sqrt{\text{km}}$).

Several techniques have been proposed in order to compensate for the PMD. The return-to-zero modulation improves the receiver sensitivity to the PMD than the non-return-to-zero format [22]. In [23], electrical equalizers for 40 Gb/s systems were proposed to mitigate the PMD, so improve system performance. Lastly, the coherent detection with advanced digital signal processing can equalize the PMD using MIMO equalization [24].

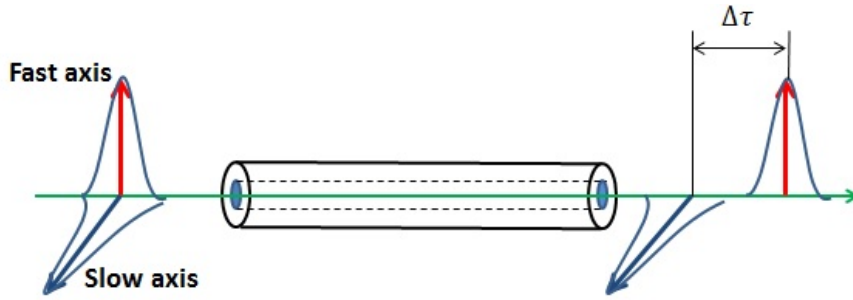


Figure 1.11: Polarization mode dispersion effect

1.1.2.2 Polarization dependent loss (PDL)

The PDL rises from non-ideal devices installed during the transmission, such as amplifiers, connectors and couplers [25][26]. Moreover, it has been proven that the standard deviation of the PDL increases linearly with the number of the PDL elements [27] and the global PDL follows a Maxwellian distribution [28]. The PDL degrades the optical transmission performance due to the loss of orthogonality between the two polarizations. Another factor is the orientation angle θ between the polarization axes. Therefore, it is known that the PDL is a subject of two cases shown in Fig. 1.12. First, the polarization suffers from different attenuation while maintaining the orientation angle ($\theta = 0$ [90°]). Second, the polarization loses the orthogonality while maintaining the same attenuation.

As mentioned previously, the polarization dependent loss (PDL) results from different attenuation for the two polarizations. The PDL can be modeled by:

$$H_{PDL} = R_{\theta} \begin{pmatrix} \sqrt{1+\gamma} & 0 \\ 0 & \sqrt{1-\gamma} \end{pmatrix} R_{\theta}^{-1} \quad (1.19)$$

where R_{θ} is a random rotation matrix for the polarization axes, $\sqrt{1+\gamma}$ is the least attenuated polarization and $\sqrt{1-\gamma}$ is the most attenuated polarization. Thus, the PDL is

1. THE ROAD TO SPACE DIVISION MULTIPLEXING

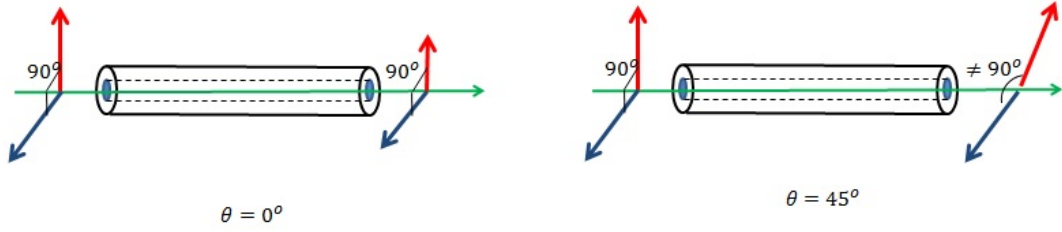


Figure 1.12: Polarization dependent loss effect

defined in dB as:

$$\Gamma_{dB} = 10 \log_{10} \left(\frac{1 + \gamma}{1 - \gamma} \right) \quad (1.20)$$

In [29][30], digital solutions have been proposed for PDL mitigation. One is the use of polarization time codes as an efficient solution to mitigate the PDL for 1000 km transmission considering distributed PDL.

1.1.3 Wavelength Division Multiplexing (WDM)

In WDM system, independent data streams are transmitted in different wavelengths (channels) in the same fiber, as shown in Fig. 1.13. The WDM system expanded the optical transmission capacity with a low cost to suit the traffic demands. However, the WDM implementation could not happen without the manufacturing of powerful wide-band optical amplifiers (EDFA amplification) and wavelength multiplexing/demultiplexing devices. Besides, the wavelengths could propagate without any exchanging power (crosstalk) between the channels even for dense WDM systems, according to ITU-T G.694.1 recommendation, where the wide channels are 50 GHz and 25 GHz.

Furthermore, the WDM is affected by the nonlinearity caused by the XPM and FWM as mentioned previously. This effect can be reduced by enlarging the separation between the channels in the case of XPM. Also, techniques such as unequal channel spacing and dispersion management can mitigate the FWM [31][32].

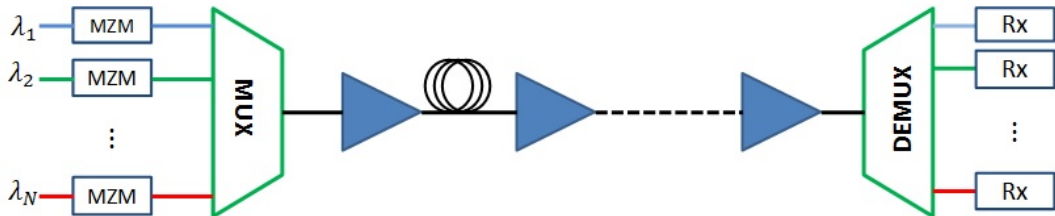


Figure 1.13: Wave division multiplexing transmission scheme

1.2 Space Division Multiplexing (SDM)

1.2.1 State-of-the-Art

The concept of the space division multiplexing (SDM) was first proposed back to 1979 and 1982 [33][34]. However, it did not get much attention because the single mode fiber could easily achieve the optical network capacity requirement as cost-efficient solution, including optical amplifiers, wave division multiplexing (WDM), and polarization division multiplexing (PDM). The capacity crunch, anticipated to happen when the optical commercial expected to offer capacity per fiber more than 80 Tbit/s [35], as shown in Fig. 1.14. It has been foreseen that the bandwidth growth will exceed the maximum achievable capacity of SMF caused by the nonlinear effect (nonlinear Shannon limit) by the year 2023, especially with the arrival of technologies such as the fifth-generation mobile communication (5G) and the Internet of Things (IoT). Several options are possible to be applied, such as multi-cable solutions, multi-fiber cables with higher fiber count, or multi- $\{\text{core}/\text{mode}\}$ fibers. The choice will be based on the type of application, maturity of technologies, standards, energy consumption and operational complexity.

Companies like Google and Facebook that operate in a massive bandwidth started contributing to the subsea infrastructure by deploying their subsea cables. Nowadays, These cables break the 120 Tbits/s and 160 Tbits/s. Today, companies look for the best trade-off between cable capacity, cost, and energy, it is better to stop maximizing the capacity per fiber and optimize capacity per cable, by playing with fiber count, fiber type, fiber performance, and energy efficient amplification technologies.

Nevertheless, the available technologies cannot compete with future traffic demands a few years from now. Therefore, many experts are working to provide a solution for the capacity crunch in the space division multiplexing. Space is the last degree of freedom to be discovered and to increase the optical bandwidth to deliver speed equal to Petabyte per second and avoid the capacity crunch.

The SDM technologies were first deployed to the data center due to the short distance (<100 km) and low strict requirements [36]. In order to implement the SDM in other telecommunication ranges [access - submarine], the reliability of the transmission system should be proved, as shown in Table 1.1 [1]. Since the SMF cannot be renewed to catch up with new requirements, the SDM becomes the primary systems to be deployed with new infrastructure and optical networks. However, this transition should be done smoothly and based on the existing infrastructure. Above that, the emerging SDM technologies have to validate their advantages compared to the deployed SMF-based solutions in terms of cost efficiency and energy efficiency [1].

1. THE ROAD TO SPACE DIVISION MULTIPLEXING

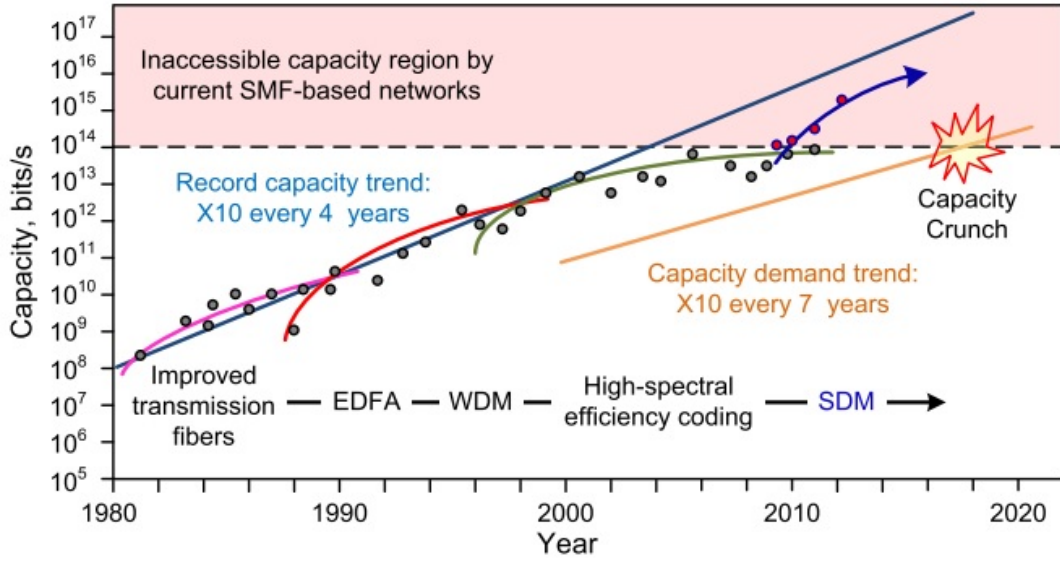


Figure 1.14: The evolution of the optical transmission capacity over the years [1]

Table 1.1: System requirements for different region, '*' indicates the requirement level

	Distance (km)	Component cost	Reliability
Submarine	$\leq 12,000$	*****	*****
Long-haul	≤ 4000	****	****
Metro	$\leq 200 - 500$	***	***
Access	≤ 100	**	**
Data center	$\leq 1 - 10$	*	*

Realizing the SDM system required specific multiplexing devices, the spatial multiplexing SMUX aims to convert the signal from bundle SMFs into modes or separate cores in SDM fiber, as shown in Fig. 1.15. The SMUX can be implemented using several technologies which have been evolved from bulk optics by using spot-based excitation or mode-selective excitation [37] [38] to photonic integrated devices such as 3-dimensional waveguide (3DW) and fiber-bundle (also referred as Fan-{In/Out}) [39] [40]. The performance difference between these technologies is based on the insertion loss, the mode dependent loss and the core dependent loss which will be discussed later.

Deploying the SDM systems mainly depends on implementing low complex digital signal processing techniques and realization amplification devices that match the optical communication standard. Amplifying the optical signal in SDM fibers is categorized into two main techniques. The core pumping, the amplification of the optical signal occurs separately by using an erbium-doped amplifier (EDFA) and the spatial multiplexing and demultiplexing before combining the core or the modes into the SDM fiber as illustrated in Fig. 1.16(a). With this scheme, the power controlling gain in each spatial path is achieved



Figure 1.15: Spatial multiplexing and demultiplexing scheme

using single components at the cost of high cost amplification. Better scheme in term of cost efficiency is the cladding-pumped amplifiers as shown in Fig. 1.16(b). The challenge in such a scheme is to provide a uniform power gain between the spatial paths. However, a lot of research and experimental demonstration have been reported in the SDM amplification fields [41][42][43]. In our work, we do not consider the amplification components in the transmission link. At the same time, we focus on the transmission losses knowing that it could be implemented in future works.

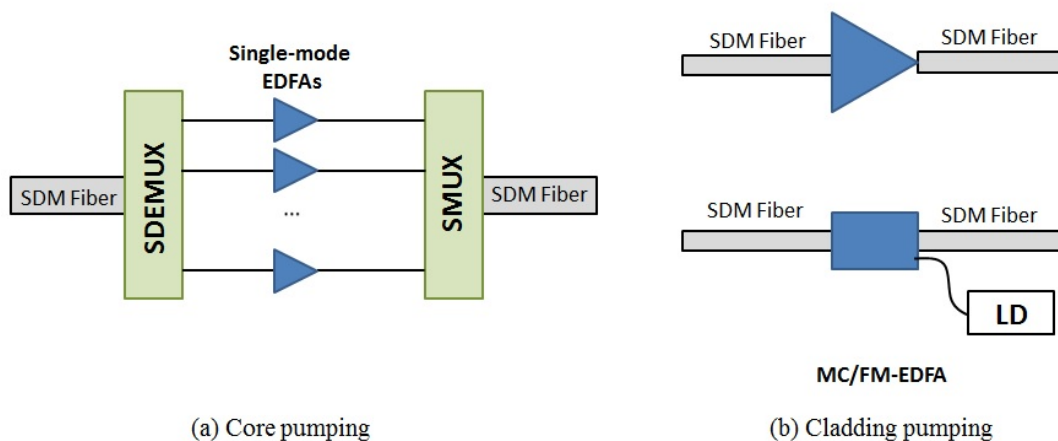


Figure 1.16: Amplification schemes: (a) core pumping and (b) cladding pumping

1.2.2 SDM Fiber Approaches

The new emerging SDM fiber has different implementation approaches, as shown in Fig. 1.17. The different approaches in order to realize SDM fibers can be summarized as follow:

1. THE ROAD TO SPACE DIVISION MULTIPLEXING

- **Fiber bundles:** the simplest way to realize a SDM system is to compose independent SMFs with separate cladding as shown in Fig. 1.17(a) [1]. However, the fiber bundles provide a large core packing densities compared to the conventional SMFs so large footprint. Besides, the management of each fiber should be done separately in term of amplification, photonic circuit devices consequently lower cost-efficiency compared to the multi-mode or multi-core fibers.
- **Few-mode fibers (FMFs)/Multi-mode fibers (MMFs):** has a larger core compared to the SMF as shown in Fig. 1.17(b) and (c); referred to mode division multiplexing (MDM). In case of FMFs, the fiber supports propagation of small number of modes that depends on the characterization of the fiber and the normalized frequency V in Eq. 1.4. The modes are combined in a set of M linearly polarized (LP) modes each represents a solution of the wave equation taking into account the boundary limits and can be approximated by Bessel functions. The mode is represented as LP_{lq} where l is the azimuthal order and q is the radial order of the mode, the mode has two orthogonal spatial distribution when $l \neq 0$ and denoted as $LP_{lq,a}$ and $LP_{lq,b}$. In Table 1.2, we illustrate an example of the parameters for FMFs and the corresponding propagating modes as reported in [3] for $\lambda = 1.55\mu m$ and numerical aperture $NA = 0.205$. The conventional multi-mode fibers (MMFs)

Table 1.2: FMF parameters for 3, 6 and 10 modes, for $\lambda = 1.55\mu m$ and $NA = 0.205$. [3]

number of modes	core radius	propagating modes
3	$6\mu m$	$LP_{01}, LP_{11a,b}$
6	$8.7\mu m$	$LP_{01}, LP_{11a,b}, LP_{21a,b}, LP_{02}$
10	$11\mu m$	$LP_{01}, LP_{11a,b}, LP_{21a,b}, LP_{02}, LP_{12a,b}, LP_{31a,b}$

are designed with core diameter equal to $50\mu m$ in $125\mu m$ cladding. The MMFs are mostly deployed for short-distance communication due to the low restriction and high modal dispersion. However, in MDM each mode or group of modes is modulated independently with separate data information. In addition to the physical impairments such as the chromatic dispersion or polarization mode dispersion, the FMFs/MMFs are affected by the differential mode group delay (DMGD) and mode dependent loss (MDL) that needs to be addressed in the design of the fiber link.

- **Multi-core fibers (MCFs):** it integrates multiple cores in one cladding. The MCF can be manufactured using different techniques based on the coupling relation between the cores and the core arrangement. In SDM based on MCF, each core carries separate modulated data stream that supports the fundamental mode LP_{01} or few modes depends on the core radius as mention previously. However, Table 1.3

give a brief comparison between the FMF and the MCF. The MCF can be designed with larger effective area A_{eff} so more tolerant to the fiber nonlinearities [42] [44]. Also, the authors showed that the coupled MCF has higher nonlinearity tolerance compared to the uncoupled MCF. Regards the DSP processing, the complexity is reduced for MCF due to low MDGD. Moreover, the spatial utilization efficiency of FMF/MMF is higher than the MCF using the standard $125\mu\text{m}$ cladding diameter.

Table 1.3: Comparison between the FMF/MMF and the MCF

	Spatial efficiency	DSP complexity	Nonlinearity tolerance	Scalability
FMF/MMF	High	High	Medium	High
MCF	Medium	Medium	Medium/High	Medium

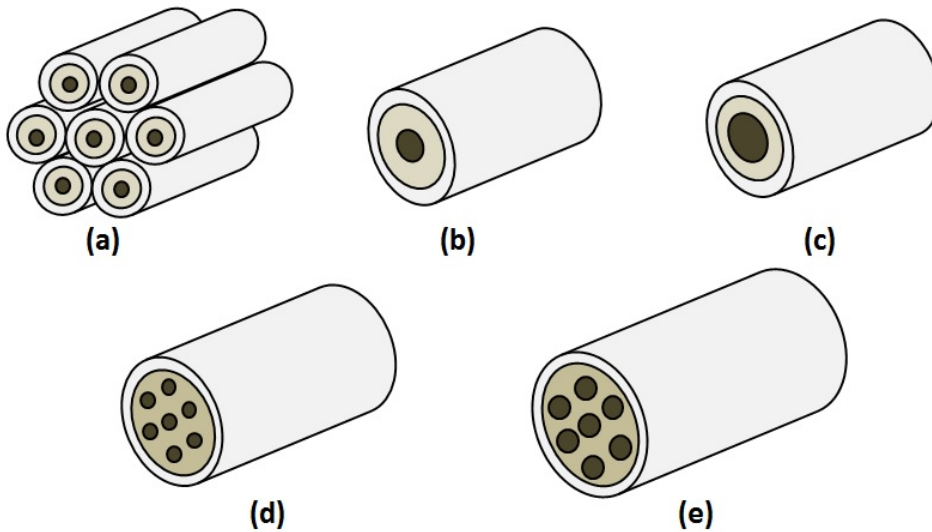


Figure 1.17: SDM approaches:(a) Fiber bundles, (b) FMF, (c) MMF, (d) MCF and (e) Massive SDM (MCF and FMF)

Summary

In this chapter, we reviewed the evolution of the optical communication systems, we concerned to present the several technologies which have been introduced until now in order to enhance the system capacity. We started by illustrating the basic principle of single mode fiber and the propagation impairments. After, we reviewed the DoF that helps to improve the optical transmission performance such as: the EDFA along with the WDM, the coherent detection and PDM systems. Finally, we introduced the SDM system

as the last degree of freedom to be developed. We illustrated the different techniques to realize SDM systems (Fiber bundles, FMF and MCF).

In this thesis, we are interesting in investigating the performance of the SDM based on the MCF fiber since several studies have been done in the field of FMF systems in [45][3]. Besides, more investigation is currently concerned with MCF systems since it showed more implementation visibility compared to the MDM. As mentioned previously, MCF systems have lower complex devices compared to the MMF such as the MCF-amplifications and multiplexing (Fan-{In and Out}), one of the main reasons is the low MDGD in the MCF systems. Thus, it is expected that the first SDM system generation will be MCF based. However, several questions should be answered concerning the fiber design, propagation impairments, channel model and system performance before providing standard MCF system. The next chapter is dedicated to provide detailed information on the MCF fiber design and system limitation that affects the system performance.

Chapter 2

Multi-Core Fiber Structures and Limitations

We have reviewed in the previous chapter the SMF optical communication evolution over the years until now. We explained all the degrees of freedom already deployed until reaching the space as the last degree of freedom. The SDM system is a potential solution to keep up with the increasing the capacity demand and overcome the Shannon capacity limitation of single mode channel. In this thesis, we are interested in the MCF transmission system as an alternative approach for spatial multiplexing. In fact, the optical community investigates more on evaluating the MCF system than the MMF since the DSP complexity of MMF is much higher than the MCF systems.

The ITU standards for MCF fiber is not yet established. Therefore, manufacturing SDM based on MCF is very challenging in order to optimize different core parameters such as the cutoff wavelength, the effective area, the cladding diameter and also managing the mode coupling between the cores. The MCFs is categorized into two regimes. In the weak-coupling regime, sufficient separation between cores is required, which reduces the number of neighbor cores surrounding to limit the crosstalk level that affects each core. In the strong-coupling regime, the design limitations are more relaxed at the cost of shifting the load to the receiver side. However, in the literature, several MCF layout designs have been proposed for specific core numbers. These layouts will be our references to evaluate the MCF transmission systems.

In this chapter, we start by discussing the design limitations of MCFs. We present the most common techniques used in the literature in order to design MCF. Also, we illustrate the analytical coupling expression for each technique and make the comparison between them. Afterward, we present some of the experimental demonstrations that have been

2. MULTI-CORE FIBER STRUCTURES AND LIMITATIONS

carried on in laboratories. Lastly, we focus on the MCF layout which will be evaluated in our thesis; we explain all the required parameters which have been applied in each fiber design.

2.1 Multi-Core Fiber Design Techniques

2.1.1 Crosstalk Estimation

In MCF, the crosstalk between the neighbor cores is one of the main parameters that need to be evaluated. In the literature, there are two approaches to estimate the value of the crosstalk for a certain bending radius (R_b). The first approach is the coupled-mode theory (CMT), which is a well-known technique for the coupling process such as the coupler devices. However, it is challenging to adapt CMT for the optical fiber; a large number of samples must be simulated to obtain an accurate value of the crosstalk without taking into account the propagation constant fluctuation [2]. Therefore, relying on the CMT to estimate the crosstalk is not desirable. The second approach is the coupled-power theory (CPT), where the averaged crosstalk values are obtained by only one simulation and taking into account the fluctuation in the propagation constant [46]. In order to realize fast and accurate estimation of the crosstalk, an analytical expression of the power coupled coefficients (PCC) based on an autocorrelation function is preferable [2]. In the following, a detailed explanation of the two approaches will be discussed.

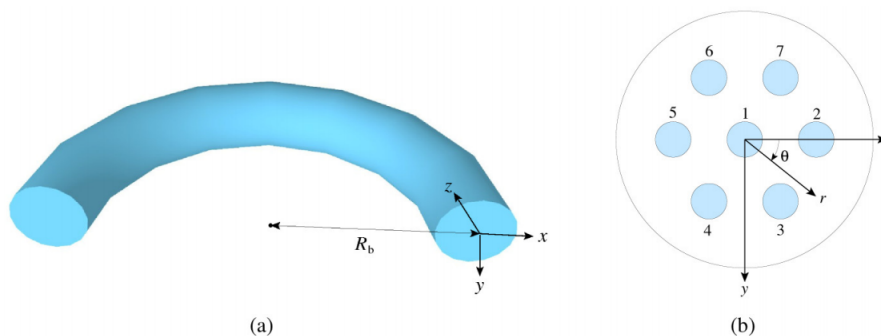


Figure 2.1: Schematics of (a) bent multi-core fiber and (b) fiber cross-section [2]

2.1.1.1 Coupled-Mode Theory

The crosstalk evaluation for MCFs should consider the effects of the bending and twisting in the transmission line due to the impact on the propagation constant difference between the cores ($\Delta\beta$). The bending and twisting are considered as random process which have a direct impact on the crosstalk level between the cores.

The crosstalk expression based on the CMT is presented as [47]:

$$\frac{dA_n}{dz} = -j \sum_{n \neq m} k_{nm} A_m(z) \exp(-j\Delta\beta_{nm}z) f(z) \quad (2.1)$$

k_{nm} is the coupling coefficients between core n and m . $\Delta\beta_{nm}$ is the effective propagation constant different which is given as:

$$\Delta\beta_{nm} = \Delta\beta_{core,nm} + \Delta\beta_{bend,nm}(z) \quad (2.2)$$

where $\Delta\beta_{core,nm}$ is the intrinsic propagation constant difference between core n and core m and $\Delta\beta_{bend,nm}$ is the bending and twisting induced propagation constant difference along the optical transmission link.

In Eq. 2.1, $f(z)$ is the phase function which is represented as:

$$f(z) = \exp[j(\phi_m - \phi_n)]\delta f(z) \quad (2.3)$$

where ϕ_n and ϕ_m are the phase in core n and m , respectively. $\delta f(z)$ is a random part due to the crosstalk fluctuation in the longitudinal direction, which should be considered in MCFs caused by the crosstalk statistical characteristics. Without the random part, Eq. 2.1 is presented as the conventional coupled mode equation. In [2], the total length is divided into finite equal segments (d_s) and random phase-offsets ($\exp(j\phi_{rnd})$) as shown in Fig. 2.2. Solving Eq. 2.1 provides the crosstalk between the cores. However, since the crosstalk given by the CMT shows a statistical characteristics shown in Fig. 2.3, in order to obtain an accurate average value of the crosstalk a large number of simulations are required. Thus, coupled-power theory (CPT) is introduced to obtain more accurate and fast estimation of the crosstalk.

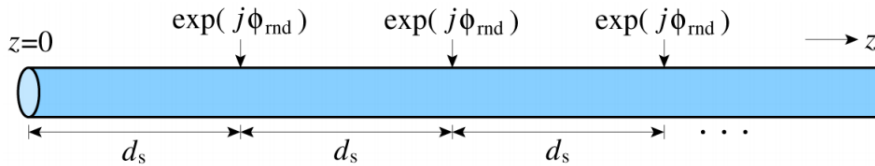


Figure 2.2: Random phase-offsets applied to all cores at every segment [2]

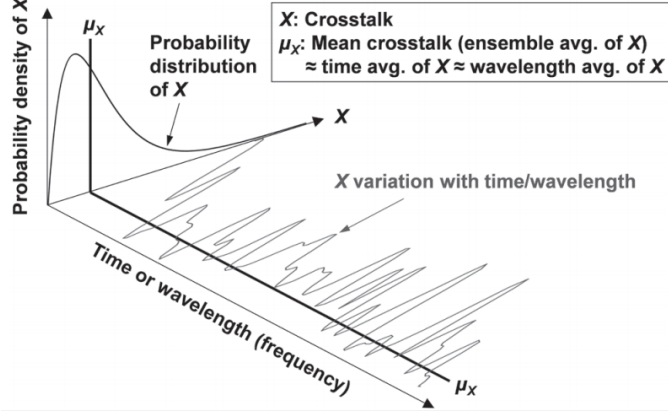


Figure 2.3: Schematic diagram explaining stochastic behaviors and statistical parameters of XT in MCF [2]

2.1.1.2 Coupled-Power Theory

From Eq. 2.1, small segment $[z_1, z_2]$, the crosstalk increment in power is given as[47]:

$$\begin{aligned} \Delta XT_{nm} &= \left\langle \left| \frac{\Delta A_n}{A_m} \right|^2 \right\rangle = k_{nm}^2 \int_{z_1}^{z_2} \int_{z_1}^{z_2} \exp[-j\Delta\beta_{nm}(z-z')] \cdot \langle f(z) \cdot f^*(z') \rangle dz dz' \\ &= k_{nm}^2 \int_{z_1}^{z_2} \int_{z_1-z'}^{z_2-z'} \exp[-j\Delta\beta_{nm}\zeta] \cdot \langle f(z'+\zeta) \cdot f^*(z') \rangle d\zeta dz' \end{aligned} \quad (2.4)$$

where $f(z)$ is the random fluctuation of the bending and twisting which can be considered as stationary random process with an autocorrelation function $R(\zeta) = \langle f(z'+\zeta) \cdot f^*(z') \rangle$. After substituting the autocorrelation function in the previous expression, we obtain[47]:

$$\Delta XT_{nm} = k_{nm}^2 \int_{z_1}^{z_2} dz' \int_{+\infty}^{-\infty} \exp[-j\Delta\beta_{nm}\zeta] \cdot R(\zeta) d\zeta = k_{nm}^2 \cdot \Delta z \cdot S(\Delta\beta_{nm}) \quad (2.5)$$

where $S(\Delta\beta_{nm})$ is the power spectral density of f . In [47], it has been proved that the exponential autocorrelation function can describe the randomness of the bending and twisting of the MCF ($R(\zeta) = \exp(-|\zeta|/d)$), where d is the correlation length between the bending and the twisting).

Given the local power coupling coefficient $h_{nm}(z) = \Delta XT_{nm}/\Delta z$ [47], the power coupling coefficient can be derived as:

$$h_{nm}(z) = \frac{2k_{nm}^2 d}{1 + \Delta\beta_{nm}^2(z) \cdot d} \quad (2.6)$$

According to CPT, the average power coupling coefficient $\langle h_{nm} \rangle$ can be obtained after

a propagation length L that results in crosstalk expression as follows:

$$XT_{nm} = \tanh((h_{nm})L) \quad (2.7)$$

The previous expression is applicable for homogeneous cores where the cores are identical (homogeneous MCFs) or heterogeneous cores where the cores are different in reflective index or core radius (heterogeneous MCFs). In [48] [49], the authors provide a modified XT expression taking into account the crosstalk frequency dependence. However, in our model, we consider the average power that gives an accurate and fast estimation of the crosstalk level. In the following, we will explain the different manufacturing techniques and the corresponding coupling expression based on the CPT.

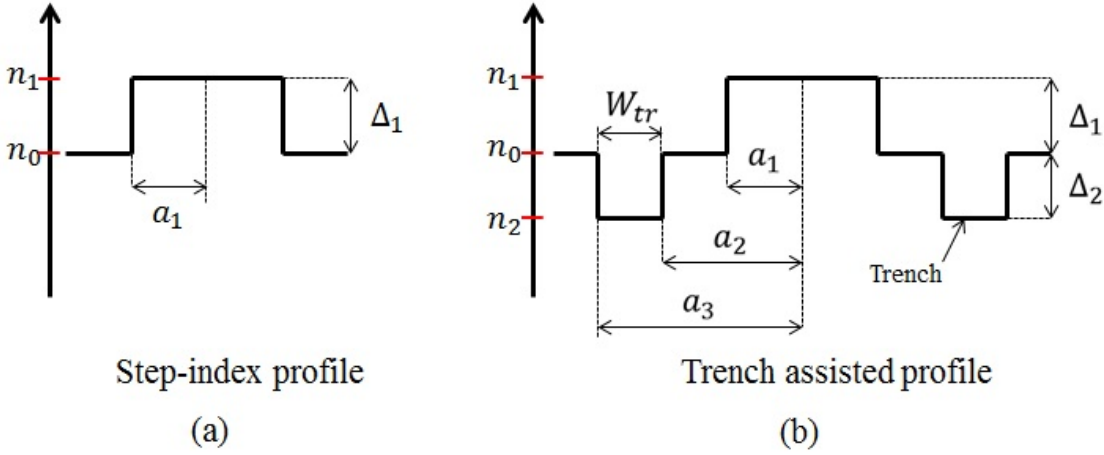


Figure 2.4: Core index profile: (a) Step-index profile and (b) Trench assisted profile.

2.1.2 CPT expressions for MCF Designs

2.1.2.1 Homogeneous MCF

MCF with homogeneous cores induces high crosstalk levels since the propagation constant is the same between the cores ($\Delta\beta = 0$). In order to realize a weakly coupled system, a large separation between the core is necessary. The crosstalk between two adjacent cores based on Eq. 2.7 is estimated by [50]:

$$XT_{n,m} = \frac{2k_{nm}^2 R_b}{\beta^2 \Lambda} L \quad (2.8)$$

The crosstalk is proportional to the coupling coefficient (k_{nm}) and the bending radius (R_b). Λ and L are the core pitch and the fiber length, respectively. Furthermore, the

2. MULTI-CORE FIBER STRUCTURES AND LIMITATIONS

coupling coefficient between two cores with step index profile as shown in Fig. 2.4(a) is given by [50]:

$$k_{nm} = \frac{\sqrt{\Delta_1}}{a_1} \frac{U_1^2}{V_1^3 K_1^2(W_1)} \sqrt{\frac{\pi a_1}{W_1 \Lambda}} \exp\left(-\frac{W_1}{a_1} \Lambda\right) \quad (2.9)$$

where $U_1^2 = a_1^2(k^2 n_1^2 - \beta^2)$ and $W_1^2 = a_1^2(\beta^2 - k^2 n_0^2)$. $V_1 = ka_1 n_1 (2\Delta_1)^{0.5}$ is the V number which determines the modes propagation in a fiber. $K_1(\cdot)$ is the modified Bessel function of the 2nd kind of 1st order.

In Fig. 2.5, a fiber composed of a core surrounded by six neighbor cores is considered; this is the worst case scenario. We plot the crosstalk value in dB function of the core pitch for the different MCF design techniques. We set the bending radius's value to be equal to 140mm and the fiber length equal to 100 km. The yellow points represent the experimental achievements in the literature [51][52][53]. In the case of homogeneous cores, we notice the high crosstalk value with significant core separation where the crosstalk is equal to 22dB with $\Lambda = 45\mu m$. Consequently, the homogeneous approach shows design limitations imposed by the crosstalk, since applying more core separation is not desirable due to the mechanical failure which limits the cladding diameter to $255\mu m$ [54].

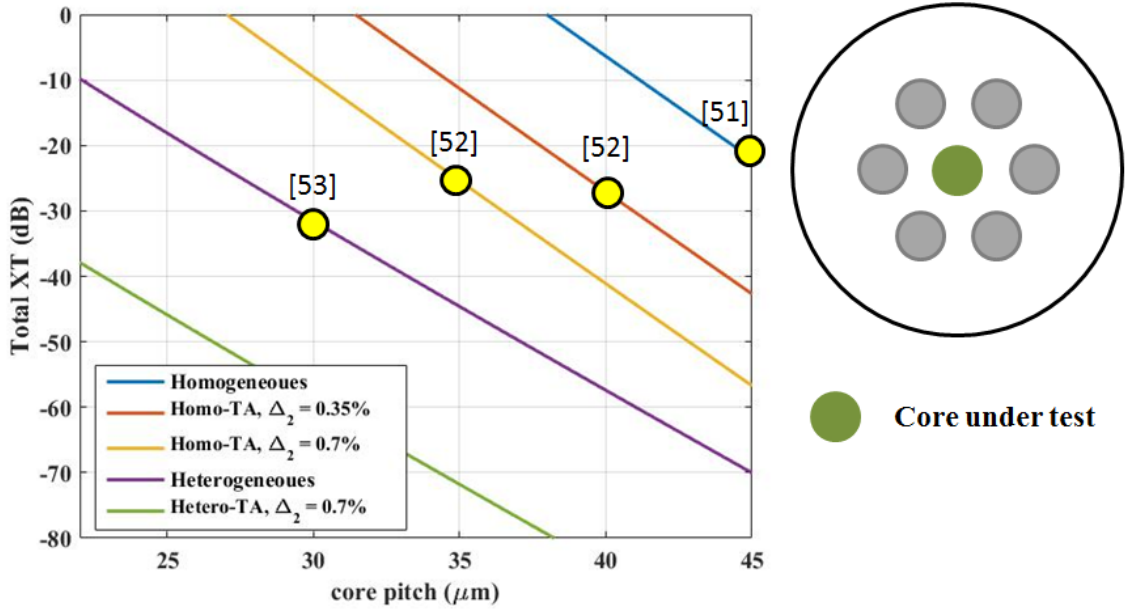


Figure 2.5: The total crosstalk versus core pitch for different MCF core design

2.1.2.2 MCF with Trench Assistance

Caused by the limitation of the conventional homogeneous MCF, it becomes necessary to depart from the step index core profile to trench assisted core, as shown in Fig. 2.4(b). a_1 , a_2 and a_3 are respectively the core radius, the distance between the core center and

the inner edge of the trench and the distance between the core center. W_{tr} is the trench thickness. n_0 the refractive indices for the 1st and 2nd cladding. Δ_1 is the relative refractive index differences between the core and 1st cladding and Δ_2 is the relative refractive index differences between the trench and 2nd cladding. The field confinement in each core is reinforced by using the refractive index trench and allowing decreasing the crosstalk due to the trench assistance.

The estimation of the crosstalk between homogeneous cores with trench assistance and step index profile remains the same as Eq. 2.8. Except, the coupling coefficient expression, in this case, is given as [54]:

$$k_{nm} = \frac{\sqrt{\Delta_1}}{a_1} \frac{U_1^2}{V_1^3 K_1^2(W_1)} \sqrt{\frac{\pi a_1}{W_1 \Lambda}} \exp\left(-\frac{W_1}{a_1} \Lambda\right) \exp\left[-\frac{W_1 \Lambda + 2(W_2 - W_1)W_{tr}}{a_1}\right] \quad (2.10)$$

$W_2 = (V_2^2 + W_1^2)^{1/2}$, where $V_2 = ka_1(n_0^2 - n_2^2)^{1/2}$, in which n_2 is the refractive index of the trench assistance. In order to notice the effect of the trench assistance on the crosstalk value, we can represent the crosstalk of trench assisted MCF function of the conventional MCF (step index profile)(Eq. 2.8)[54]:

$$XT_{trench} = XT_{step} \Gamma \exp\left[-4(W_2 - W_1)W_{tr}/\Lambda\right] \quad (2.11)$$

where XT_{step} is the conventional MCF crosstalk in Eq. 2.8 and Γ is given by[54]:

$$\Gamma = \frac{W_1}{[(W_2 - W_1)W_{tr}/\Lambda]} \quad (2.12)$$

From the expression in Eq. 2.11, the trench width W_{tr} and the trench depth Δ_2 are the major parameters for crosstalk reduction. In [54], the authors show that more than 30dB crosstalk reduction is achievable with a typical trench width of $W_{tr}/a_1 = 1$, which will be used in our study.

In Fig. 2.5, we show the crosstalk level of the homogeneous cores with trench assistance for $\Delta_2 = \{0.35\%, 0.7\%\}$. We observe that the crosstalk is reduced by 20dB and 30dB for Δ_2 equal to 0.35% and 0.7% respectively compared to the core with step index profile. Moreover, the trench assistance technique allows us to reach 30 μm core pitch at the cost of high crosstalk value equal to -10dB at $\Delta_2 = 0.7\%$. On the other hand, air-holes assisted structure is another technique used to suppress the crosstalk between the cores [55]. Despite the existence of air-holes MCF structure, it is not frequently applied in the literature. Thus, we do not evaluate the air-holes MCF structure in this thesis.

2.1.2.3 Heterogeneous MCF

The heterogeneous core techniques are considered a promising technique to obtain a sufficient crosstalk reduction and increase the number of cores in the fiber. In this case, the core can be non-identical in the refractive index, the core diameter or both. Consequently, different propagation constant is induced between the neighbor cores ($\Delta\beta \neq 0$), which drastically reduces the coupling level. Based on the CPT, the crosstalk characterization in the heterogeneous cores is divided into two regions, as shown in Fig. 2.6. In the first region (red region), the bending radius is small compared to a determined parameter $R_{pk} = \frac{n_{eff}}{\Delta n_{eff}} \Lambda$ [51]. n_{eff} and Δn_{eff} are the effective refractive index and the difference between two cores. In this region, where the number of phase-match is high ($\Delta\beta = 0$), the crosstalk is proportional to the bending radius similar to the homogeneous MCF. After exceeding R_{pk} , the fiber enters the second region (blue region), where the number of phase-match is negligible, and the crosstalk becomes independent of the bending radius and proportional to the correlation length. As shown in Fig. 2.6, the crosstalk is reduced drastically compared to homogeneous system. In the heterogeneous MCF, it is assumed to operate in the second region where the crosstalk between two adjacent cores is estimated by [56]:

$$XT_{n,m} = \frac{2k_{nm}^2 L}{\Delta\beta^2 d} \quad (2.13)$$

where d is the correlation length, furthermore, the coupling coefficient between two heterogeneous cores is obtained by [57]:

$$k_{nm} = \frac{k(n_p^2 - n_{cl}^2) W_{1-p} U_{1-q} \sqrt{\frac{\pi a_{1-q}}{2W_{1-q} D}} \exp\left(-W_{1-q} \frac{D}{a_{1-q}} + 2(W_{1-q} - W_{2-q} \frac{a_{3-q} - a_{2-q}}{a_{1-q}})\right)}{\sqrt{n_p n_q} a_{1-p} a_{1-q} V_{1-p} V_{1-q} J_1(U_{1-p}) J_1(U_{1-q})} \\ \times \int_0^{a_{1-p}} J_0\left(U_{1-p} \frac{r}{a_{1-p}}\right) I_0\left(\frac{W_{1-q}}{a_{1-q} r}\right) r dr \quad (2.14)$$

where

$$\begin{aligned}
 & \int_0^{a_{1-p}} J_0\left(U_{1-p} \frac{r}{a_{1-p}}\right) I_0\left(\frac{W_{1-q}}{a_{1-q} r}\right) r dr \\
 &= \frac{J_0\left(\frac{U_{1-p}}{a_{1-p}}\right) \frac{W_{1-q}}{a_{1-q}} I_1\left(\frac{W_{1-q}}{a_{1-q}}\right) + I_0\left(\frac{W_{1-q}}{a_{1-q}}\right) \frac{U_{1-p}}{a_{1-p}} J_1\left(\frac{U_{1-p}}{a_{1-p}}\right)}{\left(\frac{U_{1-p}}{a_{1-p}}\right)^2 \left(\frac{W_{1-q}}{a_{1-q}}\right)^2} \quad (2.15)
 \end{aligned}$$

a_{1-m} is the radius of core m , a_{2-m} is the distance from the center of core m to the inner circumference of trench m . a_{3-m} is the distance from the center of core m to the outer circumference of trench m . $J_0(\cdot)$ and $J_1(\cdot)$ are the 0th-order and the 1st-order of the Bessel function, respectively. $I_0(\cdot)$ and $I_1(\cdot)$ are the 0th-order and the 1st-order of the 1st kind modified Bessel function. Finally, in Fig. 2.5 we plot the crosstalk value of

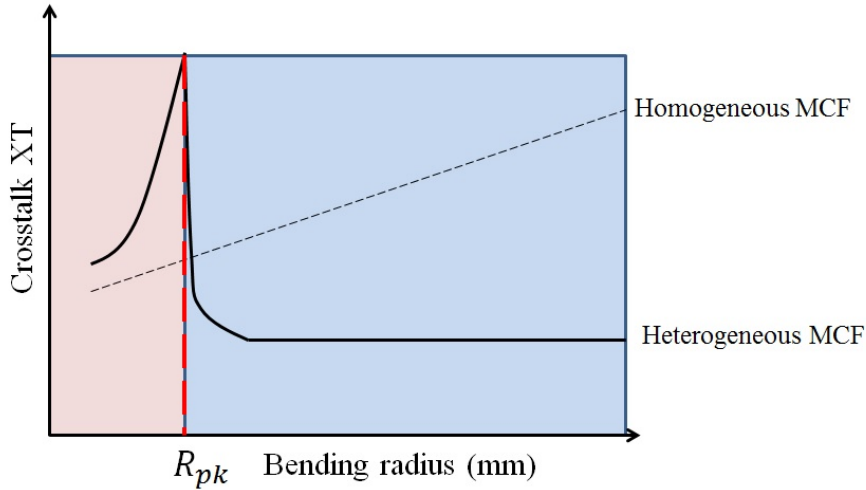


Figure 2.6: Schematic of the dependence of bending diameter of the heterogeneous and homogeneous MCF

the heterogeneous core without and with trench assistance at $\Delta_2 = 0.7\%$. We notice the advantage of applying the heterogeneous technique since the crosstalk value is reduced up to 50dB at core pitch equal to $30\mu_m$ compared to the homogeneous core with trench assistance. We also notice that the core pitch can be reduced to $22\mu_m$, which allows us to increase the core number.

2.2 Multi-Core Fiber Layouts

2.2.1 Experimental Achievements in MCF

Series of successful experiments deploying the MCF system has been carried out in optical transmission systems. In this section, we review some achievements shown in Table 2.1. These experiments aim to achieve high throughput and transmission reach without applying MIMO processing at the receiving side. Recently, the University of L'Aquila, with cooperation with Sumitomo Electric and Optoscribe, has deployed the world's first MCF testbed for SDM fiber optic communications in a real field environment in the city of L'Aquila as part of INCIPICT project[58][59]. The project is a big step toward implementing the MCF fiber in the industry. The testbed consists of two fiber types: 4-core Homo-MCF [58] and 8-core Homo-MCF with ring structure [59] for transmission distance 6.3 km. Moreover, others achieved several experimental demonstrations aiming to reach long distances, higher bit rate, or higher core numbers. In [60], J.Sakaguchi *et al.* achieved 109 Tbit/s over 16.8 km for 7-core Homo-MCF. In other work [61], the authors could achieve a higher bit rate equal to 112 Tbit/s over 76.8 km for 7-core Homo-MCF. Further, Takeshima and others demonstrated longer transmission reach equal to 2520 km after installing MCF amplifier (MCF-EDFA) [62]. On the other side, Y.Sasaki *et al.* designed MCF transmission with 7-core Hetero-MCF with three types of cores [51]. Takara *et al.* proposed 12-core Hetero-MCF with ring layout for low crosstalk value over 40km transmission distance [63]. For the same number of cores, the authors in [64] proposed a 12-core Hetero-MCF square layout aiming to increase the number of cores while maintaining the crosstalk value as low as possible. Moreover, Sakoguchi *et al.* could achieve 305 Tbit/s transmission over 10.1 km by using 19-core Homo-TA-MCF [65]. In [56], high density multi-core fiber is achieved by manufacturing 30-core Hetero-MCF with three types of cores and transmission distance equal to 96 km. Moreover, Mizuno *et al.* achieved 32-core Hetero-MCF for long transmission distance equal to 1600km by using recirculating loop system [66]. Finally, Puttnam and others demonstrated 2.15 Pbit/s using a 22-core MCF structure for transmission link equal to 31 km.

Noticeably, several experimental demonstrations have been realized, the performance of each structure varies based on different configuration parameters such as the crosstalk level, the MCF structure and transmission distance.

2.2.2 Multi-Core Fiber Layouts under Evaluations

This section aims to introduce the MCFs which will be studied and evaluated in our works and detail all the necessary information concerning each layout. The choices have been

Table 2.1: Recently Achievement reported for MCF transmission

Reference	Core number	Core Type	distance	bit rate
L'Aquila [58]	4-core	Heterogeneous with Trench	6.3 km	N/A
J.Sakaguchi [60]	7-core	Homogeneous	16.8 km	109 Tbit/s
B.Zhu [61]	7-core	Homogeneous	76.8 km	112 Tbit/s
Y.Sasaki [51]	7-core	Heterogeneous	N/A	N/A
K.Takeshima [62]	7-core	Homogeneous	2520 km	51.1 Tbit/s
L'Aquila [59]	8-core (Ring)	Homogeneous with Trench	6.3 km	N/A
Takara [63]	12-core (Ring)	Heterogeneous	40 km	N/A
T.Mizuno [64]	12-core	Heterogeneous with Trench	40 km	N/A
J.Sakaguchi [65]	19-core	Homogeneous with Trench	10.1 km	305 Tbit/s
Puttnam [67]	22-core	Homogeneous	31 km	2.15 Pbit/s
V.Amma [56]	30-core	Heterogeneous	9.6 km	N/A
T.Mizuno [66]	32-core	Heterogeneous with Trench	1600 km	100 Gbit/s

made based on the most commonly used structures according to the literature. As shown in Fig.2.7, the considered MCFs are: **(A)** 7-core Heterogeneous MCF (7-core Hetero-MCF) [51], **(B)** 7-core Heterogeneous MCF with Trench Assisted (7-core Hetero-TA-MCF) [51] [56], **(C)** 12-core Heterogeneous MCF (12-core Hetero-MCF) [63], **(D)** 12-core Heterogeneous MCF with Trench Assisted (12-core Hetero-TA-MCF) [63], **(E)** 19-core Heterogeneous MCF (19-core Hetero-MCF) [52], **(F)** 19-core Homogeneous MCF (19-core Homo-MCF) [68] and **(H)** 32-core Heterogeneous MCF (32-core Hetero-MCF) [53] [66].

We can classify the structures depending on the core coupling where it is strong (crosstalk $XT > -30\text{dB}$) in structures **A**, **C** and **F** and weak (crosstalk $XT < -30\text{dB}$) in structures **B**, **D**, **E** and **H**. In the other side, the structures can be categorized according to the number of different type of cores in the fiber. In structures **A**, **B** and **E** the fibers contain three types of cores while structures **C**, **D** and **H** the fibers are constructed by selecting two types of cores. Lastly, structure **F** is the only fiber that contains homogeneous cores. Fig.2.7 with Table. 2.2 illustrate the design details of the fiber and the core parameter for each structure. The core radius, the distance between the core center and

2. MULTI-CORE FIBER STRUCTURES AND LIMITATIONS

the inner edge of the trench and the distance between the core center are a_1 , a_2 and a_3 , respectively. W_{tr} is the trench thickness. n_0 the refractive indices for the 1st and 2nd cladding. Δ_1 is the relative refractive index differences between the core and 1st cladding and Δ_2 is the relative refractive index differences between trench and 2nd cladding. The cladding diameter in the {7, 12}-core MCF (CD_1) is equal to $125\mu_m$ while in the 19-core MCF the cladding diameter (CD_2) is equal to $210\mu_m$ and (CD_3) is equal to $243\mu_m$ for the 32-core Hetero-MCF.

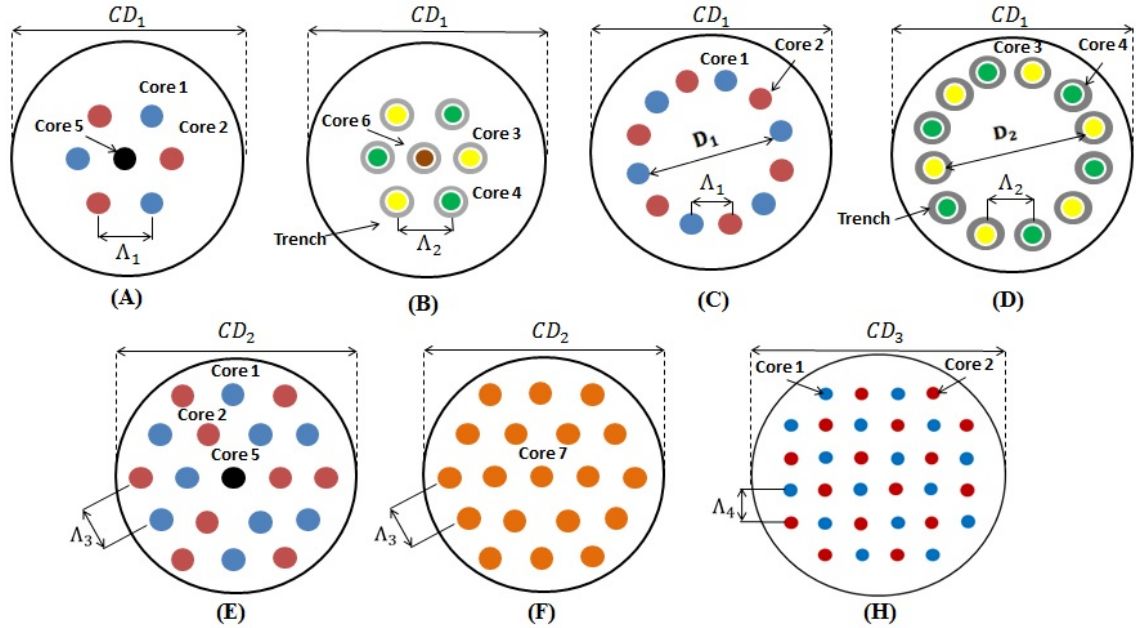


Figure 2.7: MCF structures, the cladding diameter $CD_1 = 125\mu_m$, $CD_2 = 210\mu_m$ and $CD_3 = 243\mu_m$, core pitch $\Lambda_1 = 24\mu_m$, $\Lambda_2 = 33\mu_m$, $\Lambda_3 = 40\mu_m$ and $\Lambda_4 = 33\mu_m$, $D_1 < D_2$.

Table 2.2: Cores parameters

core	1	2	3	4	5	6	7
$a_1[\mu_m]$	4.68	4.76	4.68	4.76	4.68	4.68	4.5
a_2/a_1	-	-	1.7	1.7	-	1.7	-
W_{tr}/a_1	-	-	1	1	-	1	-
n_0	1.45	1.45	1.45	1.45	1.45	1.45	1.45
$\Delta_1[\%]$	0.388	0.338	0.388	0.338	0.305	0.305	0.335
$\Delta_2[\%]$	-	-	0.7	0.7	-	0.7	-

2.3 Propagation in Multi-Core Fiber

First, to simplify the considered MCF structures that will be evaluated in this thesis, Fig. 2.8 arranges all the considered MCF structures based on the two categories: Coupling level and the Core structure.

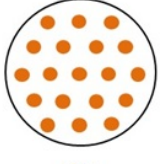
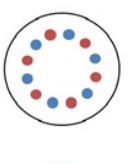
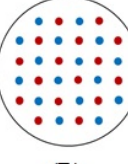
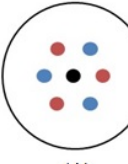
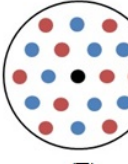
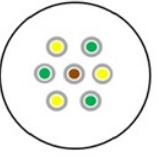
	Core Types		
	Homogenous Cores	Heterogeneous Cores with Two Types of Core	Heterogeneous Cores with Three Types of Core
Strong Coupled	 <p>(F)</p>	 <p>(C)</p>  <p>(D)</p>	 <p>(A)</p>  <p>(E)</p>
Weak Coupled		 <p>(D)</p>	 <p>(B)</p>

Figure 2.8: MCF under evaluation to organize various the coupling level and the core design

In MCF transmission, each core is modulated with an independent data stream. In this case, the capacity of the optical fiber increases linearly with the core number. In a real system, the MCF is affected by different impairments that impact fiber performance. In addition to the well-known physical impairments in the conventional single mode fiber such as chromatic dispersion or polarization mode dispersion, the MCF fiber suffers from additional effects caused by the core's existence in the same cladding and the simultaneous propagation of the data in each core. First, the linear coupling between the neighbor cores that depends on the MCF structure and the design techniques. Second, the imperfection of the inline components installed during the transmission causes differential misalignment losses or amplification gain which vary from one core to another depending on the core position and core type. Combining these two impairments induce non-unitary effect known as the core dependent loss (CDL) that impacts the MCF systems' capacity and performance.

2.3.1 Linear Crosstalk

Manufacturing a multi-core transmission system where each path (core) transmits a signal without interference from the neighbors is the ideal MCF system. However, the existence of the core in the same cladding without sufficient separation causes field overlap between the transmitted signals. In fact, the core coupling is a transfer of energy from core to another core where occurs at discrete points such as Fan-{In/Out} devices, connector and an optical amplifier. In addition, the coupling can originate from the propagation through

2. MULTI-CORE FIBER STRUCTURES AND LIMITATIONS

the MCF due to the bending or mechanical stress. The coupling can be non-unitary that induces power fluctuations between the cores resulting in SNR penalties. The coupling level between the cores is an important factor to be considered during the design process of the MCF systems. The amount of coupling depends on the constant propagation difference $\Delta\beta$ and core pitch between the cores in addition to the in-line components.

In the weakly coupled fiber, the main challenge is to reduce the coupling level to the minimum. One approach is designing the MCF with a sufficient separation, large enough to reduce the linear coupling. Thus, the requirement of low coupling limits the spatial density of cores in the MCF. Therefore, in this category, we mostly focus on fiber fabrication with a large spatial density of cores while preventing linear core coupling induced by fabrication or environment conditions. Moreover, the privilege of weakly coupled fiber is the ability to avoid using full MIMO processing at the receiver, as shown in Fig. 2.9(a). However, even for the weak coupling regime, full MIMO processing brings enhancement in the transmission performance. For example, in [69], the authors proved that the full MIMO improves the reach by 8% of the transmission in weakly coupled MCFs.

In the strongly coupled fiber, the linear coupling is permitted which makes the fiber design constraints more relaxed. Therefore, fewer specifications are needed to manufacture optical components that induce coupling such as Fan- $\{\text{In/Out}\}$ devices. In this case, a large spatial density of cores can be approached since there is no longer needed for significant core separation. However, the drawback of the coupled MCF is the DSP and the requirement of full MIMO processing that increases the receiver complexity, as shown in Fig. 2.9(b) [70].

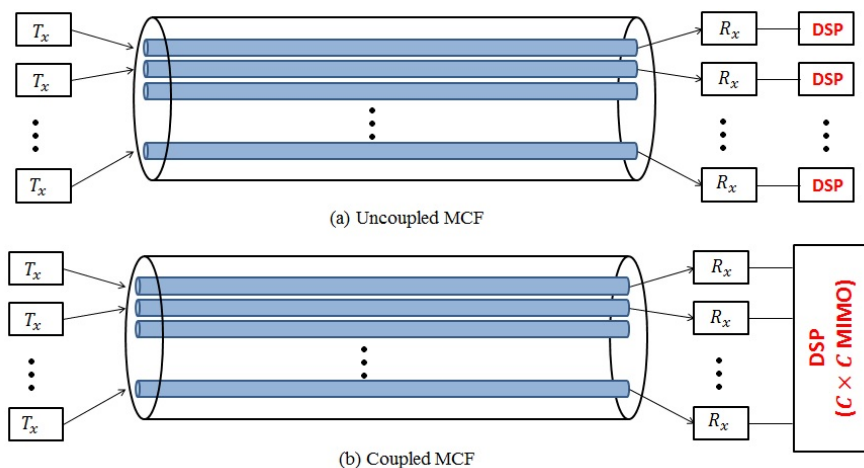


Figure 2.9: Multi-core Fiber transmission scheme for: (a) uncoupled MCF and (b) coupled MCF. DSP: digital signal processing and MIMO: multiple-input-multiple-output.

2.3.2 Misalignment Loss

The transmission chain of the MCF system contains several installed components such as the connectors, link splicing, optical amplifiers and Fan-{In/Out} devices [71]. The imperfection of the components, as well as the splicing parts, induces the misalignment losses. The fields of single-mode fibers are represented by Gaussian field distributions with form [72]:

$$E = a \exp\left(-\frac{r^2}{w^2}\right) e^{-i\beta z} \quad (2.16)$$

where a is a constant function of the field power and fiber parameter, w are the fiber mode field radius and r is the core radius. Then, the fiber misalignment can be differentiated into three main types as follow [72]:

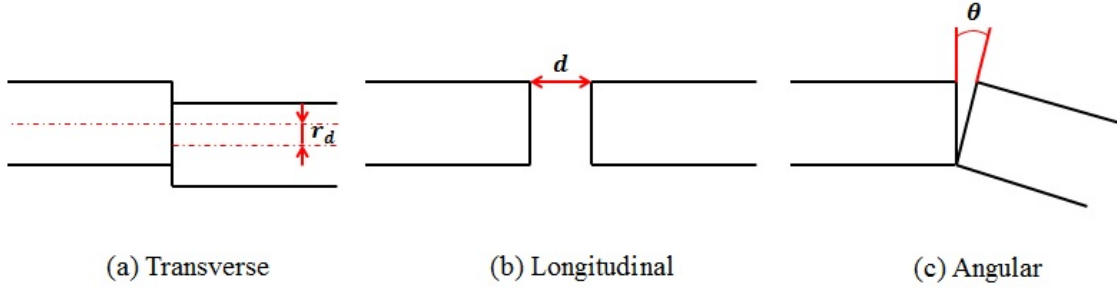


Figure 2.10: Fiber Misalignment Types: (a) Transverse Misalignment, (b) Longitudinal Misalignment and (c) Angular Misalignment

2.3.2.1 Longitudinal Misalignment

The splicing point is shown in Fig. 2.10, the power transmission coefficient is calculated as:

$$\alpha = \frac{4w_1^2 w_2^2}{\frac{d^2}{k_0^2} + (w_1^2 + w_2^2)^2} \quad (2.17)$$

where d is the value of the longitudinal misalignment, $k_0 = \frac{2\pi}{\lambda}$ and w_1 and w_2 are the fiber mode fields radius before and after the splicing, respectively.

2.3.2.2 Angle Misalignment

For the splicing with tilt, as shown in Fig. 2.10, the power transmission coefficient is calculated as:

$$\alpha = \frac{4w_1^2 w_2^2}{(w_1^2 + w_2^2)^2} \exp\left(-\frac{k_0^2 \theta^2 w_1^2 w_2^2}{2(w_1^2 + w_2^2)}\right) \quad (2.18)$$

where θ is the angular displacement of the fibers.

2.3.2.3 Transverse Misalignment

The power transmission coefficient of the transverse misalignment shown in Fig. 2.10 is obtained by:

$$\alpha = \frac{4w_1^2 w_2^2}{(w_1^2 + w_2^2)^2} \exp\left(\frac{-2r_d^2}{w_1^2 + w_2^2}\right) \quad (2.19)$$

where d is the value of the longitudinal misalignment.

In [71] [73], the authors showed that the transverse misalignment is the main factor affecting the fiber losses in MCF. Therefore, in our work, we consider all the misalignment losses source caused by the transverse coefficient.

2.3.3 Differential mode group delay

The modes in each core propagate in different velocity depending on the propagation constant β . The difference between the propagation constant is called the differential mode group delay (DMGD). In fact, MCFs are less affected by the DMGD than the MDM. However, several contributions have been made in order to manufacture MMF with low DMGD [74] [75]. Still, the accumulated DMGD can appear especially for the long-haul transmission system [76]. In addition, heterogeneous MCF can be affected by large DMGD due to the existence of different core types; each fundamental mode propagates with a different velocity corresponding to the core type. For C cores, the modal dispersion is represented by:

$$T_k = \begin{pmatrix} \exp(-i(\phi_1 + w\tau_1)) & & 0 \\ & \ddots & \\ 0 & & \exp(-i(\phi_C + w\tau_C)) \end{pmatrix} \quad (2.20)$$

where ϕ_i and τ_i are respectively the phase noise and the group delay of core i due to thermal and random mechanical stress applied on the core, where $i \in [1, \dots, C]$.

The coherent SDM transmission systems allow mitigating most of the propagation impairments. In the time domain, an equalizer (TDE) with a finite-impulse-response (FIR) filter can recover the mixed spatial channels. In order to recover MCF transmission system, the MIMO equalizer requires $N \times N \times L$ FIR filters [1][77]. Moreover, a tremendous reduction in the computational complexity of MIMO processing for mitigating the large DMGD is obtained through the frequency domain equalizers (FDE) with block-by-block processing and Fast Fourier Transform (FFT) implementation [1]. Another solution that can be implemented to enable lower complexity is the OFDM format [78], with a suitable choice of cycle prefix inserted to absorb the DMGD. OFDM's compensation comes at

the cost of a small added overheads which limits the net throughput of the transmission slightly.

2.3.4 Core Dependent Loss

Core dependent loss (CDL) is considered the main issue in designing the MCF transmission system, especially for high coupling MCF. CDL causes mode power fluctuation between the cores, resulting in a non-unitary effect and orthogonality losses, leading to SNR penalties. In fact, the effect of the CDL is similar to the MDL in MMFs or the PDL in polarization multiplexing on single mode fiber [79] [80] [81]. In MCF systems, the CDL is generated from the crosstalk and misalignment losses accumulation during the transmission. These two factors rise due to the fiber structures, studies have been proven that the cores in the outer circle (far from the fiber center) are more affected by losses than the cores in the inner circle (near to the fiber center) which induce power fluctuation so increase the CDL level. Furthermore, MCF amplifiers are one of the components that impact the CDL level. Therefore, designing the MCF amplifier with unitary power gains is a challenge and still under research to provide a sufficient amplification technique in order to ensure core power equality. The CDL definition is obtained by applying the singular value decomposition (SVD) on the consider channel model, which will be discussed in detail in the next chapter.

Summary

In this chapter, we provided all the details concerning designing MCF for several configurations. We illustrated the conventional MCF fiber designs, the homogeneous core, the trench assistance and the heterogeneous cores. We provided the analytical expressions in order to obtain the coupling between the cores for each solution. These expressions will help to evaluate the transmission performance and providing the MCF channel model in the following chapters. Also, comparisons between the three techniques have been shown based on the crosstalk and the core pitch, which illustrates each technique's advantages and disadvantages. Further, we focused on the mode propagation in MCF. The MCF transmission link is impacted by several impairments represented by the core crosstalk, the DMGD and the misalignment losses. We illustrated the effect of the crosstalk on the performance and system design. Besides, we introduced the different misalignment type which occurs during the transmission link. Finally, we ended up defining the CDL on the MCF as a non-unitary effect caused by the crosstalk and the misalignment losses that impact the MCF performance.

Chapter 3

Performance of Multi-Core Fiber Systems Impaired by CDL

In the last chapter, we studied the possible designing techniques based on the coupling between the cores. Each MCF geometry is affected by specific coupling level which gives different channel characterization that makes the MCF transmission performance unpredictable. Thus, determination of channel model is required for CDL degradation. In MDM, mathematical channel model is already available in the literature that describes the MDL effects and the coupling between the modes [45][3]. In MCF channel several design structures have been proposed resulting difficulty in order to obtain a channel model. In this chapter, we propose a mathematical MCF channel model which is valid for all the layouts. The model provides an estimation of the CDL level induced by the transmission system depending on the crosstalk and the misalignment level. Moreover, we compute an upper bound of the error probability based on the Maximum-Likelihood (ML) and Zero-Forcing (ZF) detection techniques.

In our work, we investigate the performance of the MCF structures presented in the previous chapter (Fig. 2.8). DMGD is a dispersion effect that can be mitigated by time or frequency domain equalizers[1][77]. Therefore, we consider that the DMGD is already compensated by applying one of these two methods. On the other side, current MIMO-DSP cannot compensate the CDL at the receiver which impacts the MCF system capacity and transmission performance.

In this chapter, we begin by introducing a channel matrix taking into account both the crosstalk and the misalignment losses based on the design techniques. After, we propose a model of the MCF transmission system in order to investigate the CDL impact. Later, we develop MCF mathematical channel model and estimate the CDL level for any MCF structure that helps us in the error probability analyses. Finally, we derive an upper

bound error probability for the MCF system applying optimal and sub-optimal decoding methods.

3.1 MCF Transmission System Model

This section evaluates the MCF transmission performance and studies the effect of both the crosstalk and the misalignment level, which are induced by the in-line devices such as Fan-{In/Out} and amplifiers. In our work, we presents the effects of these components by introducing crosstalk and misalignment channel metrics for several MCF structures. Then, we investigate the CDL impact on MCF transmission performance.

3.1.1 Core Crosstalk and Misalignment Loss Channel Matrix

Crosstalk and misalignment are the main factors that affect system performance. In this part, we introduce the crosstalk representation between the cores. Also, we represent the misalignment losses for each core, depending on the transmission link configuration.

3.1.1.1 Crosstalk Channel Matrix

Considering MCF with C number of cores, each core is affected by specific crosstalk levels induced by the core neighbors. The transfer matrix representing the coupling between the cores is given by:

$$\mathbf{H}_{XT} = \begin{pmatrix} XT_1 & XT_{1,2} & \cdots & XT_{1,C} \\ XT_{2,1} & \ddots & & XT_{2,C} \\ \vdots & & \ddots & \vdots \\ XT_{C,1} & XT_{C,2} & \cdots & XT_C \end{pmatrix} \quad (3.1)$$

$XT_i = 1 - \sum_{n \neq m} XT_{n,m}$ which represents the losses induced by the crosstalk from the neighbours, $i \in [1, \dots, C]$. $XT_{n,m}$ is the linear crosstalk between core n and core m based on the CPT as mention in chapter. 2 [54]. As shown in the last chapter, the crosstalk for homogeneous and heterogenous cores are estimated by Eq.2.8 and Eq.2.13, respectively. For coupled MCF, \mathbf{H}_{XT} is a full $C \times C$ matrix. For full uncoupled MCF, \mathbf{H}_{XT} is diagonal matrix representing the power transfer in each core.

3.1.1.2 Misalignment Losses Channel Matrix

In MCF, each core in MCF is affected by different misalignment losses due to the imperfection at the splices, the connectors, the Fan-{In/Out} devices and the core position

fluctuation [73] [72] [82]. As mentioned previously, we consider the transverse misalignment loss (α) due to its large impact compared to the other misalignment types. The transverse misalignment loss is given by:

$$\alpha = \exp(-br_d^2), \quad r_d = \sqrt{d_x^2 + d_y^2}, \quad b = \frac{2}{w_1^2 + w_2^2} \quad (3.2)$$

w_1 and w_2 are the fiber mode fields radius before and after the splicing, respectively. However, in our study, the splicing applies to an identical span which means that w_1 and w_2 are equal. r_d is the transverse displacement of the fiber in the x and y directions.

The misalignment channel matrix \mathbf{M} for MCF while single mode propagating in each core can be expressed as a diagonal matrix containing different loss values:

$$\mathbf{M} = \begin{pmatrix} \alpha_1 & & \\ & \ddots & \\ & & \alpha_C \end{pmatrix} \quad (3.3)$$

we assume the misalignment loss values as Gaussian random variables of *zero* mean and standard deviation (std) ($\sigma_{x,y}$), as a percentage of the fiber core radius a_1 .

3.1.2 MCF Channel Model

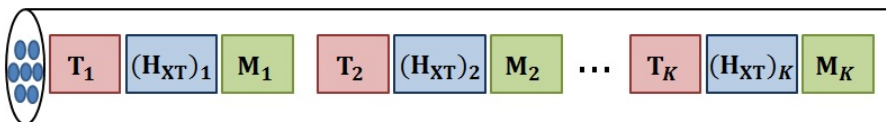


Figure 3.1: Illustration of MCF channel model

In our analysis, we consider a physical description of the fiber with a realistic non-unitary CDL effect generated by the core coupling and fiber splices. The channel matrix for MCF transmission link \mathbf{H} can be modeled as shown in Fig. 3.1 which is represented mathematically as:

$$\mathbf{H} = \sqrt{\ell} \prod_{k=1}^K (\mathbf{T}_k (\mathbf{H}_{\mathbf{XT}})_k \mathbf{M}_k) \quad (3.4)$$

where \mathbf{H} results from concatenation of K spans (fiber sections), each span is equivalent to the multiplication of the crosstalk channel matrix $\mathbf{H}_{\mathbf{XT}}$, the misalignment channel matrix \mathbf{M} and \mathbf{T} is a diagonal matrix with random phase entries $\exp(i\phi_C)$ where $\phi_C \in [0, 2\pi]$ representing the fluctuation on the propagation constant between the different cores. The reflective index variation is due to temperature or mechanical stress. ℓ is a normalization

3. PERFORMANCE OF MULTI-CORE FIBER SYSTEMS IMPAIRED BY CDL

factor used to compensate the link loss, such that $Tr(\mathbf{H}\mathbf{H}^H) = C$ (with $Tr(\cdot)$ represent the trace of a matrix operator), where \mathbf{H}^H is the conjugate transpose of MCF channel model \mathbf{H} .

The channel model \mathbf{H} can be described as $\mathbf{H} = \mathbf{U}\mathbf{\Sigma}\mathbf{V}^H$ after applying the single value decomposition (see Appendix. A.3), \mathbf{U} and \mathbf{V}^H are random unitary matrices and $\mathbf{\Sigma}$ contains the singular values. The CDL is defined as the ratio between the maximum eigenvalue (λ_{max}) and the minimum eigenvalue (λ_{min}) of $\mathbf{H}\mathbf{H}^H$ in decibel as:

$$CDL_{dB} = 10 \log_{10}(\varepsilon) = 10 \log_{10} \left(\frac{\lambda_{max}}{\lambda_{min}} \right) \quad (3.5)$$

The CDL limits the transmission capacity of the SDM system, unlike the dispersive effects. In the MIMO channel system, the CDL breaks the orthogonality of the parallel data streams which makes retrieving the data more difficult at the receiver side. Therefore, keeping the CDL value as low as possible in the transmission link is essential to obtain channel close to the Additive White Gaussian Noise (AWGN) channel and reduce the decoding complexity at the receiver side.

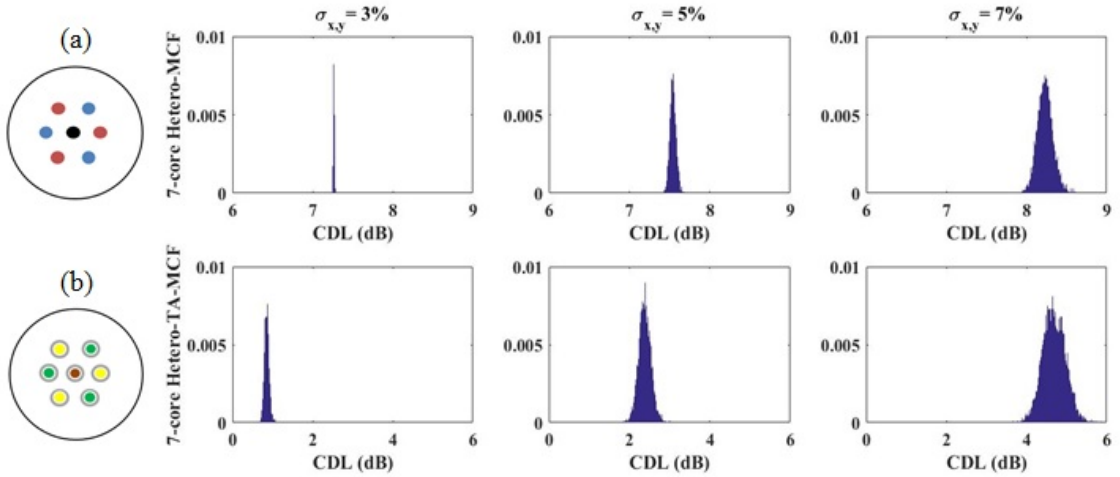


Figure 3.2: PDF of the CDL distribution for: (a) 7-core Hetero-MCF and (b) 7-core Hetero-TA-MCF with $\sigma_{x,y} = \{3\%,5\%,7\%\}a_1$

In order to investigate the crosstalk and the misalignment impact on the CDL level, we simulate 10^5 channel realizations of several MCFs where $K = 300$ misaligned fiber sections with $\sigma_{x,y} = \{3\%,5\%,7\%\}a_1$. Fig.[3.2, 3.3 and 3.4], illustrate the probability density function (PDF) of the CDL. In Fig.3.2, we compare between the 7-core Hetero-MCF and Hetero-TA-MCF where the crosstalk has been decreased after applying the trench assistance, since the trench provides more mode confinement as explained in Chapter. 2. In this

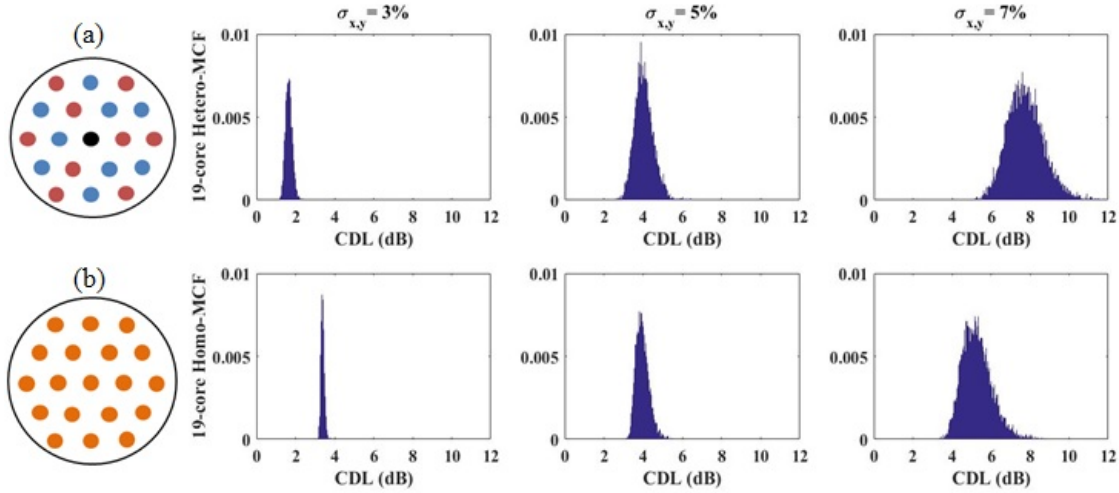


Figure 3.3: PDF of the CDL distribution for: (a) 19-core Hetero-MCF and (b) 19-core Homo-MCF with $\sigma_{x,y} = \{3\%, 5\%, 7\% \} a_1$

comparison, we observe that the CDL level is directly proportional to the misalignment offset and the crosstalk level. Moreover, in Fig.3.3 we compare the 19-core Hetero-MCF and Homo-MCF. We notice that the MCF with homogeneous cores has higher CDL value than the heterogeneous cores at small misalignment levels (3%) due to the high crosstalk between the homogeneous cores. At large misalignment levels, the CDL of heterogeneous exceeds the homogeneous MCF. We conclude that the heterogeneous cores have an increasing impact on the CDL, especially at high misalignment levels, since it forces the signals to follow different paths despite decreasing the core coupling, especially for long-haul transmission systems. However, the Homo-MCF has a core number limitation that arises from the need to have sufficient core pitch distance between the cores. At the same time, the cladding diameter should respect the mechanical failure probability of the fiber. Thus, applying heterogeneous or homogeneous cores does not necessarily determine the CDL level caused by the losses induced in the system. Lastly, in Fig. 3.4, we evaluate the 12-core Hetero-MCF and 12-core Hetero-TA-MCF, the special characteristic of the ring structures that all the cores are surrounded by the same number of neighbors and the MCF does not have a center core. Consequently, we notice the same CDL values for both structures resulting from the ring layout, where the same crosstalk values almost impact all the cores. In conclusion, first, the crosstalk and the misalignment level directly impact the CDL level. Second, it is difficult to estimate the CDL level on the system based on the MCF structure.

3. PERFORMANCE OF MULTI-CORE FIBER SYSTEMS IMPAIRED BY CDL

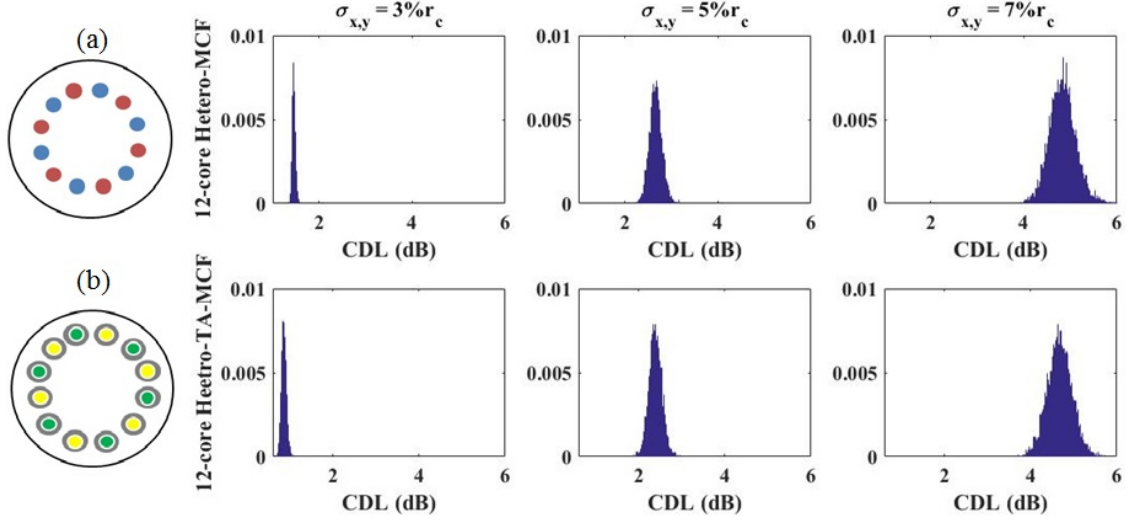


Figure 3.4: PDF of the CDL distribution for: (a) 12-core Hetero-MCF and (b) 12-core Hetero-TA-MCF with $\sigma_{x,y} = \{3\%, 5\%, 7\% \} a_1$

3.1.3 MIMO-MCF Transmission Performance

Considering a MIMO transmission channel for C cores where single mode with single polarization propagates in each core of MCF structures to focus on the CDL impact on the transmission performance. We do not consider fiber non-linearities effects, the resulting MIMO channel is given by:

$$\mathbf{Y}_{C \times 1} = \mathbf{H}_{C \times C} \mathbf{X}_{C \times 1} + \mathbf{N}_{C \times 1} = \sqrt{\ell} \prod_{k=1}^K (\mathbf{T}_k (\mathbf{H}_{\mathbf{XT}})_k \mathbf{M}_k) \mathbf{X}_{C \times 1} + \mathbf{N}_{C \times 1} \quad (3.6)$$

where \mathbf{X} and \mathbf{Y} are respectively the emitted and the received vectors. For the AWGN channel, the channel matrix is equal to the identity matrix \mathbf{I} . \mathbf{N} is an Additive White Gaussian Noise with *zero* mean and variance N_0 . In fact, the non-whiteness noise can be neglected in the case of strong core coupling [68]; in our model, the white noise will be considered for all the coupling levels as it was done in [83] [80] [84] [85]. MIMO processing

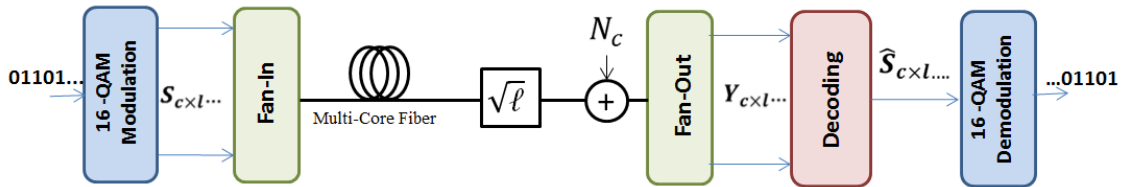


Figure 3.5: MCF transmission system scheme

is mainly required for strong coupling MCF. However, R. S.Luis *et al* in [69] shows that MIMO improves the transmission reach even for weakly coupled systems. In order to

illustrate the benefit of applying MIMO processing over MCF transmission, in Fig. 3.6 we plot the BER of the 7-core Hetero-TA-MCF (weak coupling) over the transmission distance with and without applying MIMO decoding techniques at SNR = 10dB. The obtained result proves the enhancement that MIMO decoding brings to the short reach and long-haul transmission system. Moreover, we evaluate the effect of the transmission distance on the accumulated CDL. We notice that the CDL impact is much higher in the long-haul transmission, where the CDL is equal to 22dB after 1000km distance.

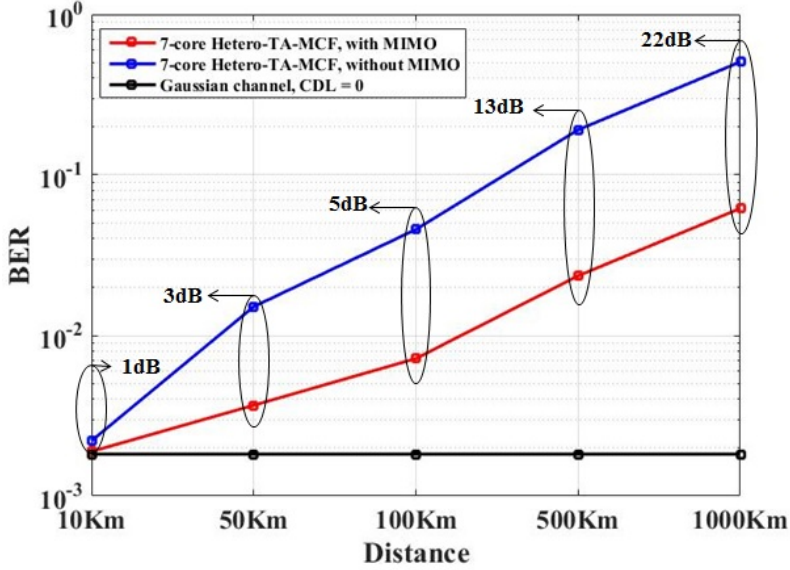


Figure 3.6: 7-core Hetero-MCF Performance function of the transmission distance, with and without full MIMO and at SNR = 10dB and $\sigma_{x,y} = 7\% a_1$.

Further, we plot the bit error rate (BER) versus the signal to noise ratio SNR = $10\log_{10}(E_b/N_0)$ for different CDL values corresponding to $\sigma_{x,y} = \{3\%, 7\%\} a_1$. A 16-QAM modulation is used at the transmitter and ML decoder is used at the receiver side. In Fig.3.7(a), we show the performance of 7-core Hetero-MCF. We observe SNR penalty equal to 1.5dB at BER = 10^{-3} with CDL = 7.2dB compared to the Gaussian channel (CDL=0) and 3.5dB penalty with CDL = 8.3dB caused by increasing the misalignment level. Moreover, we evaluate the performance of 12-core Hetero-MCF as shown in Fig.3.7(b). We notice that the system performance with CDL value equal to 1dB has SNR penalty = 0.1dB at BER = 10^{-3} and the penalty increases to 2dB with CDL = 4.6dB. 12-core Hetero-MCF does not have a central core which gives better performance compared to 7-core Hetero-MCF. Thus, in our following evaluation the ring structure has the advantage to perform better than the other structures.

3. PERFORMANCE OF MULTI-CORE FIBER SYSTEMS IMPAIRED BY CDL

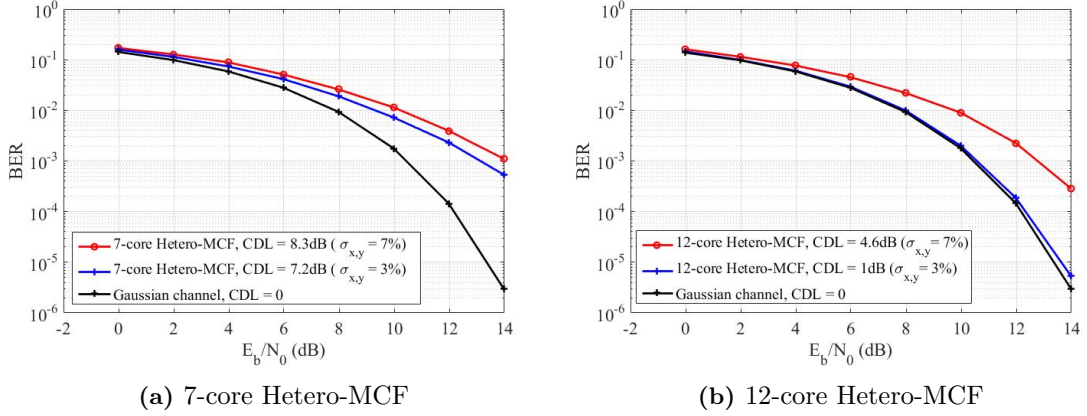


Figure 3.7: BER performance: (a) 7-core Hetero-MCF and (b) 12-core Hetero-MCF, with $3\%a_1$ misalignment level (red curve) and $7\%a_1$ misalignment level (blue curve).

3.2 Theoretical Analysis of MCF Channel

The fact that the transmission system configuration and the MCF structure determine the CDL level push us to investigate a solution to predict the MCF performance. Thus, deriving a theoretical channel model as a tool to estimate the CDL for the several MCF systems is required. In this section, we aim to model the MCF channel \mathbf{H} theoretically by using the singular value decomposition of \mathbf{H} as: $\mathbf{H} = \mathbf{U}\mathbf{\Sigma}\mathbf{V}^H$, where \mathbf{U} and \mathbf{V}^H are random unitary matrices and $\mathbf{\Sigma}$ is a diagonal matrix with singular value elements λ_i .

3.2.1 Analytical Derivation

The equivalent channel matrix \mathbf{H} is a concatenation of each section as:

$$\mathbf{H} = \underbrace{\mathbf{T}_1(\mathbf{H}_{XT})_1\mathbf{M}_1}_{\mathbf{H}_1} \underbrace{\mathbf{T}_2(\mathbf{H}_{XT})_2\mathbf{M}_2}_{\mathbf{H}_2} \dots \underbrace{\mathbf{T}_K(\mathbf{H}_{XT})_K\mathbf{H}_K}_{\mathbf{H}_K} \quad (3.7)$$

by applying the QR decomposition (see Appendix A.1) starting from the last section (\mathbf{H}_K). Then, we apply the **QR** decomposition on the previous section \mathbf{H}_{K-1} after multiplying by the orthogonal matrix \mathbf{Q}_K :

$$\begin{aligned} \mathbf{H} &= \mathbf{H}_1 \mathbf{H}_2 \dots \mathbf{H}_{K-1} \underbrace{\mathbf{H}_K}_{\mathbf{Q}_K \mathbf{R}_K} \\ &= \mathbf{H}_1 \mathbf{H}_2 \dots \underbrace{\mathbf{H}_{K-1} \mathbf{Q}_K}_{\mathbf{Q}_{K-1} \mathbf{R}_{K-1}} \mathbf{R}_K \end{aligned} \quad (3.8)$$

due to the unitary property of \mathbf{Q} , the multiplication of \mathbf{Q} doesn't change the singular value of the upper triangular of each \mathbf{R}_k , $k \in [1, \dots, K]$. We continue the process until reaching

\mathbf{Q}_1 which is the equivalent unitary matrix of the product:

$$\mathbf{H} = \mathbf{Q}_1 \mathbf{R}_1 \mathbf{R}_2 \dots \mathbf{R}_K \quad (3.9)$$

where the diagonal value of each \mathbf{R}_k approximately can be given as:

$$r_i = \alpha_i \sqrt{XT_i^2 + \sum_{j=1}^C XT_{i,j}^2} \quad (3.10)$$

The singular values of the equivalent channel \mathbf{H} are equal to the diagonal values of the product of \mathbf{R}_k given that \mathbf{Q}_1 is a unitary matrix. Hence, the singular values are equal to:

$$\lambda_i = \prod_{k=1}^K r_{i,k} = \prod_{k=1}^K \left(\alpha_{i,k} \sqrt{XT_i^2 + \sum_{j=1}^C XT_{i,j}^2} \right) \quad (3.11)$$

We can notice that the effect of the random noise phase does not appear since the $\mathbf{T}^H \mathbf{T} = \mathbf{I}$. Based on the singular values distribution behavior, obtaining the CDL differs from heterogeneous MCF and homogeneous MCF. Thus, the following explains in detail the CDL derivation for both cases.

3.2.1.1 Heterogeneous MCF

For simplification, the summation of the crosstalk squared ($\sum_{j=1}^C XT_{i,j}^2$) can be neglected since we noticed that the values are very small compared to XT_i^2 , meaning that the crosstalk level is very small compared to the actual losses in each core. Therefore, the singular values are expressed as:

$$\lambda_i = (XT_i)^K \prod_{k=1}^K \alpha_{i,k} \quad (3.12)$$

$(XT_i)^K$ and $\alpha_{i,total} = \prod_{k=1}^K \alpha_i^k$ are respectively the total crosstalk and the total misalignment losses of core i at the end of the link where:

$$\alpha_{i,total} = \prod_{k=1}^K \alpha_i^k = \exp(Z), \quad Z = \sum_{k=1}^K -b(dx_{k,i}^2 + dy_{k,i}^2) \quad (3.13)$$

$dx_{k,i}^2$ and $dy_{k,i}^2$ are Chi-squared distributed with 1 degree of freedom $\sim \sigma_{x,y}^2 \tilde{\chi}_1^2$. So, $dx_{k,i}^2$ and $dy_{k,i}^2$ have mean $\sigma_{x,y}^2$ and variance $2\sigma_{x,y}^4$. For high number of sections K , we can apply the Central Limit Theorem (CLT) on Z . This leads to set that Z is normally distributed with mean $\mu_z = -2Kb\sigma_{x,y}^2$ and variance $\sigma_z^2 = 4Kb^2\sigma_{x,y}^4$.

As Z is normally distributed, $\alpha_{i,total} = \exp(Z)$ has a lognormal distribution with parameters:

3. PERFORMANCE OF MULTI-CORE FIBER SYSTEMS IMPAIRED BY CDL

$$\mu_{\alpha_i, total} = \exp(\mu_z + \sigma_z^2/2) = \exp(2Kb_i(b_i\sigma_{(x,y)_i}^4 - \sigma_{(x,y)_i}^2)) \quad (3.14)$$

$$\sigma_{\alpha_i, total}^2 = (\exp(\sigma_z^2) - 1) * \mu_{\alpha_i}^2 = (\exp(4Kb_i^2\sigma_{(x,y)_i}^4) - 1) * \mu_{\alpha_i}^2 \quad (3.15)$$

thus λ_i is lognormally distributed with mean $\mu_{\lambda_i} = (XT_i)^K \mu_{\alpha_i, total}$ and variance $\sigma_{\lambda_i}^2 = (XT_i)^{2K} \sigma_{\alpha_i, total}^2$.

Obtaining the singular values distribution for each core allows to estimate the CDL value theoretically. From Eq.3.14 and Eq.3.15, we can determine the singular value of each core and then determine the maximum and minimum values ($\lambda_{max}, \lambda_{min}$). Thus, the CDL ends up as Gaussian distribution $\mathcal{N}(\mu_{CDL}, \sigma_{CDL})$ where:

$$\mu_{CDL} = \left(\frac{20}{\ln(10)}\right) \times \left(K \ln\left(\frac{XT_{max}}{XT_{min}}\right) + (\mu_{z, \lambda_{max}} - \mu_{z, \lambda_{min}})\right), \quad (3.16)$$

$$\sigma_{CDL} = \left(\frac{20}{\ln(10)}\right)^2 \times (\sigma_{z, \lambda_{max}}^2 + \sigma_{z, \lambda_{min}}^2) \quad (3.17)$$

3.2.1.2 Homogeneous MCF

The homogeneous cores follow the same lognormal distribution, which leads to obtaining each of μ_{max} and μ_{min} by using a different methodology. In the case of heterogeneous MCF, it is easier to define λ_{max} and λ_{min} by determining the singular values with maximum and minimum means (μ_{max}, μ_{min}). The CDF of $\max\{\lambda_i\}$ and $\min\{\lambda_i\}$ are respectively defined as $F(x)^C$ and $1 - (1 - F(x))^C$ where $F(x)$ is the CDF of random variable λ_i .

Since $Z \sim \mathcal{N}(\mu_z, \sigma_z)$. the PDF of $X = \min\{Z\}$ and $Y = \max\{Z\}$ are given as (see Appendix.A.2):

$$f_X(z) = \frac{C}{\sigma_z \sqrt{2\pi}} \left[\operatorname{erfc}\left(\frac{z - \mu_z}{\sigma_z \sqrt{2\pi}}\right) \right]^{C-1} e^{-\left(\frac{z - \mu_z}{\sigma_z \sqrt{2\pi}}\right)^2} \quad (3.18)$$

$$f_Y(z) = \frac{C}{2^{n-2} \sigma_z \sqrt{2\pi}} \left[1 + \operatorname{erf}\left(\frac{z - \mu_z}{\sigma_z \sqrt{2\pi}}\right) \right]^{C-1} e^{-\left(\frac{z - \mu_z}{\sigma_z \sqrt{2\pi}}\right)^2} \quad (3.19)$$

we notice that σ_z has a very small value, which allows us to assume that $\operatorname{erf}(\cdot)$ and $\operatorname{erfc}(\cdot)$ reach the saturation. Therefore, we can claim that the PDF of the X and Y are normally distributed.

Further, the mean values of X and Y are given by [86]:

$$\mu_{max} = E[X] = \mu_z + \sigma_z E_C \quad (3.20)$$

$$\mu_{min} = E[Y] = \mu_z - \sigma_z E_C \quad (3.21)$$

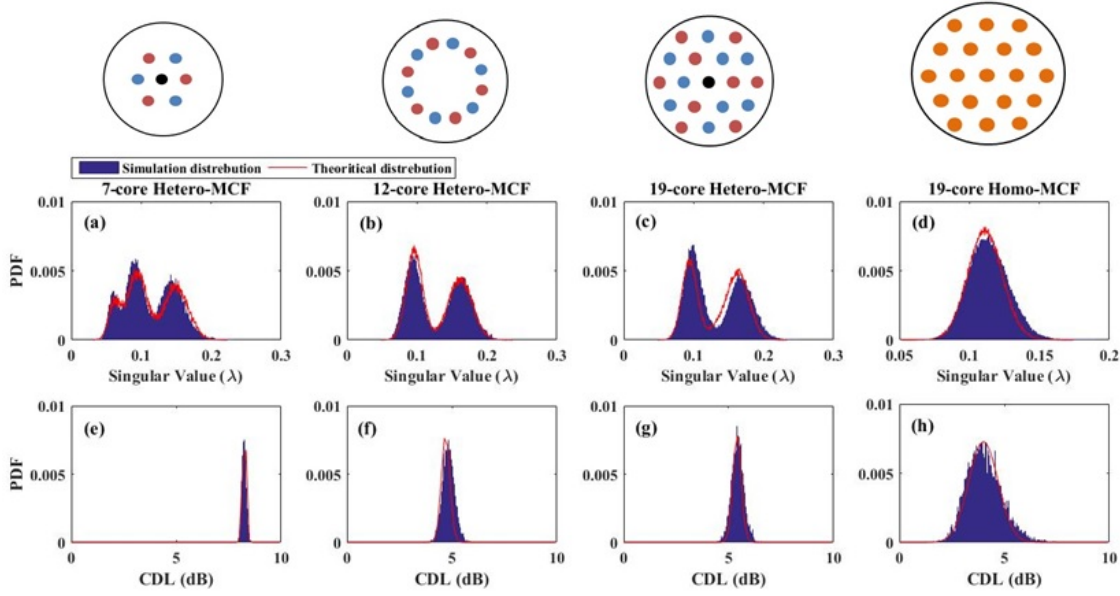


Figure 3.8: Comparison between the simulated and the Theoretical PDF distribution, the upper figures are the PDF of the singular value and the bottom figures are the PDF of the CDL

where E_C is defined as:

$$E_C = \int_{-\infty}^{\infty} z \frac{d}{dz} F_z(z) dz \quad (3.22)$$

It has been shown in [86] that E_C can be approximated by $E_C \sim \sqrt{2 \log(C)}$ which depends on the number of cores C in the MCF. Thus, the CDL can be rewritten as:

$$\mu_{CDL} = \left(\frac{20}{\ln(10)} \right) \times \left(\ln \left(\frac{XT_{max}}{XT_{min}} \right) + (2E_C \sigma_z) \right), \quad (3.23)$$

$$\sigma_{CDL} = \left(\frac{20}{\ln(10)} \right)^2 \times (2\sigma_z^2) \quad (3.24)$$

3.2.2 Theoretical Channel Model Validation

We compare the proposed mathematical channel model with the simulated results for specific MCF structures that serve our purpose of illustrating all the observations. However, the following results can be obtained for any MCF structure. We simulate 10^5 realizations of the optical channel where $K = 300$ misaligned fiber sections with $\sigma_{x,y} = 7\%a_1$, R_b is equal to $140mm$, the correlation length d is equal to $100mm$ and $100km$ fiber length. In Fig.3.8, we plot in the upper figures the PDF of the singular values (λ_i) of \mathbf{H} . In Fig.3.8[(a),(c)], we observe three distributions which correspond to the three kinds of cores coexisting in the same structure, the third distribution in Fig.3.8(c) is overlapped in the

3. PERFORMANCE OF MULTI-CORE FIBER SYSTEMS IMPAIRED BY CDL

middle of the two distributions with low probability. The same observation in Fig.3.8(b) since we notice two distributions related to the two types of cores in the 12-core Hetero-MCF. The singular values in the 19-core Homo-MCF follow one distribution as shown in Fig.3.8(d). Then, the bottom figures compare the simulated and theoretical CDL by plotting the PDF of the CDL. We notice that the two distributions are in good agreement for all the structures.

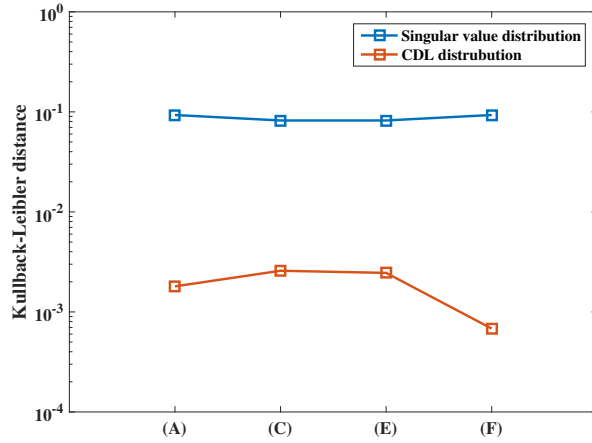


Figure 3.9: The Singular value and CDL distribution Kullback divergence structures: **(A)** 7-core Hetero-MCF, **(C)** 12-core Hetero-MCF, **(E)** 19-core Hetero-MCF and **(F)** 19-core Homo-MCF.

Further, in order to have statistical information about the fitting between the two probability distributions, we apply the Kullback–Leibler divergence that measures the difference between two distributions. For continuous random variables of two probability distributions P and Q , the Kullback is defined as [87]:

$$D_{KL}(P||Q) = \int_{-\infty}^{\infty} p(x) \log \frac{p(x)}{q(x)} dx \quad (3.25)$$

the divergence of 0 indicates that the two distributions exactly fit each other while the divergence of 1 indicates completely different behavior. We calculate the Kullback divergence for each MCF structure obtained in Fig.3.8. As shown in Fig. 3.9, the Kullback divergence of the singular value distributions is around 0.1, while for the CDL distribution, the divergence is around 0.01 which gives a complete validation of the accuracy of the proposed mathematical channel model.

3.3 Analytical Study of Multi-Core Fiber Performance

This section aims to analyze the performance of the MCF optical system by deriving an upper bound error probability based on the theoretical channel model obtained in the previous section. In this analysis, we apply two detection methods; the ML decoder and the ZF decoder. These two methods differ in performance and computational complexity. First, we begin our studies by deriving the error probability upper bound for the wireless channel. We then extend our analysis to reach the MCF optical transmission system and develop an upper bound expression for ML and ZF detections. We derive an upper bound error probability of the wireless channel based on the transmission channel. In this analysis, we assume a perfect channel state information (CSI) at the receiver side. The ML decoder estimates the transmitted symbols \hat{X} which are computed among the set of all possible symbols \mathcal{C} according to:

$$\hat{X}_{ML} = \underset{X \in \mathcal{C}}{\operatorname{argmin}} \|Y - \mathbf{H}X\|^2 \quad (3.26)$$

where $\|\cdot\|$ is the Frobenius Norm, the error probability of wrongly estimated X is given by:

$$\begin{aligned} Pr_{error} &= \Pr(\hat{X} \neq X) \\ &= \sum_{X \in \mathcal{C}} \Pr(X) \cdot \Pr(\hat{X} \neq X | X) \end{aligned} \quad (3.27)$$

by applying the union bound error probability, the upper bound on the error probability of all i.i.d. transmitted symbols are obtained as follow [88]:

$$Pr_{error} \leq \frac{1}{\operatorname{card}(\mathcal{C})} \sum_{\hat{X} \neq X} \Pr(X \rightarrow \hat{X}) \quad (3.28)$$

$\operatorname{card}(\mathcal{C})$ is the cardinality of \mathcal{C} and the pairwise error probability (PEP) where detecting \hat{X} given that X has been transmitted is $\Pr(X \rightarrow \hat{X})$. Given channel matrix \mathbf{H} , the PEP is given as [88]:

$$\Pr(X \rightarrow \hat{X}) = Q\left(\sqrt{\frac{\|\mathbf{H}(\hat{X} - X)\|^2}{2\sigma^2}}\right) \quad (3.29)$$

where Q is the tail function that can be expressed as:

$$Q(x) = \frac{1}{\sqrt{2\pi}} \int_x^\infty \exp\left(-\frac{t^2}{2}\right) dt \quad (3.30)$$

the $Q(x)$ can be upper bounded by using the Chernoff bound ($Q(x) \leq \frac{1}{2} \exp(-\frac{x^2}{2})$). Then, by averaging Eq. 3.29 over all channel realizations, we obtain:

$$\Pr(X \rightarrow \hat{X}) \leq \mathbb{E}_{\mathbf{H}} \left[\exp \left(\frac{-\|\mathbf{H}(\hat{X} - X)\|^2}{8\sigma^2} \right) \right] \quad (3.31)$$

3.3.1 Error probability upper bound of MCF optical system with ML decoder

In this part, we move forward to derive an upper bound error probability for MCF impacted by the CDL. First, we start by investigating the performance of the ML.

3.3.1.1 Maximum-likelihood Decoder

The ML decoders give the optimal BER performance. However, the MIMO decoding algorithm's primary challenge is to achieve the required performance with feasible decoding complexity. Several ML techniques can realize the optimal decoding, one is the exhaustive search for the transmitted signals which obtained by minimizing the quadratic Euclidean distance $\|Y - \mathbf{H}X\|^2$ over the set of all possible symbols. The computational complexity of this method depends on the constellation size and the MIMO dimension.

3.3.1.2 Derivation of error probability upper bound for ML decoder

The data symbols can be estimated at the receiver side by using the ML decoder. The optimal detection should satisfy the ML criteria in estimating the emitted vector \mathbf{X} as mentioned previously. The PEP where detecting \mathbf{X}_2 given that \mathbf{X}_1 has been transmitted and known the optical channel matrix \mathbf{H} obtained in section. 3.2 is:

$$\Pr\{\mathbf{X}_1 \rightarrow \mathbf{X}_2 | \mathbf{H}\} = \Pr\{\hat{\mathbf{X}} = \mathbf{X}_2 | \mathbf{X}_1, \mathbf{H}\} \quad (3.32)$$

$$\Pr\{\mathbf{X}_1 \rightarrow \mathbf{X}_2 | \mathbf{H}\} = Q \left(\frac{\ell \|\mathbf{H}\mathbf{X}_\Delta\|}{\sqrt{2N_0}} \right) \quad (3.33)$$

where $\mathbf{X}_\Delta = \mathbf{X}_2 - \mathbf{X}_1$. To obtain an upper bound of the error probability, the PEP is averaged over all the channel realizations. Replacing the matrix \mathbf{H} by the corresponding channel model ($\mathbf{H} = \mathbf{U}\Sigma\mathbf{V}^H$). Then, applying the permutation property of the trace with the fact that \mathbf{U} is a unitary matrix, Eq. 3.33 is given as:

$$\Pr\{\mathbf{X}_1 \rightarrow \mathbf{X}_2 | \mathbf{H}\} = Q \left(\sqrt{\frac{\ell \text{trace}(\Lambda \mathbf{V}^H \mathbf{X}_\Delta \mathbf{X}_\Delta^H \mathbf{V})}{2N_0}} \right) \quad (3.34)$$

Λ is a diagonal matrix with eigenvalues elements λ_i .

3.3 Analytical Study of Multi-Core Fiber Performance

At high SNR, the closest neighbors where the distance between them is equal to d_{min} (the minimum distance of the corresponding QAM constellation) are dominating the error probability. Moreover, for all the codewords differences in the closest neighbours set has $\mathbf{X}_{\Delta}^H \mathbf{X}_{\Delta} = d_{min}^2 \mathbf{I}_C$. Then, by developing the trace(.), the upper bound can be written as:

$$P_e \lesssim N_{min} Q \left(\sqrt{\frac{\ell d_{min}^2}{2N_0} \sum_i \sum_j \lambda_i |v_{i,j}|^2} \right) \quad (3.35)$$

where N_{min} is the kissing number. An upper bound of the above expression can be obtained by substituting each $\ell \lambda_i$ by the minimum over the maximum. In this case, the V factor is removed by applying the unitary property of V .

$$P_e \lesssim N_{min} Q \left(\sqrt{\frac{d_{min}^2}{2N_0} \frac{\min\{\lambda_i\}}{\max\{\lambda_i\}}} \right) \quad (3.36)$$

the previous expression can be developed by applying three scenarios as follow.

• First upper bound

One can directly substitute $\max\{\lambda_i\}$ and $\min\{\lambda_i\}$ by λ_{max} and λ_{min} , respectively:

$$P_e \lesssim N_{min} Q \left(\sqrt{\frac{d_{min}^2}{2N_0} \frac{\lambda_{min}}{\lambda_{max}}} \right) \quad (3.37)$$

$$P_e \lesssim N_{min} Q \left(\sqrt{\frac{d_{min}^2}{2N_0 \varepsilon}} \right) \quad (3.38)$$

here, we notice the Gaussian behavior of the MCF transmission performance directly with an SNR reduced by the CDL (ε).

• Second upper bound

To obtain tighter upper bound than the one in Eq. 3.38, we only substitute $\max\{\lambda_i\}$ by the practical λ_{max} , the expression in Eq. 3.35 can be rewritten as:

$$P_e \lesssim N_{min} E_X \left[Q \left(\sqrt{\frac{\gamma}{\lambda_{max}} X} \right) \right] \quad (3.39)$$

where $X = \min\{\lambda_i\}$ and γ is the SNR.

Substituting X by the PDF which is already defined in Eq. 3.18, the chernoff upper

bound is given as:

$$P_e \lesssim K \int_0^\infty e^{\frac{-\gamma}{2\lambda_{max}}x} \left[\operatorname{erfc}\left(\frac{x-\mu}{\sigma\sqrt{2\pi}}\right) \right]^{n-1} e^{-\left(\frac{x-\mu}{\sigma\sqrt{2\pi}}\right)^2} dx \quad (3.40)$$

with $K = \frac{CN_{min}}{\sigma\sqrt{2\pi}}$. The previous expression can be approximated knowing that the standard deviation of the eigenvalues of the MCF channel model is very small ($\sigma \ll 1$) [89]. Thus, $\operatorname{erfc}(\cdot)$ tends to 1 and Eq. 3.40 is given as:

$$P_e \lesssim K \int_0^\infty e^{\frac{-\gamma}{2\lambda_{max}}x} e^{-\left(\frac{x-\mu}{\sigma\sqrt{2\pi}}\right)^2} dx \quad (3.41)$$

$$P_e \lesssim N_{min}\beta \frac{\sqrt{\pi}\sigma}{2} e^{\frac{1}{4}a(a\sigma^2-4\mu)} \left[1 - \operatorname{erfc}\left(\frac{a^2-2\mu}{2\sigma}\right) \right] \quad (3.42)$$

with $a = \frac{\gamma}{2\lambda_{max}}$ and $\beta = \frac{C}{\sqrt{2\pi}}$.

• Third upper bound

In the last two upper bounds were approximated in order to obtain the upper bound error probabilities. Here, we give tighter upper bound by developing Eq. 3.40 without any approximation. $\operatorname{erfc}(z)$ can be upper bounded as $e^{(-\frac{z}{2})^2}$. Then, by completing the square after multiplying the three exponential terms, Eq.3.40 is expressed as:

$$P_e \lesssim K \int_0^\infty e^{\frac{-\gamma}{2\lambda_{max}}x} e^{-(C-1)\left(\frac{x-\mu}{\sigma\sqrt{2\pi}}\right)^2} e^{-\left(\frac{x-\mu}{\sigma\sqrt{2\pi}}\right)^2} dx \quad (3.43)$$

$$P_e \lesssim K \int_0^\infty e^{-C\left(\frac{x-\mu}{\sigma\sqrt{2\pi}}\right)^2 - \frac{\gamma}{2\lambda_{max}}x} dx \quad (3.44)$$

$$P_e = K e^{-\frac{\mu^2}{2\pi\sigma^2}} \left[\pi \sqrt{\frac{\sigma^2}{2C}} e^{-\frac{b}{4a}} \operatorname{erfc}\left(\frac{1}{2}\sqrt{\frac{b}{a}}\right) \right] \quad (3.45)$$

where $b = \frac{C\gamma}{\lambda_{max}}$ and $a = \frac{C}{2\pi\sigma^2}$.

In order to compare the three upper bounds, we present the system performance of ML detection through numerical simulations and compare them to the analytical upper bound expressions. We plot BER versus SNR for structure **A** (7-core Hetero-MCF) as shown in Fig. 3.10. A 16-QAM modulation is used at the transmitter and the MCF system is affected by the CDL level equal to 8dB. We notice that the first approach obtained in Eq. 3.37 is loose with 2.5dB penalty compare to the simulation result. In contrast, expression (3.42) with the applied approximation ($\sigma \ll 1$) gives a tighter upper

bound especially at high SNR. Finally, the last expression in Eq. 3.45 of the ML error probability upper bound is tight at low SNR and exact at high SNR.

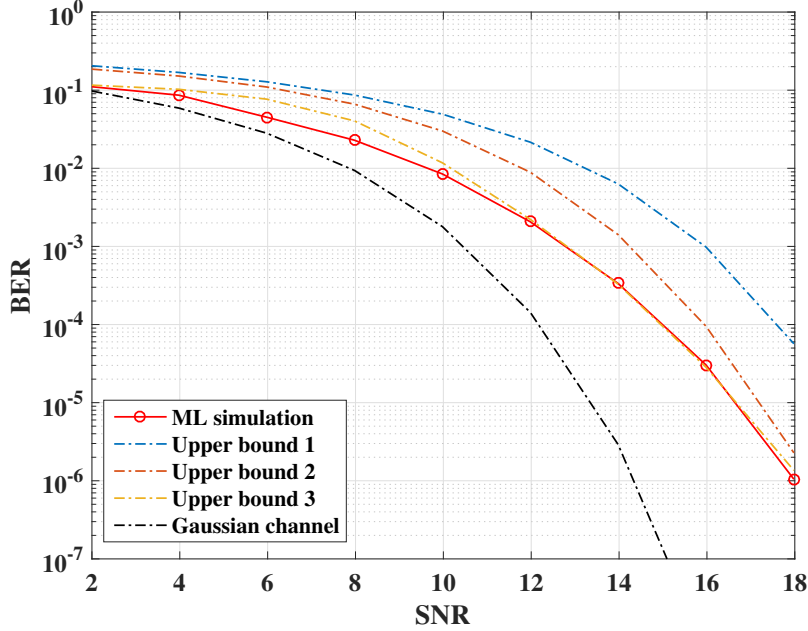


Figure 3.10: Simulation and analytical upper bound of ML detection for 7-core Hetero-MCF

3.3.2 Error probability upper bound of MCF Optical System with ZF Decoder

3.3.2.1 Zero-Forcing Decoder

In this section, we focus on the simplest sub-optimal decoders, which is the Zero-Forcing decoding [90]. This method aims to undo the crosstalk between the cores by multiplying the received signal Y by an equalization matrix generated by obtaining the pseudo-inverse of the channel matrix as follows:

$$\mathbf{H}^\dagger = (\mathbf{H}^H \mathbf{H})^{-1} \mathbf{H}^H \quad (3.46)$$

for square channels, the pseudo-inverse is simplified into the inverse of \mathbf{H}^{-1} . The received signal with ZF decoders can be expressed as:

$$Y_{ZF} = \mathbf{H}^{-1}(\mathbf{H}X + N) = X + \underbrace{\mathbf{H}^{-1}N}_{N'} \quad (3.47)$$

from the last expression, we notice that the ZF decoder performance depends on the noise vector N . The covariance matrix of the noise N is given by:

$$\begin{aligned}
 R_{N'} &= \mathbb{E}[N'N'^H] \\
 &= \mathbb{E}[\mathbf{H}^{-1}NN^H\mathbf{H}^{-H}] \\
 &= \mathbf{H}^{-1}\mathbb{E}[NN^T]\mathbf{H}^{-H} \\
 &= 2\sigma^2(\mathbf{H}^H\mathbf{H})^{-1}
 \end{aligned} \tag{3.48}$$

3.3.2.2 Derivation of Error probability upper bound for ML decoder

The Zero-Forcing decoder is the simplest linear decoder. The received signal \mathbf{Y} is multiplied by the channel pseudo-inverse to remove the crosstalk in all the channels. The post-detection SNR of the ZF detection is expressed as [88] [91]:

$$\gamma = \frac{\gamma_0}{[\mathbf{H}^H\mathbf{H}]_{ll}^{-1}} \tag{3.49}$$

where γ_0 is the normalized received SNR. From the definition of the optical channel matrix \mathbf{H} :

$$[\mathbf{H}^H\mathbf{H}]^{-1} = \ell^{-1}V\Lambda^{-1}V^H. \tag{3.50}$$

by substituting in Eq.(3.49):

$$\gamma = \frac{\gamma_0\ell}{\sum_{i=1}^C \lambda_i^{-1}|u_{il}|^2} \tag{3.51}$$

the error probability with the ZF decoder is bounded by $Q(\sqrt{\beta\gamma})$ where β depend on the constellation (q -QAM) [88] [91].

$$P_e \leq \mathbb{E}[Q(\sqrt{\beta\gamma})] \tag{3.52}$$

$$P_e \leq \mathbb{E}\left[Q\left(\sqrt{\frac{\ell \beta \gamma_0}{\sum_i \lambda_i^{-1}|u_{il}|^2}}\right)\right] \tag{3.53}$$

the expression can be simplified to obtain an upper bound of the error probability as:

$$\gamma = \frac{\ell \beta \gamma_0}{\sum_{i=1}^C \lambda_i^{-1}|u_{il}|^2} > \frac{\beta \gamma_0 \min\{\lambda_i\}}{\max\{\lambda_i\}} \tag{3.54}$$

with the same methodology as the previous section by substituting $\max\{\lambda_i\}$ by the practical λ_{max} and $X = \min\{\lambda_i\}$, the upper bound error probability of the ZF detection is given as:

$$P_e \leq \mathbb{E}_X \left[Q\left(\sqrt{\frac{\beta \gamma_0}{\lambda_{max}} X}\right) \right] \tag{3.55}$$

We notice that we end up with almost the same expression as the upper bound when using ML decoder. Thus, we develop the expectation with the same methodology in the previous section, which leads to:

$$P_e = M e^{-\frac{\mu^2}{2\pi\sigma^2}} \left[\pi \sqrt{\frac{\sigma^2}{2n}} e^{-\frac{b}{4a}} \operatorname{erfc} \left(\frac{1}{2} \sqrt{\frac{b}{a}} \right) \right] \quad (3.56)$$

with $M = \frac{C}{\sigma\sqrt{2\pi}}$, $b = \frac{C\gamma}{\lambda_{max}}$ and $a = \frac{C}{2\pi\sigma^2}$.

With the same simulation setup for the ML systems (subsection.3.3.1.1), we validate the expression obtained in Eq. 3.56 for the 7-core Hetero-MCF with ZF decoder at the receiver side. In Fig. 3.11, we notice that the error probability upper bound is in agreement with the ZF performance. However, we observe that the ZF decoder performance is worse than the ML decoder, which is evident from the high CDL value.

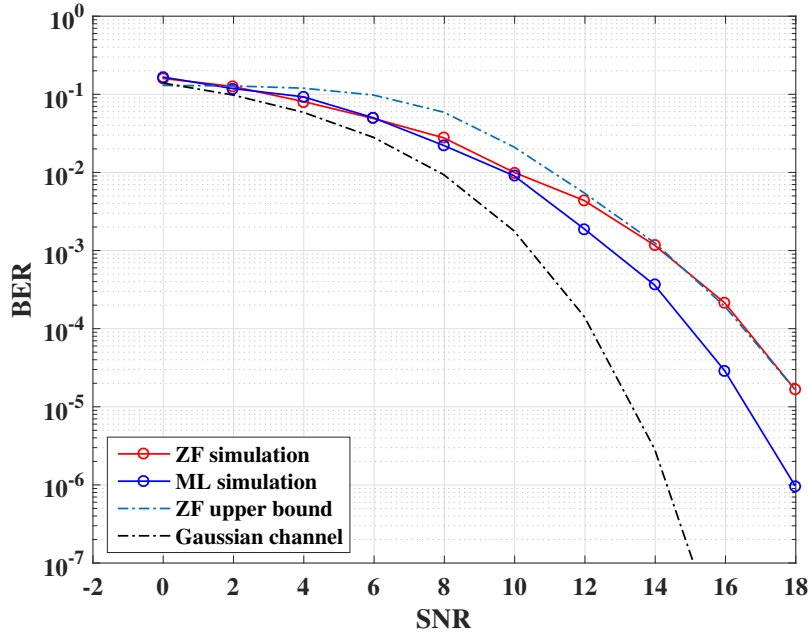


Figure 3.11: Simulation and analytical upper bound of ZF detection for 7-core Hetero-MCF

Summary

This chapter evaluated the transmission performance of the MCF, taking into consideration the impact of the CDL. We investigated the crosstalk and the misalignment channel matrices. We proposed a mathematical channel model in order to predict the CDL level function of the MCF system configurations. We proved that the proposed model gives

3. PERFORMANCE OF MULTI-CORE FIBER SYSTEMS IMPAIRED BY CDL

an accurate estimation of the CDL for several structures. Moreover, we derived an upper bound error probability by developing expressions for the optimal ML decoder and the sub-optimal ZF decoder. Based on our results obtained in this chapter concerning the channel model and the upper bound analysis. In the next chapter, we propose several optical and digital techniques to mitigate the CDL over the MCF transmission system.

Chapter 4

Core Scrambling Techniques for Multi-Core Fiber

The MCF system's performance is degraded in the presence of the CDL. In the previous chapter, we introduced the MCF channel model taking into account the crosstalk and the misalignment losses. We noticed that the level of the CDL depends mostly on the MCF structure. Therefore, we proposed a valid mathematical channel model for all the MCF structures and provided an accurate estimation of the CDL level. We ended up driving a numerical analysis of the error probability of the MCF systems which illustrates that ML decoders outperform the ZF decoders at the cost of high complexity at the receiver side. This chapter aims to provide an optical solution based on the core scrambling to reduce the CDL. Besides, solving the decoding complexity at the receiver side by proving that ML and ZF decoders perform the same thanks to the core scrambling.

This chapter starts by introducing the channel model after installing core scrambling in the transmission link. After, we propose three different deterministic scrambling strategies for different MCF structures related to the MCF profile geometry. These strategies proved their efficiency to mitigate the CDL. Afterward, we drive a theoretical channel model with the presence of the scrambling aiming to understand the performance behavior and to determine the optimal number of scramblers that should be installed in the transmission link. Finally, we investigate the performance of the ML and ZF decoders by driving upper bound error probability expressions for both decoders.

4.1 Performance Enhancement of MCF using Core Scrambling

The scrambling technique was previously investigated in order to reduce the MDL in MDM system [3]. The first use of the mode scrambling was to overcome the MMF frequency dependence on mode distribution [92] [93]. As shown in chapter. 3, the CDL impacts the MCF system performance, caused by the different losses that face the propagating signal in each core. In this section, we study the core scrambling (CS) as an optical method to mitigate the CDL so enhance the MCF system performance.

4.1.1 MCF Transmission Channel Model Including Core Scrambling

The core scrambling strategy is to install a core permutation after K_{scr} spans, as shown in Fig. 4.1. However, the received signal after transmission including the scrambling matrices is similar to Eq. 3.6 which is given by:

$$\mathbf{Y}_{C \times 1} = \sqrt{\ell} \prod_{k=1}^K (\mathbf{T}_k (\mathbf{H}_{XT})_k \mathbf{M}_k \mathbf{P}_k) \mathbf{X}_{C \times 1} + \mathbf{N}_{C \times 1} \quad (4.1)$$

\mathbf{P}_k are the permutation matrices that represent the scramblers when k is equal to the scrambling period K_{scr} and identity matrices in other cases. \mathbf{P}_k can be chosen either in a random or deterministic manner. The advantages and disadvantages of these two scrambling methods will be explained in the following subsections.

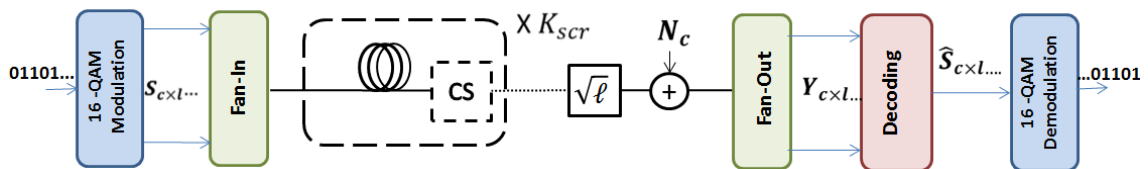


Figure 4.1: Multi-Core Fiber transmission system with random core scramblers

4.1.2 Core Scrambling Strategies

4.1.2.1 Random Core Scrambling

The core scrambling function is illustrated in Fig. 4.2. Assuming MCF with three different cores (black, red and blue), we send three messages in each core (S_1 , S_2 and S_3). Then, the scrambler is installed after K_{scr} and the signals are permuted randomly (random core scrambling) and transmitted through different cores. In this case, the signals face the average losses induced by all the cores. An example of \mathbf{P}_k in the case of random core

scrambling for 7-core MCF is represented as follows:

$$\mathbf{P}_k = \begin{pmatrix} 1 & 0 & 0 & 0 & 0 & 0 & 0 \\ 0 & 0 & 1 & 0 & 0 & 0 & 0 \\ 0 & 0 & 0 & 0 & 1 & 0 & 0 \\ 0 & 1 & 0 & 0 & 0 & 0 & 0 \\ 0 & 0 & 0 & 0 & 0 & 0 & 1 \\ 0 & 0 & 0 & 0 & 0 & 1 & 0 \\ 0 & 0 & 0 & 1 & 0 & 0 & 0 \end{pmatrix} \quad (4.2)$$

The permutation matrix changes randomly at each scrambling point. The effect of the scrambling is illustrated in Fig. 4.3, where we simulate 10^5 channel realizations of the 7-core Hetero-MCF configuration after we set the transverse offset to be equal to $7\%r_c$ and $K = 300$, we plot the PDF of the singular values of channel matrix with and without scrambling. In Fig.4.3(a), we notice three distributions which illustrate that the signals are affected by three different losses corresponding to the types of cores existing in the MCF. In Fig.4.3(b), we can observe the effect of the scrambling since all the cores follow single distribution after averaging the losses by using 15 random core scrambling.

In real optical transmission systems, the scrambling can be realized by applying the demultiplexing and multiplexing (DEMUX/MUX) devices to permute the signal, as shown in Fig. 4.4. However, installing a large number of random core scramblers in the transmission link is the main drawback to approach a sufficient CDL reduction. Thus, introducing a new strategy to solve this issue is needed.

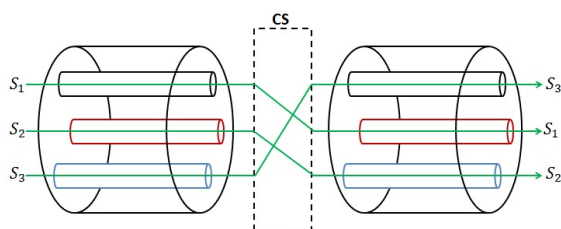


Figure 4.2: 7-core Hetero-MCF with corresponding core parameters

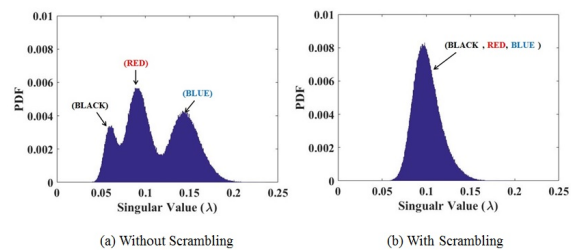


Figure 4.3: Simulated and theoretical channel model

4.1.2.2 Deterministic Core Scrambling

We propose the deterministic scrambling strategy to overcome the random core scrambling limitations. In that strategy, we ensure that in each scrambling period (K_{scr}) the permutation of the particular core should be with different core types. In this case, we allow the propagating signals to experience all the channel losses induced in the MCF system.

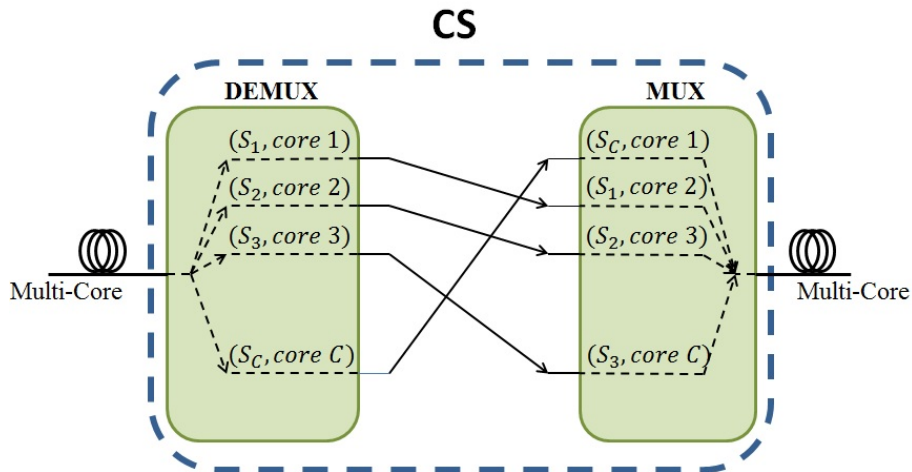


Figure 4.4: Core scrambling implementation using DEMUX/MUX

Moreover, switching from random to deterministic core scrambling makes the permutation matrices \mathbf{P}_k fixed after each K_{scr} as follows:

$$P_k = \begin{pmatrix} 0 & 1 & 0 & 0 & 0 & 0 & 0 \\ 0 & 0 & 1 & 0 & 0 & 0 & 0 \\ 0 & 0 & 0 & 1 & 0 & 0 & 0 \\ 0 & 0 & 0 & 0 & 1 & 0 & 0 \\ 0 & 0 & 0 & 0 & 0 & 1 & 0 \\ 0 & 0 & 0 & 0 & 0 & 0 & 1 \\ 1 & 0 & 0 & 0 & 0 & 0 & 0 \end{pmatrix} \quad (4.3)$$

the last matrix is an example of 7×7 matrix, which can be implemented for a higher dimension. However, we propose three similar functions of MCF structures.

• Snail Scrambling

The Snail scrambling is proposed for 7-core Hetero-MCF with three type of cores (structure **A** and **B**) as shown in Fig. 4.5(a). In this strategy, after small scrambling periods, all the signals will be affected by the losses induced by all the different core types, especially the central core, which has the worst performance among the other cores due to the large crosstalk impact comes from the neighboring cores. A comparison between the random and Snail scrambling is presented in Fig.4.6. We simulate 10^5 channel realizations and plot the average CDL of the channel function of the number of scramblers installed in the link where the number of sections $K = 300$. We notice that the CDL can be decreased to 2.5dB in structure **A** (7-core Hetero-MCF) by installing only 5 deterministic scramblers instead

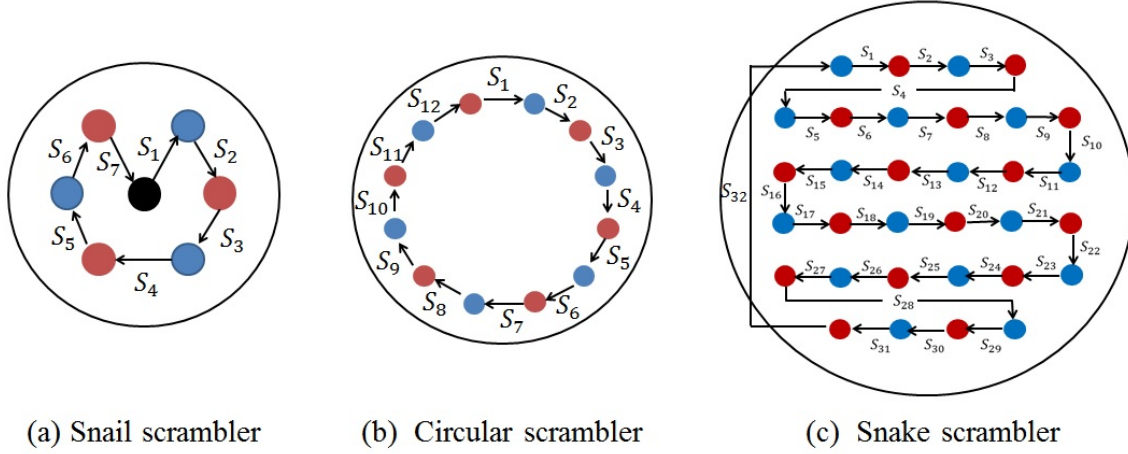


Figure 4.5: Deterministic scramblers strategies: (a) Snail scrambler, (b) Circular scrambler and (c) Snake scrambler

of 35 random scramblers. Further, we evaluate the performance of the Snail scrambling over the 7-core Hetero-MCF. In Fig.4.7, we plot the BER versus the SNR with the same transmission system configuration for the random core scrambling. We notice that the 7-core Hetero-MCF without scrambling has SNR penalty equal to 2dB at $\text{BER} = 10^{-3}$ compared to the Gaussian channel. Installing 5 Snail scramblers in the transmission link decreases SNR penalty to 0.5dB instead of 1dB by applying the random scramblers at $\text{BER} = 10^{-3}$.

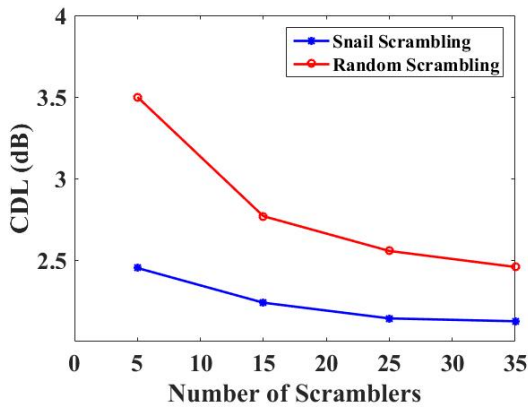


Figure 4.6: Comparison between the Snail scramblers and random scramblers with number of section equal to 300

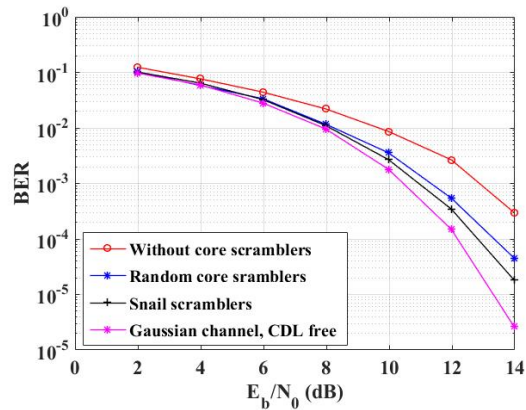


Figure 4.7: Snail scrambling System performance after applying 5 core scramblers.

• Circular Scrambling

We introduce the Circular scrambling for the 12-core Hetero-MCF with two different type of cores (structure **C** and **D**) as shown in Fig. 4.5. The no presence of the center core is the privilege of the ring structure, which makes the scrambling more effective in terms of CDL reduction. In Fig.4.8, we illustrate the performance of the Circular scramblers in the ring structure **C** (12-core Hetero-MCF). We notice that to decrease the CDL level almost to the minimum, which is equal to 0.4dB after installing only 5 deterministic scramblers. Fig.4.9 illustrates the Circular scrambling BER performance, we observe that installing 5 Circular scramblers for the 12-core Hetero-MCF mitigates the CDL completely from 2.5dB SNR penalty without scrambling and 1.5dB penalty with the random scrambling.

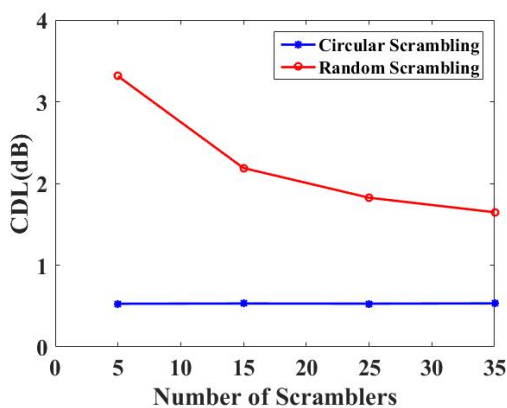


Figure 4.8: Comparison between the Circular scramblers and random scramblers with number of section equal to 300

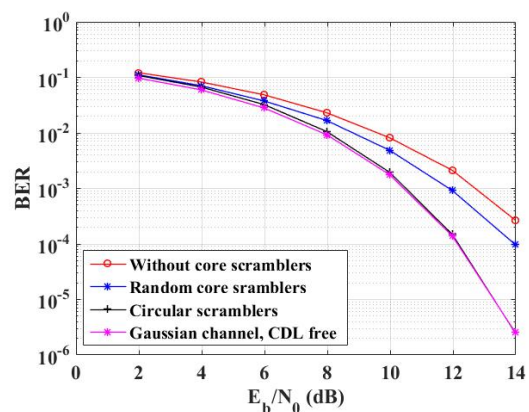


Figure 4.9: Circular scrambling System performance after applying 5 core scramblers.

• Snake Scrambling

Finally, the Snake scrambling is proposed for the 32-core Hetero-MCF with two different types of cores (structure **H**) as illustrated in Fig. 4.5. The existence of a large core number makes the random scrambling technique challenging to be implemented due to a large number of scrambling needed to be installed in the transmission link. In 32-core Hetero-MCF, we can decrease the number of scramblers from 35 random scramblers to 5 deterministic scramblers to obtain CDL equal to 1.8dB as shown in Fig.4.10. Moreover, Fig.4.11 illustrates the BER performance of the Snake scramblers for the 32-core Hetero-MCF, the system without scrambling has SNR penalty equal to 2.5dB at $BER = 10^{-4}$. However, installing the random scramblers decreases the penalty to 0.4dB while applying the Snake scramblers strategy reduces the SNR penalty to 0.1dB by utilizing only 5

scramblers. However, the optimal number of deterministic scramblers to be installed in the system should be determined. Therefore, obtaining the theoretical channel model with core scrambling is necessary to answer the question.

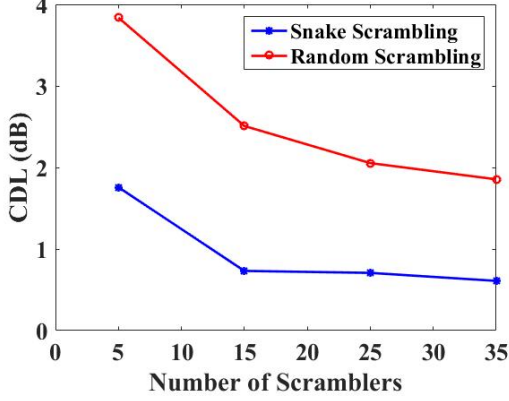


Figure 4.10: Comparison between the Snake scramblers and random scramblers with number of section equal to 300

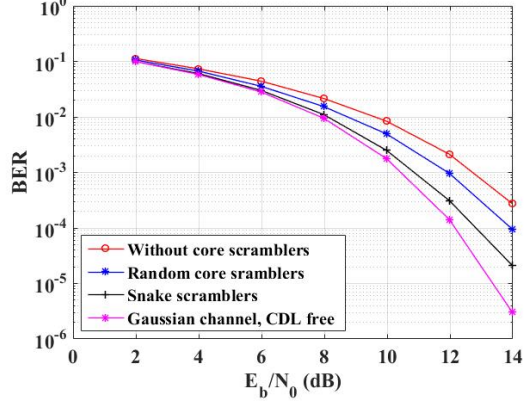


Figure 4.11: Snake scrambling System performance after applying 5 core scramblers.

4.2 Theoretical Analysis of MCF Channel with Scrambling

In the previous section, we introduced the core scrambling as a promising solution to mitigate the CDL in the MCF systems. One of the remaining questions is the optimal number of deterministic scramblers required to sufficiently reduce the CDL level. To reach the answer, we first introduce a theoretical channel model for the MCF transmission system with core scrambling. As in Chapter. 3, we model the MCF channel \mathbf{H} in Eq. 4.1 theoretically using the singular value decomposition ($\mathbf{H} = \mathbf{U}\Sigma\mathbf{V}^H$).

4.2.1 Analytical Derivation including the Scrambling

With the same methodology in section. 3.2, we start our derivation to obtain a theoretical channel model for MCF transmission system with deterministic core scrambling. The equivalent channel matrix \mathbf{H} in (4.1) with core scrambling is given as:

$$\mathbf{H} = \prod_{k=1}^K (\mathbf{T}_k(\mathbf{H}_{XT})_k \mathbf{M}_k \mathbf{P}_k) \quad (4.4)$$

by permuting the misalignment channel matrix \mathbf{M}_k after the multiplication of \mathbf{P}_k , we obtain:

$$\mathbf{H} = \prod_{k=1}^K (\mathbf{T}_k(\mathbf{H}_{XT})_k \mathbf{M}_{p,k}) \quad (4.5)$$

4. CORE SCRAMBLING TECHNIQUES FOR MULTI-CORE FIBER

where $\mathbf{M}_{p,k}$ is the matrix after the permutation. Then, we apply the **QR** decomposition with the same steps as in subsection. 3.2.1. The channel matrix \mathbf{H} can be expressed as:

$$\begin{aligned}\mathbf{H} &= \underbrace{\mathbf{T}_1(\mathbf{H}_{XT})_1\mathbf{M}_{p,1}}_{\mathbf{H}_{p,1}} \underbrace{\mathbf{T}_2(\mathbf{H}_{XT})_2\mathbf{M}_{p,2}}_{\mathbf{H}_{p,2}} \dots \underbrace{\mathbf{T}_k(\mathbf{H}_{XT})_k\mathbf{M}_{p,K}}_{\mathbf{H}_{p,k}} \\ &= \mathbf{Q}_{p,1}\mathbf{R}_{p,1}\mathbf{R}_{p,2}\dots\mathbf{R}_{p,K} = \mathbf{Q}_{p,1} \mathbf{R}_{p,eq}\end{aligned}\quad (4.6)$$

The product of $\mathbf{R}_{p,k}$ matrices is a random combination of all the misalignment loss values α existing in the system as a resulting of the permutation matrices. So, the diagonal value of the upper triangular $\mathbf{R}_{p,eq}$ is given as:

$$r_{p,i} = \left(\prod_{k=1}^{K_1} \alpha_1^k \times \dots \times \prod_{k=1}^{K_T} \alpha_T^k \right) \left(\sqrt{XT_i^2 + \sum_{j=1}^C XT_{i,j}^2} \right)^K \quad (4.7)$$

by neglecting $(\sum_{j=1}^C XT_{i,j}^2)$, the singular values with scrambling $(\lambda_{p,i})$ are equivalent to the diagonal value of the upper triangular matrix \mathbf{R}_{eq} :

$$\lambda_{p,i} = \underbrace{\left(\prod_{k=1}^{K_1} \alpha_1^k \times \dots \times \prod_{k=1}^{K_T} \alpha_T^k \right)}_{(\alpha_{p,i})_{total}} (XT_i)^K, \quad \text{where } i \neq j \quad (4.8)$$

$(\alpha_{p,i})_{total}$ is the total losses after the scrambling at the end of the link and it is given as:

$$(\alpha_{p,i})_{total} = \prod_{k=1}^{K_1} \alpha_1^k \times \dots \times \prod_{k=1}^{K_T} \alpha_T^k = \exp(Z_p), \quad (4.9)$$

$$Z_p = \underbrace{\left[-b_1 \sum_{k=1}^{K_1} (dx_{k,i}^2 + dy_{k,i}^2) \right]}_{X_1} \underbrace{\left[-b_2 \sum_{k=1}^{K_2} (dx_{k,i}^2 + dy_{k,i}^2) \right]}_{X_2} \dots \underbrace{\left[-b_T \sum_{k=1}^{K_T} (dx_{k,i}^2 + dy_{k,i}^2) \right]}_{X_T} \quad (4.10)$$

where T is the number of different type of cores. K_t is the number of sections correspond to each core type where $t \in [1, \dots, T]$. After applying the Central Limit Theorem on each term. X_t can be presented as normal distribution with mean $\mu_{X_t} = -2K_t b_t \sigma_{(x,y)_t}^2$ and variance $\sigma_{X_t}^2 = 4K_t b_t^2 \sigma_{(x,y)_t}^4$ which makes Z_p normally distributed with mean $\mu_z = \sum_{t=1}^T \mu_{X_t}$ and variance $\sigma_z^2 = \sum_{t=1}^T \sigma_{X_t}^2$. Thus, $(\alpha_{p,i})_{total} = \exp(Z_p)$ has a lognormal distribution with parameters:

$$\mu_{(\alpha_{p,i})_{total}} = \exp(\mu_z + \sigma_z^2/2) \quad (4.11)$$

$$\sigma_{(\alpha_{p,i})_{total}}^2 = (\exp(\sigma_z^2) - 1) * \mu_{(\alpha_{p,i})_{total}}^2 \quad (4.12)$$

Finally, $\lambda_{p,i}$ is lognormally distributed with mean $(XT_i)^K \mu_{(\alpha_{p,i})_{total}}$ and standard deviation $(XT_i)^{2K} \sigma_{(\alpha_{p,i})_{total}}^2$.

4.2.2 Number of Optimal Core Scrambling

Obtaining the optimal number of deterministic scramblers (S_{opt}) is achievable by using the proposed channel model in the previous section. S_{opt} occurs when all the cores almost have the same losses during the transmission so obtains the minimum CDL value. The calculation of S_{opt} differ from one structure to another. In general, S_{opt} is the number of steps in order to reach all the cores $S_{opt} = C - 1$, where C is the number of cores. The ring structures are considered as special cases where $S_{opt} = T/2$, T is the number of different types of cores. In Fig.4.12, we plot the CDL function of the number of core scramblers. We observe that $S_{opt} = 1$ for the 12-core Hetero-MCF since it has two type of cores ($T=2$). On the other side, the 7-core Hetero-MCF and 32-core Hetero-MCF respectively have $S_{opt} = 6$ and 31 which proved our formulas.

Achieving the optimal deterministic scrambling allows to obtain the K_t values in Eq.4.10 since the permutations are known in this case:

$$K_t = K \times w_t, \quad (4.13)$$

where $w_t = \frac{N_t}{C}$, N_t is the number of cores with the same type and C is the total number of cores.

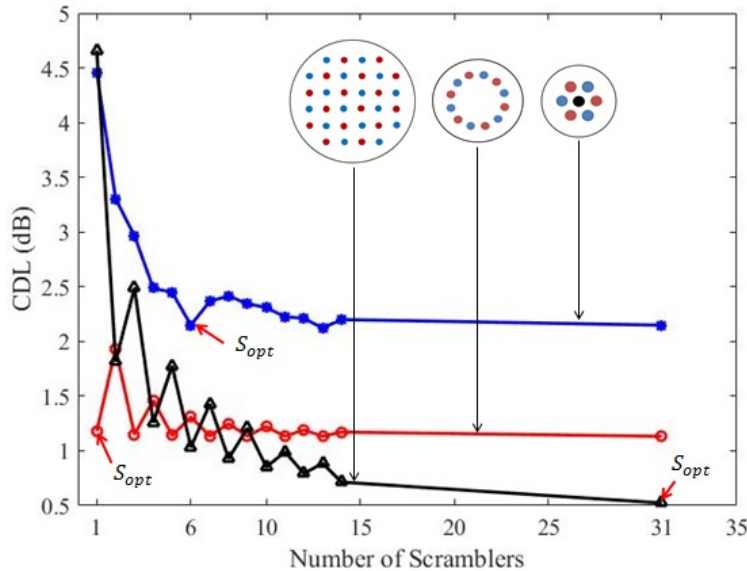


Figure 4.12: The CDL function of the number of deterministic scramblers

We compare the proposed theoretical channel model using deterministic core scrambling with the simulated results for MCF structures. By realizing 10^5 of the optical channel where $K = 300$ misaligned fiber sections with $\sigma_{x,y} = 7\%a_1$ and $100km$ fiber length. We apply Eq.4.13 for the two ring structures which leads to set both K_1 and K_2 to 150. In the case of the 7-core Hetero-MCF and 7-core Hetero-TA-MCF, we set the values of K_1 , K_2 to be equal to 150 and K_3 to 50. In Fig.4.13, we plot the PDF function of the singular value decomposition after the scrambling. We observe that the theoretical results fit the simulation with Kullback divergence around 0.01.

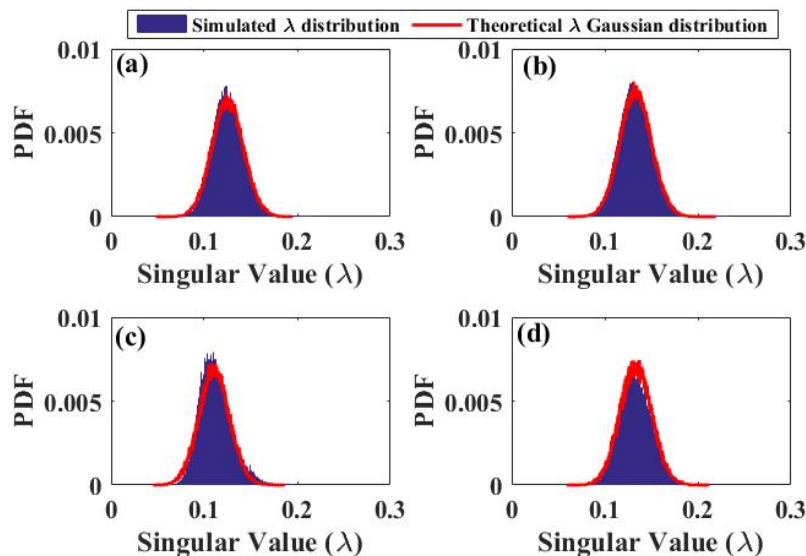


Figure 4.13: Simulated and Theoretical PDF of the singular value (λ) with Optimal deterministic scrambling for: (a) 12-core Hetero-MCF, (b) 12-core Hetero-TA-MCF, (c) 7-core Hetero-MCF and (d) 19-core Homo-MCF

4.3 Analytical Study of Multi-Core Fiber Performance with Core Scrambling

The core scrambling enhances the system performance by uniforming the different loss distributions over the different cores. We can estimate the CDL level for the MCF system with scrambling thanks to the proposed theoretical channel mode. However, the last step remains to evaluate the performance of the MCF channel analytically after introducing the core scrambling to the system. This section provides a numerical analysis of the error probability upper bound for the MCF system, including core scrambling and considering the ML and ZF decoders. From these expressions, we show that ML and ZF decoders have the same performance after installing the core scrambling in the transmission link.

4.3 Analytical Study of Multi-Core Fiber Performance with Core Scrambling

4.3.1 Error Probability Upper Bound of MCF System with Core Scrambling

We start by deriving an error probability upper bound of the MCF system for both ML and ZF decoders. Using the theoretical channel model obtained in section 4.2, we observed that the singular values have the same lognormal distribution, which simplifies the upper bound derivation significantly. We apply the first upper bound presented in section 3.3 by using the practical value of the maximum and minimum singular values.

4.3.1.1 Maximum-likelihood Decoder with Scrambling

We begin our derivation by the expression obtained in Eq. 3.35:

$$P_e \lesssim N_{min} Q \left(\sqrt{\frac{d_{min}^2 \min\{\lambda_i\}}{2N_0 \max\{\lambda_i\}}} \right) \quad (4.14)$$

Taking the privilege of the scrambling where all the cores have the same distribution, the CDL follows the same behaviour as homogeneous MCF. Therefore, we can define the PDF of the $\max\{\lambda_i\}$ and the $\min\{\lambda_i\}$ by Eq. 3.18 and Eq. 3.19, respectively. After that, we substitute the two values by the means illustrated in Eq. 3.20 and Eq. 3.21. Thus, the CDL ($\varepsilon = \max(\lambda_i)/\min(\lambda_i)$) is lognormally distributed and the upper bound is obtained by substituting the CDL by its mean $\frac{1}{\mu_\varepsilon}$ as follows:

$$P_e \lesssim N_{min} \mathbb{E}_\varepsilon \left[Q \left(\sqrt{\frac{d_{min}^2}{2N_0 \varepsilon}} \right) \right] \quad (4.15)$$

$$P_e \lesssim N_{min} Q \left(\sqrt{\frac{d_{min}^2}{2N_0 \mu_\varepsilon}} \right) \quad (4.16)$$

From the last expression, we observe that MCF optical channel with scrambling is similar to the Gaussian channel with an SNR reduction equal to μ_ε .

4.3.1.2 Zero Forcing Decoder with Scrambling

For the ZF decoder, the error probability of the ZF detection is given as:

$$P_e = \mathbb{E} \left[a Q \left(\sqrt{\frac{\ell \beta \gamma_0}{\sum_i \lambda_i^{-1} |u_{il}|^2}} \right) \right] \quad (4.17)$$

then, the upper bound can be simplified as:

$$\gamma_l = \frac{\ell \beta \gamma_0}{\sum_{i=1}^C \lambda_i^{-1} |u_{il}|^2} > \frac{\beta \gamma_0 \min\{\lambda_i\}}{\max\{\lambda_i\}} \quad (4.18)$$

4. CORE SCRAMBLING TECHNIQUES FOR MULTI-CORE FIBER

Finally, we define both $\min\{\lambda_i\}$ and $\max\{\lambda_i\}$ to obtain an upper bound error probability of the ZF detection which is given as:

$$P_e < a \mathbb{E} \left[Q \left(\sqrt{\frac{\beta \gamma_0}{\varepsilon}} \right) \right] \quad (4.19)$$

$$P_e < a Q \left(\sqrt{\frac{\beta \gamma_0}{\mu_\varepsilon}} \right) \quad (4.20)$$

We notice that the upper bound error probability of ML and ZF have the same expression (Eq.4.16 and Eq.4.20) which it is not the case for the MCF system without applying the core scrambling.

4.3.1.3 Simulation results of the Scrambling

To validate our observation, we evaluate the system performance of the ML and the ZF detection after applying the core scrambling by plotting the BER versus the SNR, as shown in Fig. 4.14. We apply the Snail scrambling with $K = 300$ fiber sections for 7-core Hetero-MCF. We notice that the ML and the ZF detection have the same performance with $\text{CDL} = 1.8\text{dB}$; this observation confirms our prediction through the theoretical expression obtained. In addition, the upper bound error probability of the ML and ZF (Eq.(4.16) and Eq.(4.20), respectively) show close estimation of the MCF system performance with the core scrambling, since the difference between the simulation and the upper bound is equal to 0.3dB at $\text{BER} = 10^{-4}$ (tight upper bound). We also notice that the gap between the ZF and the Gaussian channel is equal to 1.8dB.

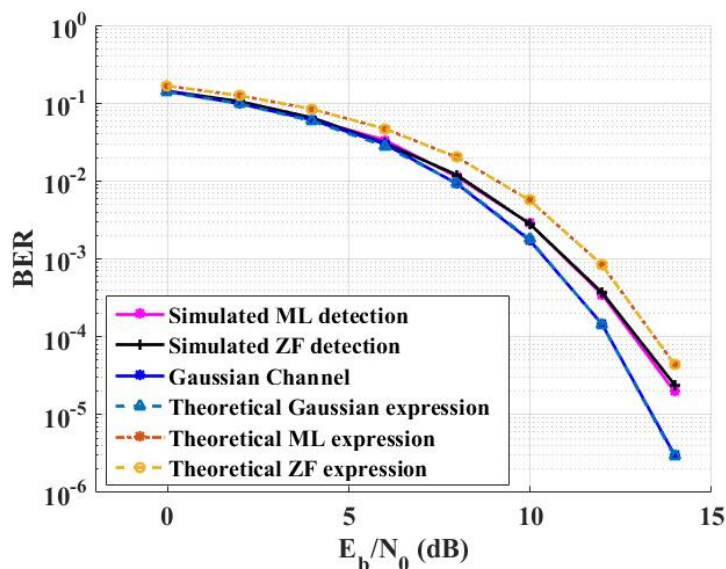


Figure 4.14: Simulation and theoretical upper bound of ML and ZF detection with core scrambling for 7-core Hetero-MCF, $\text{CDL} = 1.8\text{dB}$

Summery

This chapter proposed the core scrambling as an optical solution to enhance the MCF systems impaired by the CDL. We have shown that the core scrambling is very efficient in reducing the CDL in the MCF transmission system. Averaging the losses allows all the spatial channels to follow the single distribution. We introduced three deterministic techniques (Snail, Circular and Snake scrambling) to overcome the random scrambling limitations. Thanks to the theoretical channel model developed in this chapter, we obtained the optimal scrambling number installed in the link for maximum CDL reduction. Finally, we derived an upper bound error probability for the MCF system with the scrambling. We showed the advantage of the scrambling from these expressions since we can apply a sub-optimal decoder (ZF decoder), which offers very low complexity and the same performance as the ML decoder. The remaining chapters will be dedicated to the digital solutions for CDL mitigation also more investigation to obtain more gain and provide further enhancement to system performance.

Chapter 5

Pre-Compensation Technique for Multi-Core Fiber

Optical technique based on core scrambling strategies has been proposed in the previous chapter for CDL mitigation. Then, we obtained a theoretical channel model for the MCF system with core scrambling. We showed that the scrambling can reduce the complexity of the decoding since the ZF and the ML decoder have similar BER performance. Regardless of the performance enhancement obtained by the scrambling, yet the CDL is not completely mitigated. This chapter aims to introduce a digital technique to mitigate the CDL level on the system completely. Based on the mathematical channel model and inspired by the precoding in wireless communication, we propose a compensation technique called Zero Forcing (ZF) pre-compensation. The proposed solution does not require feedback link as wireless communication thanks to the mathematical channel model. The ZF pre-compensation shows an enhancement of the MCF transmission system performance and close to the Gaussian performance.

We start the chapter by reviewing some information and communication theory techniques. Then, we explain the difference between the open and closed loop systems. For each regime, we give the capacity expression based on the literature and the power allocation strategy proposed in the wireless communication domain. Then, we explain the ZF precoding technique's principle and end up by illustrating the challenges that interrupt the implementation of the ZF precoding concept in optical communication. Next, we propose the ZF pre-compensation as a digital CDL mitigation technique based on the theoretical MCF channel model. We prove that the ZF pre-compensation overcomes all the challenges in optical communication that face the ZF precoding. We also show that the proposed technique provides a low complex detection solution by utilizing the ZF decoder at the receiver side instead of the optimal ML decoder.

5.1 Capacity and Power Allocation in Wireless Communication

The power allocation given to each core can impact the capacity of the transmission system where the cores perform differently to each other. Therefore, applying a technique in order to adjust the power transmitted over each channel can be a solution for CDL mitigation in MCF system. In this section, we review some basic on the capacity of wireless communication and the power allocation strategies for two different communication systems.

5.1.1 Capacity of Communication Systems

In order to understand the fundamentals of communication systems, we need to review some information and communication theory principles given by Claude Shannon [94]. First, we consider a single-input-single-output (SISO) communication system. Then, we show the increasing throughput with the same bandwidth provided by MIMO systems.

5.1.1.1 SISO system

In [94], to estimate the maximum data rates, which can be transmitted with low error probability, we consider a general communication scheme, as shown in Fig. 5.1. A modulated symbols X are transmitted resulting from the mapped source sequence (message) given by the encoder. Caused by the channel, the symbols are changed from the originally transmitted symbols X . Then, the decoder retrieves the initial message. A confusable symbol means that the two symbols lead to the same output. Therefore, we can transmit a message into widely separated symbol sequences with a very low probability of error where the decoder can reconstruct the original source. The channel capacity of the previous system is defined by Shannon based on the mutual information between X and Y maximized over all the possible distributions of X as follows:

$$C = \max_{f(x)} I(X;Y) = \int_{A_X A_Y} f(x,y) \log \left(\frac{f(x,y)}{f(x) \cdot f(y)} \right) \quad (5.1)$$

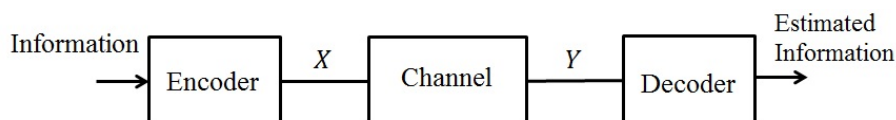


Figure 5.1: Communication channel including encoder and decoder

A_X and A_Y are the alphabet of the input symbols X and the output symbol Y , respectively. $f(\cdot)$ represents the PDF and $f(x, y)$ is the joint PDF of X and Y . In the case of AWGN channel, the achievable capacity is described with a well-known formula:

$$C = \log(1 + \gamma) \tag{5.2}$$

The previous expression represents the SISO Shannon capacity, which fixes the maximum amount of information that can be transmitted for a given AWGN channel. The Shannon coding theorem in [95] states that if one transmits information with a rate $R < C$, it is always possible to find an encoder such that the transmission error tends to zero when the transmitted sequence length tends to infinity. On the other side, no encoder allows transmission error-free given that the transmitted rate $R > C$.

5.1.1.2 MIMO system

Switching from point-to-point (SISO) to MIMO communication link brings diversity and multiplexing gain. Sending different copies of the same transmitted signal provides a better estimation of the transmitted signal after combining these copies. The capacity obtained from the maximum of the mutual information in Eq. 5.1 for Gaussian distributed inputs is given by [96]:

$$C = \log \det \left(I + \frac{P_t}{M} H Q_x H^\dagger \right) \tag{5.3}$$

P_t is the total power and $Q_x = \mathbb{E}\{X.X^\dagger\}$ is the covariance matrix of the input X . H is the wireless channel where it is equal to identity matrix for AWGN channel and the Rayleigh fading channel H consists of random complex Gaussian with zero mean and a unit variance elements.

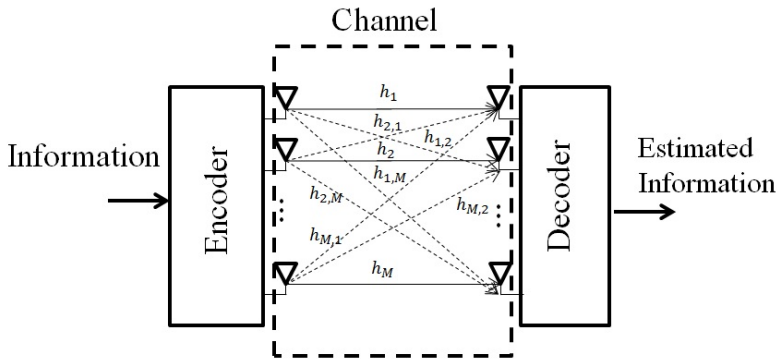


Figure 5.2: MIMO wireless system

5. PRE-COMPENSATION TECHNIQUE FOR MULTI-CORE FIBER

Noticeably, the last expression does not give any information about Q_x which represents the finite amount of power allocated strategy at the transmitter side as:

$$\text{Tr}(Q_x) = P_t \quad (5.4)$$

5.1.2 Open/Closed Loop Systems

This subsection illustrates the difference between the open and closed loop systems in the wireless channel. We highlight the advantages and disadvantages brought by each system, taking into account the power allocation provided for each regime.

5.1.2.1 Open Loop System

When the transmitter side does not know any information about the channel matrix properties known as channel state information (CSI), this system is referred to as an Open loop system, as shown in Fig. 5.3. Consequently, in the absence of the CSI the covariance Q_x in Eq. 5.3 is proven to be the identity matrix ($Q_x = I$). Thus, the capacity is represented as [97]:

$$C_{eq} = \sum_{i=1}^r \log \left(1 + \frac{P_t}{M} \frac{\lambda_i}{2\sigma^2} \right) \quad (5.5)$$

where $r \leq M$ is the rank of the channel matrix H and λ_i are the eigenvalues of HH^H . The capacity of the MIMO system is the sum of the capacity of r independent channels with gain equal to $\frac{\lambda_i}{2\sigma^2}$. The best power allocation for open loop system is to give the same amount of power in each transmitter ($\frac{P_t}{M}$) [97]. However, distributing the power equally on all the M paths provides a low-cost implementation since no algorithm is required. In contrast, it is not the best power allocation strategy since the paths face different propagation attenuation, which gives some paths better performance than others. Thus, the CSI at the transmitter is the solution to overcome this drawback.

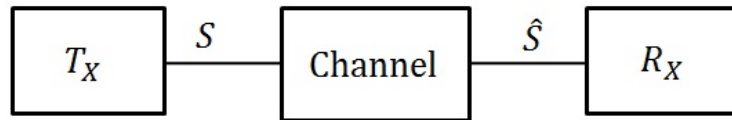


Figure 5.3: Open Loop System

5.1.2.2 Closed Loop System

The system with a feedback link from the receiver to the transmitter side is referred to as the closed loop system, shown in Fig. 5.4. The feedback link provides the transmitter with

the knowledge of the CSI; in this case, the covariance matrix Q_x is chosen to maximize the channel capacity with appropriate algorithms [98][99]. Some algorithms are applied to calculate the optimal powers, such as the waterfilling (WF) algorithm. Here, we give each path an unequal power and the capacity is represented as:

$$C_{CSI} = \sum_{i=1}^L \log \left(1 + p_i^* \frac{\lambda_i}{2\sigma^2} \right) \quad (5.6)$$

L is the number of spacial paths with a non zero power allocated by the WF algorithm. p_i^* is the optimal power allocated to each channel where $i \in [1, \dots, C]$ which is given by:

$$p_i^* = \mu - \frac{2\sigma^2}{\lambda_i} \quad (5.7)$$

The choice of μ is based on the power constraints of Eq. 5.4. However, the algorithm does not excite all the channels where other channels have zero power. The waterfilling obtains the optimal power of the channel by applying the singular value decomposition of the estimated channel matrix that comes from the feedback link ($H = U\Sigma V^H$). Then, the transmitter sends a correlated symbols vector $V.X$. Unfortunately, this technique enhances the transmission capacity at the cost of the complex implementation, as have been mentioned in M. Amhoud thesis[3]. In the next section, we will introduce a simpler technique and illustrate the challenging that faces the closed loop system in the optical communication system.

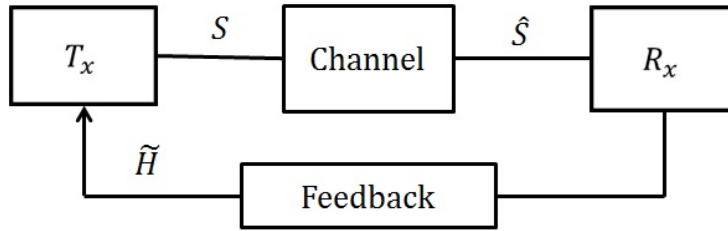


Figure 5.4: Closed Loop System

5.2 Zero-Forcing Precoding System

In wireless communication, the simplest modulation technique in order to equalize the different channels is the Zero-Forcing precoding [100]. In this technique, the transmitted vector signal is multiplied by the inversion of the estimated channel, as shown in Fig. 5.5.

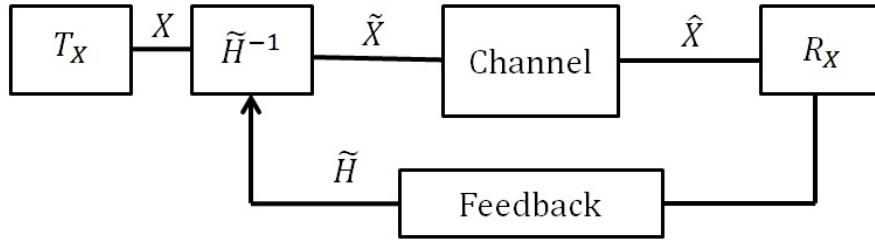


Figure 5.5: ZF precoding scheme

Considering a transmission scheme as:

$$Y = HX + N \quad (5.8)$$

where H is the wireless channel matrix. It's convenient to construct a normalized signal such as:

$$X = \frac{u}{\sqrt{\beta}} = \frac{u}{\|u\|^2} \quad (5.9)$$

where u is the unnormalized signal. With this normalization, X obeys $\|X\|^2 = 1$. In the case of ZF precoding, we transmit the inverse of the channel as:

$$\tilde{X} = H^H(HH^H)^{-1}.X \quad (5.10)$$

for square matrix, the inversion of the channel can easily be simplified as:

$$\tilde{X} = H^{-1}.X \quad (5.11)$$

Thus, the normalization constant can be rewritten as:

$$\beta = \|\tilde{X}\|^2 = X^H(HH^H)^{-1}.X \quad (5.12)$$

The normalization is necessary to satisfy the power constraints on wireless communication, leading to cost efficiency, unlike the optical communication that suffers from the non-linearity in the optical fiber.

5.2.1 ZF Precoding Challenges in Optical Systems

For MCF optical transmission system, we studied the impact of the CDL over the MCF transmission. As shown in the previous subsection, the best power allocation is to excite

all the cores with equal power where the capacity of unknown CSI for MCF is given as:

$$C_{MCF} = \sum_{i=1}^C \log\left(1 + \frac{p_t \lambda_i}{C 2\sigma^2}\right) \quad (5.13)$$

From the previous expression, we plot the average capacity for the 7-core Hetero-MCF and 19-core Hetero-MCF versus the SNR for misalignment level $\sigma_{x,y} = \{3\%, 7\%\}a_1$ as shown in Fig. 5.6. We observe that the capacity of the system increases with the increasing number of cores. Also, we notice the effect of the misalignment which induces more CDL in the system, so decrease the system capacity.

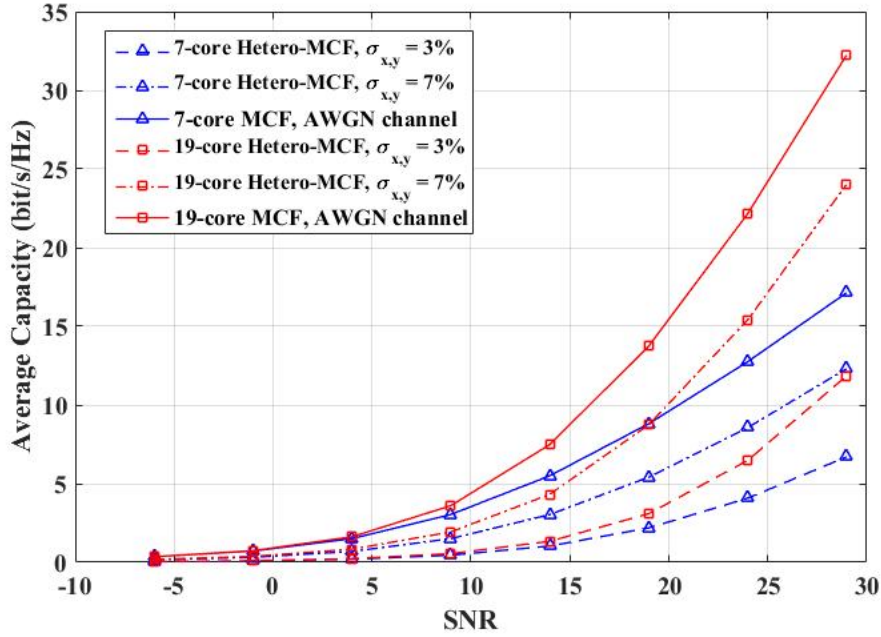


Figure 5.6: The average capacity versus the SNR for: the 7-core Hetero-MCF and 19-core Hetero-MCF with $\sigma_{x,y} = \{3\%, 7\%\}a_1$ and $K = 300$

Implementing channel equalization in the optical communication system is a challenge for ZF precoding. These challenges can be summarized in two main points:

- The accuracy of the CSI sent through the feedback link from the receiver depends on the coherence time of the channel. One condition is to transmit the equalized signal before the channel impulse response changes. In the optical system, the transmission distance is very long compared to the wireless communication system. Thus, applying channel equalization over the optical system without a feedback link solves the first issue.
- The average signal energy transmitted per symbol period and per channel core is E_0 . Thus, the total transmits energy across all cores is CE_0 per symbol. This definition

is different from the total power constraint often used in wireless MIMO, clear that due to the fiber nonlinearity the optical power per core is likely a more suitable parameter in fiber optics [101][102]. Therefore, the ZF precoded message should satisfy the optical fiber linear power constraints.

5.3 ZF Pre-compensation for MCF Transmission System

In order to address the challenges presented in optical communication, we propose a channel compensation solution based on the theoretical channel model obtained in chapter. 3 and the ZF precoding; This solution will be referred to as ZF pre-compensation. The MCF impaired by the CDL is modeled mathematically function of the MCF structure and the system configuration after performing the SVD as:

$$\mathbf{H} = \sqrt{\ell} \mathbf{U} \mathbf{\Sigma} \mathbf{V}^H \quad (5.14)$$

to recall, \mathbf{U} and \mathbf{V}^H are random unitary matrices and $\mathbf{\Sigma} = [\lambda_1, \dots, \lambda_C]$. ℓ is a normalization factor used to compensate the link loss. It has been proven that each λ_i follows lognormal distribution ($\text{lognorm}(\mu_{\lambda_i}, \sigma_{\lambda_i})$).

The strategy of the ZF pre-compensation consists of two steps:

1. At the transmitter side, we know the fiber structure and the transmission link properties. Consequently, we perform the MCF theoretical channel matrix of \mathbf{H} . Then, we determine the average singular value of each core as:

$$\bar{\mathbf{\Sigma}} = \begin{pmatrix} \bar{\lambda}_1 & & \\ & \ddots & \\ & & \bar{\lambda}_C \end{pmatrix} \quad (5.15)$$

where $\bar{\lambda}_i$ is the mean value of the singular value, $i \in [1, \dots, C]$. We define $\bar{\mathbf{H}}^{-1}$ as the inverse of the average theoretical channel model as:

$$\bar{\mathbf{H}}^{-1} = \mathbf{U}^H \begin{pmatrix} \bar{\lambda}_1^{-1} & & \\ & \ddots & \\ & & \bar{\lambda}_C^{-1} \end{pmatrix} \mathbf{V} \quad (5.16)$$

2. The transmitter applies the ZF precoding principle by multiplying the original transmitted vector \mathbf{X} by $\bar{\mathbf{H}}^{-1}$. Thus, the new codeword will be $\bar{\mathbf{X}} = \bar{\mathbf{H}}^{-1} \mathbf{X}$.

As shown in Fig. 5.7, the physical MCF channel model of the ZF pre-compensation

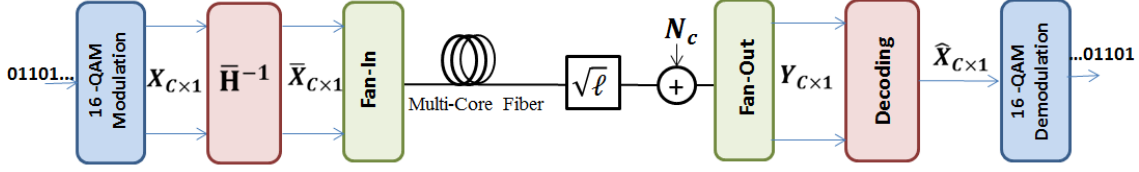
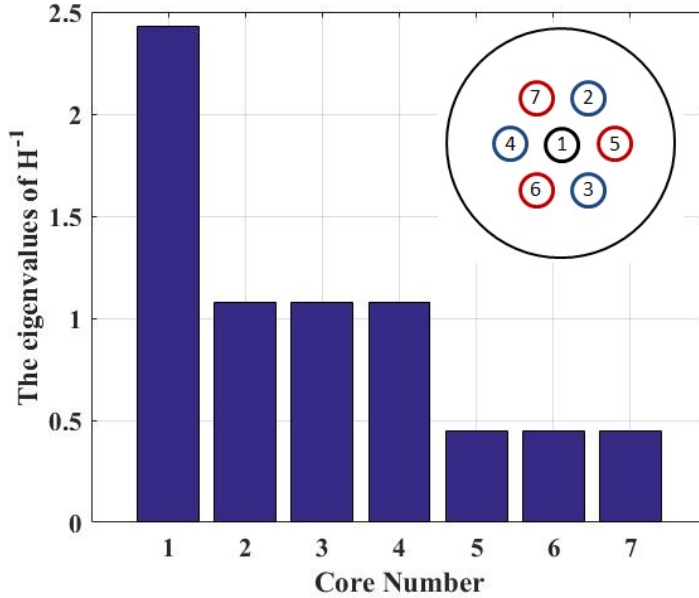


Figure 5.7: ZF pre-compensation MCF transmission system

transmission system is the same as Eq. 3.6, which is presented as:

$$\mathbf{Y}_{C \times 1} = \mathbf{H}_{C \times C} \bar{\mathbf{X}}_{C \times 1} + \mathbf{N}_{C \times 1} = \sqrt{\ell} \prod_{k=1}^K (T_k(H_{XT})_k M_k) \bar{\mathbf{X}}_{C \times 1} + \mathbf{N}_{C \times 1} \quad (5.17)$$

the only difference that we transmit the new codeword $\bar{\mathbf{X}} = \bar{\mathbf{H}}^{-1} \mathbf{X}$.


 Figure 5.8: $\bar{\mathbf{H}}^{-1}$ eigenvalues of the 7-core Hetero-MCF.

Let us investigate the performance of the ZF pre-compensation technique and see if the system satisfies the optical communication conditions and limitations. In Fig. 5.7, we can notice that the transmission system no longer needs the feedback link to have channel estimation. Instead, we obtain channel estimation from the theoretical MCF channel model that provides the transmitter by each core's power state. To address the second challenge, to ensure not exciting the fiber non-linearity, the total transmitted energy across all cores should be equal to CE_0 [101][102]. Thus, Fig. 5.8 illustrates the eigenvalues of the transmitted signal after the ZF pre-compensation for 7-core Hetero-MCF (Structure A) with $E_0 = 1$. We notice that the sum of the eigenvalues of $\bar{\mathbf{H}}^{-1}$ is equal to 7, which

5. PRE-COMPENSATION TECHNIQUE FOR MULTI-CORE FIBER

satisfies the linear regime constraints and solves the second challenge.

In order to validate the proposed ZF pre-compensation, we plot the BER versus the SNR for MCF with 100km long distance and 300 fiber sections ($K = 300$). A 16-QAM modulation is used at the transmitter and ZF decoder is applied at the receiver side. In Fig.5.9(a), we evaluate the 7-core Hetero-MCF performance with $\text{CDL} = 4.6\text{dB}$. We notice that the ZF pre-compensation enhances the system performance with SNR penalty equal to 0.6dB at $\text{BER} = 10^{-3}$ compared to the Gaussian channel and the gain obtained compare to the MCF without ZF pre-compensation is equal to 4dB . Moreover, Fig.5.9(b) shows the performance of the 12-core Hetero-MCF ring structure with $\text{CDL} = 2.5\text{dB}$. The system without the ZF pre-compensation has SNR penalty equal to 2.5dB compared to the Gaussian channel. However, we observe that we completely mitigate the CDL in the 12-core Hetero-MCF after applying the ZF pre-compensation. Besides, we provide a low complex detection solution while applying the ZF decoder and obtain performance very close to the Gaussian channel.

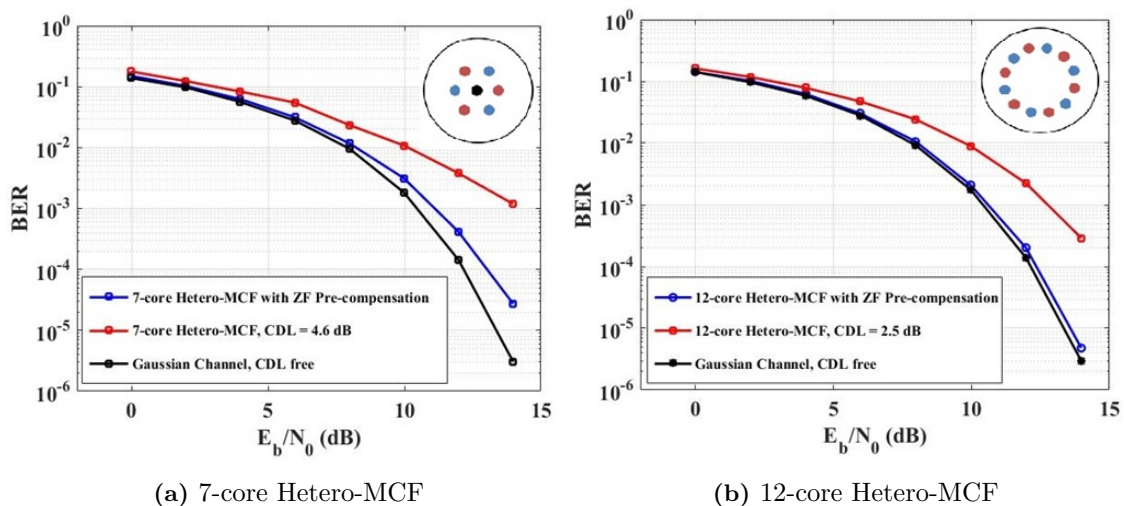


Figure 5.9: ZF pre-compensation MCF transmission system performance for: (a) 7-core Hetero-MCF and (b) 12-core Hetero-MCF

Summary

This chapter went through the capacity fundamental based on the information theory for the open loop system and the closed loop system. We illustrated the power allocation required for both regimes. We explained the ZF precoding challenges over optical communication. We proposed ZF pre-compensation for the MCF transmission system without using the feedback link. The idea is based on obtaining the mathematical MCF channel model using fiber structure and transmission link properties, in this case, we omit the

feedback link. We showed that the ZF pre-compensation enhances the performance of the MCF impaired by the CDL to be close to the Gaussian channel for {7 and 12}-core Hetero-MCF with applying the ZF decoder at the receiver side.

We observed that the CDL is not completely mitigated since we still have a 0.6dB penalty for 7-core Hetero-MCF. Therefore, for the next chapter, we are going to study an alternative digital solution to compensate for the remaining penalty by applying the space-time coding technique.

Chapter 6

Space-Time Coding for Multi-Core Fiber

The previous chapter provided a digital solution in order to mitigate the CDL that impacts the MCF performance. We proposed a ZF pre-compensation technique based on the theoretical MCF channel model and the ZF precoding principle which is applied in wireless communication. However, some configurations, such as the 7-core Hetero-MCF, still have SNR loss compared to the Gaussian channel performance. In this chapter, we study the efficiency of the space-time (ST) coding scheme over the MCF optical systems as an alternative digital solution aiming to improve the BER performance. In [30] [103], the ST codes have been already investigated in 2×2 MIMO for PDM systems impaired by the PDL. We also benefit from the ST codes to reduce the MDL on MDM systems-based FMFs for $M \times M$ MIMO configurations. Besides, the ST codes techniques have been validated experimentally for MDM with two modes and for the PDM systems [104] [105].

In the first section, we recall the ST coding technique and the upper bound error probability for the MIMO system in wireless communications. Then, we illustrate some design limitations and criteria to achieve a full rate ST codes for Rayleigh fading channel. After, we present some ST codes which have been used in the optical fiber communication system. For the second section, we introduce the ST codes to the MCF transmission systems while obtaining the error probability upper bound of the coded system after applying the ML decoder and the ZF decoder at the receiver side. Lastly, to address the decoder complexity issue for the coded system, we obtain the BER performance of the ZF decoder after applying the ST coding combined with the core scrambling techniques.

6.1 ST coding for wireless MIMO channels

The ST codes schemes have been proposed to utilize all the degrees of freedom existing in MIMO wireless systems. This coding technique provides a dependence between the spatial and temporal dimensions, so it increases the throughput and enhances the system performance. This section aims to present all the mathematical requirements and ST techniques to carry suitable tools for our study over the multi-core optical channel systems. We will highlight the main parameter affecting the coding gain brought by the ST codes in Rayleigh fading channel for further explanation and comparison to the optical channel. Then, we will discuss the decoding techniques and the ST codes in general and the ST coding family, which will be implemented in our study over the MCF transmission system.

6.1.1 ST coded for Rayleigh fading channels

For the Rayleigh fading channel matrix \mathbf{H} , we obtain the upper bound on the average PEP in Eq. 3.31 [88]:

$$\Pr(X \rightarrow \hat{X}) \leq \left(\prod_{k=1}^r \frac{1}{1 + \lambda_k \frac{SNR}{4}} \right)^{n_r} \quad (6.1)$$

where r is the rank of $\mathbf{E} = (\hat{X} - X)(\hat{X} - X)^H$. λ_k are the eigenvalues of \mathbf{E} . At high SNR the previous equation can be given as:

$$\Pr(X \rightarrow \hat{X}) \leq \left(\prod_{k=1}^r \lambda_k \right)^{-n_r} \left(\frac{SNR}{4} \right)^{-r \cdot n_k} \quad (6.2)$$

The error probability is function of n_r , λ_k and r which are respectively the number of receive antennas, the rank of \mathbf{E} and the eigenvalues of \mathbf{E} . λ_k and r depend on the transmitted codeword matrix and they define two criteria as presented in [106]:

- **Rank criteria:** the diversity gain is represented in the exponent $r \cdot n_k$ that provides the error probability asymptotic slope versus the SNR. However, achieving the full diversity of the MIMO system requires that $r = n_t$ where n_t is the number of transmitter antennas.
- **Determinant criteria:** we can rewrite Eq. 6.2 as:

$$\Pr(X \rightarrow \hat{X}) \leq \left[\left(\prod_{k=1}^r \lambda_k \right)^{-1/r} \left(\frac{SNR}{4} \right) \right]^{-r \cdot n_k} \quad (6.3)$$

first, the matrix should be full rank for all possible pairs of the codeword to achieve full diversity equal to $n_t n_r$. From Eq. 6.3, the product of the eigenvalues λ_k is

the determinant of the matrix \mathbf{E} which is the coding gain of the ST coded MIMO system. Thus, the coding gain is increased through maximizing the $\prod_{k=1}^r \lambda_k$ which is the minimum determinant of \mathbf{E} .

6.1.2 Space-Time Block Codes

In space-time block codes (STBC), the codeword matrix dimension is $n_t \times T$, where T is the time slots or channel uses (cu) to transmit one codeword. As an example of 2×2 STBC code is given as:

$$\mathbf{X}_{ST} = \begin{bmatrix} x_1(t_1) & x_1(t_2) \\ x_2(t_1) & x_2(t_2) \end{bmatrix} \quad (6.4)$$

$$= \begin{bmatrix} f_1(s_1 \dots N_s) & f_2(s_1 \dots N_s) \\ f_3(s_1 \dots N_s) & f_4(s_1 \dots N_s) \end{bmatrix} \quad (6.5)$$

The rate of the STBC is defined as:

$$r_{ST} = \frac{N_S}{T} \quad (\text{symbols/cu}) \quad (6.6)$$

N_S is the number of modulated symbols that are sent during T time slots. The STBC generates a supermatrix X_{ST} where the function f_k are linear combinations of the complex modulated symbols. Thus, we can define $n_t T \times N_S$ complex generator matrix G_c of the code by using a column-wise vectorization as:

$$\text{vec}_c(X_{ST}) = G_c S \quad (6.7)$$

$$\begin{bmatrix} x_{1,1} \\ x_{2,1} \\ \vdots \\ x_{n_t,T} \end{bmatrix} = G_c \begin{bmatrix} s_1 \\ s_2 \\ \vdots \\ s_{N_s} \end{bmatrix} \quad (6.8)$$

$\text{vec}_c(\cdot)$ is the vectorization of X_{ST} into complex vector of $n_t T \times 1$ dimension. Another representation of a STBC is also possible as:

$$\text{vec}_R(X_{ST}) = G_R S_R \quad (6.9)$$

$$\begin{bmatrix} Re(x_{1,1}) \\ Re(x_{2,1}) \\ \vdots \\ Im(x_{1,1}) \\ Im(x_{2,1}) \\ \vdots \end{bmatrix} = G_{\mathbb{R}} \begin{bmatrix} Re(s_1) \\ Re(s_2) \\ \vdots \\ Im(s_1) \\ Im(s_2) \\ \vdots \end{bmatrix} \quad (6.10)$$

where $G_{\mathbb{C}}$ is $2n_t T \times 2N_S$ generator matrix and is called a real linear code.

6.1.2.1 STBC of 2×2 MIMO channel

Several STBC constructions exist in literature, Table. 6.1 cover the most popular STBC families design for 2×2 MIMO channel with the corresponding achieved rate. Starting with the Alamouti code [107], the first design was for 2×1 MIMO systems, the code achieves a full diversity and rates 1 symbol/cu. In [108], the authors construct orthogonal ST codes for larger MIMO systems at the cost of limited rate of orthogonal codes to use transmitted antennas $n_t > 2$ the code rate is less than 1 symbol/cu. That leads us to the Golden code [109], it provides the best performance for the 2×2 MIMO Rayleigh fading channels. The Golden code transmits 4 symbols during 2 time slots which leads to rate equal to 2 symbols/cu. Finally, the Silver code [110], it has performance lower than the Golden code with the same proprieties; full diversity with a full rate for 2×2 MIMO Rayleigh fading channels. In contrast, the decoding complexity is reduced compared to the Golden code.

Table 6.1: STBC codes

STBC codes	symbol rate
Alamouti code [107]	1 symbols/cu
Silver code [108]	2 symbols/cu
Golden code [109]	2 symbols/cu
Orthogonal code [110]	≤ 1 symbols/cu

All the mentioned codes have been used to mitigate the MDL in the MDM system with two modes [3]. However, in our work, we focus on scalable STBC for any $n_t \times n_r$ MIMO system in order to be able to evaluate the performance over the MCF transmission system.

6.1.2.2 TAST codes

The minimum core multiplexing could be designed for MCF transmission is four cores (4-core MCF). At the same time, the orthogonal codes are limited in dimension and

rate. Threaded Algebraic Space-Time (TAST) codes exist for any $n_t \times n_r$ MIMO system with full rate and full diversity. This code family is known for its properties: placing each data symbol on the different core at each time slot while maintaining a minimum decoding delay. It has the same spectral efficiency as a spatially multiplexed system and uniform average energy is transmitted per spatial channel [111]. Therefore, our study focus on exploring the performance of the TAST codes over MCF systems. The TAST codes proposed by El-Gamal and Damen in [111] where it became well known for its generality, simplicity and performance. The threaded structure in general is shown in Fig. 6.1 for 3×3 TAST and 7×7 TAST code. To construct a TAST code, we need to generate a separate thread for full diversity achievement by multiplying q-QAM symbols by appropriate $n_t \times n_t$ rotation matrices. Then, to ensure a full diversity stacked threads, we threads are scaled by a set of algebraic numbers or transcendental numbers [111]. As a detailed example of the TAST code construction, we introduce the 7×7 TAST codeword matrix, as shown in Eq.6.11. Each x_i is a vector of 7 symbols where $i \in [1 : 7]$ and $\phi = \exp(j\pi/12)$. $f_\ell(x) = \sum_{k=1}^7 x_k (\psi^{\ell-1} \theta)^{k-1}$, where $\ell = [1, \dots, 7]$ with $\psi = \exp(j2\pi/7)$ and $\theta = \exp(j\pi/18)$. ϕ and θ are calculated based on the algebraic method in order to ensure the maximum coding gain [111].

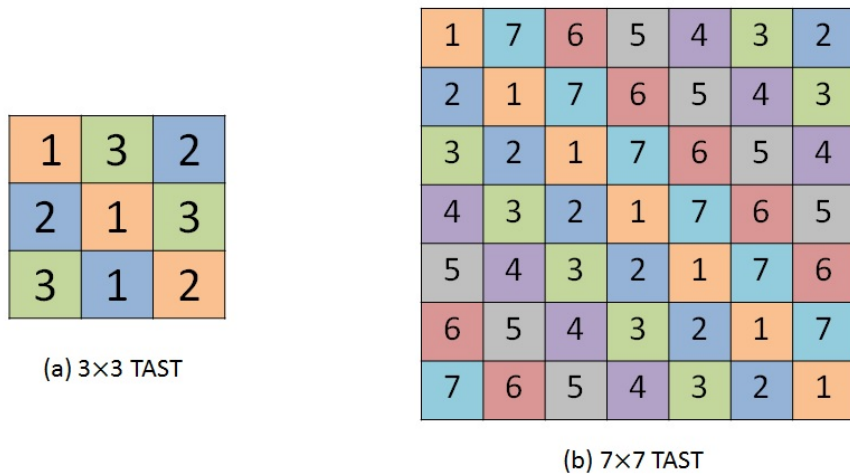


Figure 6.1: 3×3 TAST and 7×7 TAST architecture

$$X_T = \frac{1}{\sqrt{7}} \begin{bmatrix} f_1(x_1) & \phi^{\frac{6}{7}} f_2(x_7) & \phi^{\frac{5}{7}} f_3(x_6) & \phi^{\frac{4}{7}} f_4(x_5) & \phi^{\frac{3}{7}} f_5(x_4) & \phi^{\frac{2}{7}} f_6(x_3) & \phi^{\frac{1}{7}} f_7(x_2) \\ \phi^{\frac{1}{7}} f_1(x_2) & f_2(x_1) & \phi^{\frac{6}{7}} f_3(x_7) & \phi^{\frac{5}{7}} f_4(x_6) & \phi^{\frac{4}{7}} f_5(x_5) & \phi^{\frac{3}{7}} f_6(x_4) & \phi^{\frac{2}{7}} f_7(x_3) \\ \phi^{\frac{2}{7}} f_1(x_3) & \phi^{\frac{1}{7}} f_2(x_2) & f_3(x_1) & \phi^{\frac{6}{7}} f_4(x_7) & \phi^{\frac{5}{7}} f_5(x_6) & \phi^{\frac{4}{7}} f_6(x_5) & \phi^{\frac{3}{7}} f_7(x_4) \\ \phi^{\frac{3}{7}} f_1(x_4) & \phi^{\frac{2}{7}} f_2(x_3) & \phi^{\frac{1}{7}} f_3(x_2) & f_4(x_1) & \phi^{\frac{6}{7}} f_5(x_7) & \phi^{\frac{5}{7}} f_6(x_6) & \phi^{\frac{4}{7}} f_7(x_5) \\ \phi^{\frac{4}{7}} f_1(x_5) & \phi^{\frac{3}{7}} f_2(x_4) & \phi^{\frac{2}{7}} f_3(x_3) & \phi^{\frac{1}{7}} f_4(x_2) & f_5(x_1) & \phi^{\frac{6}{7}} f_6(x_7) & \phi^{\frac{5}{7}} f_7(x_6) \\ \phi^{\frac{5}{7}} f_1(x_6) & \phi^{\frac{4}{7}} f_2(x_5) & \phi^{\frac{3}{7}} f_3(x_4) & \phi^{\frac{2}{7}} f_4(x_3) & \phi^{\frac{1}{7}} f_5(x_2) & f_6(x_1) & \phi^{\frac{6}{7}} f_7(x_7) \\ \phi^{\frac{6}{7}} f_1(x_7) & \phi^{\frac{5}{7}} f_2(x_6) & \phi^{\frac{4}{7}} f_3(x_5) & \phi^{\frac{3}{7}} f_4(x_4) & \phi^{\frac{2}{7}} f_5(x_3) & \phi^{\frac{1}{7}} f_6(x_2) & f_7(x_1) \end{bmatrix} \quad (6.11)$$

6.1.2.3 STBC decoding

The ML decoding criteria is already explored in (Eq. 3.26, Chapter. 3) where the decoder search for the transmitted codeword is done by minimizing the quadratic Euclidean distance $\|Y - HX\|^2$ over all possible codewords. However, in the case of the STBC, column-wise vectorized form of Eq.5.8 is used containing the generator matrix of the ST codes as follows:

$$Y_{n_t T \times 1} = \text{vec}(Y) = \text{vec}(HX + N) \quad (6.12)$$

$$Y_{n_t T \times 1} = \begin{bmatrix} H & 0 & 0 \\ 0 & \ddots & 0 \\ 0 & 0 & H \end{bmatrix} \text{vec}(X) + \text{vec}(N) \quad (6.13)$$

$$\begin{aligned} &= H'_{n_r \times n_t} G_e S_{n_t T, 1} + N'_{n_t T \times T} \\ &= H_{eq} S_{n_t T, 1} + N'_{n_t T \times T} \end{aligned} \quad (6.14)$$

where G_e is the generator matrix of the ST code and identity matrix in the case of the uncoded system. $S_{n_t T, 1} = [s_1, \dots, s_{n_t T}]^T$ is the vector of transmitted modulated symbols.

6.1.2.4 Sphere decoder

The exhaustive search is unfeasible for real implementation for large MIMO systems. Therefore, another approach called the sphere decoder (SD) is applied by Viterbo *et al.* [83]. SD algorithm searches for the closest point in a finite sphere centered on the received point for the uncoded and coded system. One of the important parameters to reduce the algorithm complexity is the sphere radius (r_{SD}). r_{SD} is chosen function of the noise power and channel eigenvalues as follows:

$$r_{SD} = \min(\min\{\lambda_1, \dots, \lambda_{2C}\}, 4C^2) \quad (6.15)$$

the sphere decoder's searching algorithm is independent of the constellation size while reducing the computational complexity tremendously.

6.2 ST coding for MCF system impaired by CDL

In this section, we introduce the MCF system model with ST codes. Then, we study the benefits of the ST codes by deriving an upper bound error probability while applying the ML and ZF decoders at the receiver side. Finally, we extend our work by proposing a low complex solution by combining the ST codes with core scrambling to obtain performance close to the Gaussian channel and apply the sub-optimal ZF decoder.

6.2.1 Error probability of ST coded over MCF optical system

In the MCF system, we benefit from the space and time by sending multiple copies of independent q -QAM symbols in several cores at different time slots. At the receiver side, we can detect these copies and enhance the estimation of the data since it experiences the different MCF channel state. As shown in Fig. 6.2, the MIMO transmission system with ST code might be described by:

$$\mathbf{Y}_{C \times T} = \mathbf{H}_{C \times C} \mathbf{X}_{C \times T} + \mathbf{N}_{C \times T} \quad (6.16)$$

$$\mathbf{H} = \sqrt{\ell} \prod_{k=1}^K (\mathbf{T}_k (\mathbf{H}_{\mathbf{X}\mathbf{T}})_k \mathbf{M}_k) \quad (6.17)$$

where $\mathbf{X}_{C \times T}$ and $\mathbf{Y}_{C \times T}$ are respectively the transmitted and the received vectors with dimension C and $T = C$ for coded system or $T = 1$ for the uncoded system. We consider STBC category where linear combinations of q -QAM symbols are created before sending them on C cores and T time slots. We apply a threaded TAST code. In our study, we focus on the 7×7 TAST codeword matrix in Eq. 6.11 for 7-core Hetero-MCF (structure **A**). In each codeword, we send M symbols on 7 time slots where $M=CT$; in the case of 7×7 TAST code $M= 49$ symbols which means that the maximum rate is achieved and equal to 7 symbols/cu. Moreover, the coding matrix does not increase the energy of the transmitted symbols after the encoding which satisfies the linear regime of fiber optics.

6.2.1.1 ML decoder

In this part, we analyze the optimal maximum-likelihood (ML) decoder performance over coded MCF transmission system impaired by the CDL. We follow the same derivation method in (subsection. 3.3.1, Chapter. 3). In this case, we observe the effect of the ST

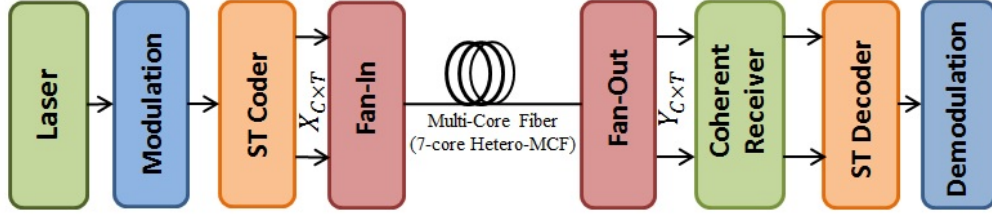


Figure 6.2: Space-Time coded MCF transmission system

codes on the BER performance. The data symbols estimation using the ML decoder should satisfy the optimal detection criteria as follows:

$$\hat{X}_{ML} = \underset{X \in \mathcal{C}'}{\operatorname{argmin}} \|\mathbf{Y}_{M,1} - \mathbf{H}_{eq} \mathbf{X}_{M,1}\|^2 \quad (6.18)$$

where \mathcal{C}' is the set of all possible transmitted codewords. Starting from (Eq. 3.33, Chapter. 3) which describes the pairwise error probability (PEP) where detecting \mathbf{X}_2 given that \mathbf{X}_1 has been transmitted:

$$P_e \lesssim N_{min} Q\left(\frac{\ell \|\mathbf{H} \mathbf{X}_\Delta\|}{\sqrt{2N_0}}\right) \quad (6.19)$$

$$P_e \lesssim N_{min} Q\left(\sqrt{\frac{\ell \operatorname{trace}(\mathbf{H} \mathbf{X}_\Delta \mathbf{X}_\Delta^H \mathbf{H}^H)}{2N_0}}\right) \quad (6.20)$$

For uncoded system (no coding, **NC**), there are $N_{min} = CN_{min}(QAM)$ words at minimum distance d_{min} , where $N_{min}(QAM)$ is the number of closest neighbours in the QAM constellation. In the case of $C \times C$ TAST coded system, there are $N_{min} = C^2 N_{min}(QAM)$ codewords at minimum distance d_{min} which has been proven in [112]. Moreover, for all the codewords differences in the closest neighbours set has $\mathbf{X}_\Delta^H \mathbf{X}_\Delta = d_{min}^2 \mathbf{I}_C$ [112]. As a simple example, we apply 4- QAM constellation ($N_{min}(QAM)=2$), each codeword has $N_{min}=7 \times 2$ closest neighbours at minimum distance d_{min} . After replacing the matrix \mathbf{H} by the corresponding channel model in Eq. 5.14. Also, applying the permutation property of the trace, Eq.6.20 is given as:

$$P_e \lesssim C^2 N_{min}(QAM) Q\left(\sqrt{\frac{\ell d_{min}^2}{2N_0} \sum_i \sum_j \lambda_i |v_{i,j}|^2}\right) \quad (6.21)$$

By having orthogonal closest neighbors λ_i , the double sum can be separated so the

expression can be rewritten as:

$$P_e \lesssim C^2 N_{min}(QAM) Q \left(\sqrt{\frac{\ell d_{min}^2}{2N_0} \sum_i \lambda_i \sum_j |v_{i,j}|^2} \right) \quad (6.22)$$

Then, ℓ can be substituted by its value ($\ell = \frac{C}{\sum_{i=1}^C \lambda_i}$) and the summation squared elements of the unitary matrix V is equal to 1. Thus, the upper bound expression in Eq. 6.22 is given as:

$$P_e \lesssim C^2 N_{min}(QAM) Q \left(\sqrt{\frac{d_{min}^2 \gamma}{2}} \right) \quad (6.23)$$

From the previous expression, the CDL can be mitigated. It shows that when the closest codeword neighbors are dominant in PEP analysis, the TAST codes mitigate the CDL and obtain C Gaussian parallel channels. The last expression shows that the MCF optical channel with TAST code is similar to the Gaussian channel, which is entirely different from the wireless MIMO channel following the Rayleigh channel model.

6.2.1.2 ZF decoder

In order to obtain an upper bound expression for the ZF decoder over the MCF transmission system, we can describe the coded MCF channel model as given in [112]:

$$\tilde{\mathbf{H}} \triangleq \text{diag}(\mathbf{H}, \dots, \mathbf{H}) \Phi \quad (6.24)$$

where Φ is the global $C^2 \times C^2$ unitary matrix [112]. As an example of TAST coded 2×2 MIMO system ($C = 2$):

$$\Phi = \frac{1}{\sqrt{2}} \begin{pmatrix} 1 & \theta & 0 & 0 \\ 1 & 0 & 1 & \theta \\ 0 & 0 & \theta & -\theta^2 \\ 1 & -\theta & 0 & 0 \end{pmatrix} \quad (6.25)$$

Then, the post-detection SNR can be rewritten as:

$$\gamma = \frac{\gamma_0}{[\tilde{\mathbf{H}}^H \tilde{\mathbf{H}}]_{ll}^{-1}} \quad (6.26)$$

hence, $\tilde{\mathbf{H}}^H \tilde{\mathbf{H}} = \Phi^H \text{diag}(\mathbf{H}^H \mathbf{H}, \dots, \mathbf{H}^H \mathbf{H}) \Phi$, we obtain:

$$\begin{aligned} (\tilde{\mathbf{H}}^H \tilde{\mathbf{H}})^{-1} &= \frac{1}{\ell} \Phi^H \text{diag}(\mathbf{V}^H \mathbf{\Lambda}^{-1} \mathbf{V}, \dots, \mathbf{V}^H \mathbf{\Lambda}^{-1} \mathbf{V}) \Phi \\ &= \frac{1}{\ell} \mathbf{\Psi}^H \text{diag}(\mathbf{\Lambda}^{-1}, \dots, \mathbf{\Lambda}^{-1}) \mathbf{\Psi} \end{aligned} \quad (6.27)$$

6. SPACE-TIME CODING FOR MULTI-CORE FIBER

where $\Psi \triangleq \text{diag}(\mathbf{U}, \dots, \mathbf{U})\Phi$ is a unitary matrix. Thus, Eq. 6.26 can be expressed as:

$$\gamma = \frac{\gamma_0 \ell}{\sum_{k=1}^C \lambda_k \sum_{i=1}^C \lambda_i^{-1}} \quad (6.28)$$

the previous equation is described as the ratio between the harmonic and the arithmetic means of λ_i . Also, we notice the effect of the TAST code by averaging the \mathbf{V} from the post-detection SNR equation.

In fact, this ratio can be simplified by the orthogonality defect factor (ODF) of $\tilde{\mathbf{H}}$ [112] which is defined as:

$$\delta(\tilde{\mathbf{H}}) \triangleq \frac{\prod_{i=1}^C \|\tilde{h}_i\|}{|\tilde{\mathbf{H}}|} \geq 1 \quad (6.29)$$

when the ODF is equal to one means that the channel $\tilde{\mathbf{H}}$ is orthogonal where the norm of $\tilde{\mathbf{H}}$ can be defined as [112]:

$$|\tilde{\mathbf{H}}| = \sqrt{\ell^{C^2}} |\mathbf{H}|^C |\Phi| = \sqrt{\ell^{C^2}} |\Lambda|^{C/2} |\mathbf{V}|^C = \sqrt{\ell^{C^2}} \prod_{i=1}^C \lambda_i^{C/2} \quad (6.30)$$

from, Eq. 6.29 and Eq. 6.30, the authors in [112] proved that the ODF of $\tilde{\mathbf{H}}$ for $C \times C$ TAST code is given by:

$$\delta = \frac{(\sum_{i=1}^C \lambda_i / C)^{\frac{C^2}{2}}}{\prod_{i=1}^C \lambda_i^{\frac{C}{2}}} \quad (6.31)$$

which could be expressed as the TAST ODF of the $\frac{C^2}{2}$ -th power of the ratio between the arithmetic and the geometric means of λ_i . The error probability with the ZF decoder is given by a $Q(\sqrt{\beta\gamma})$ where a and β depend on the constellation (q -QAM) [88] [91]:

$$\begin{aligned} P_e &= \mathbb{E} \left[a Q(\sqrt{\beta\gamma}) \right] \\ &= \mathbb{E}_\delta \left[a Q\left(\sqrt{\frac{\ell\beta\gamma_0}{\sum_{k=1}^C \lambda_k \sum_{i=1}^C \lambda_i^{-1}}}}\right) \right] \\ &= \mathbb{E}_\delta \left[a Q\left(\sqrt{\frac{\beta\gamma_0}{\delta}}\right) \right] \end{aligned} \quad (6.32)$$

One can use the maximum of the ODF to give a simple upper bound of the ZF coded system:

$$P_e \lesssim a Q\left(\sqrt{\frac{\beta\gamma_0}{\delta_{max}}}\right) \quad (6.33)$$

from the last expression, we note that the ZF performance depends on the ODF for the coded system. Hence, the ZF decoder has an optimal performance when the ODF is equal to 1 through the orthogonality of the channel matrix.

We simulate the 7×7 TAST code performance for the 7-core Hetero-MCF after applying both ML and ZF decoders. In Fig.6.3, we plot the BER function of the SNR for the coding scheme, we consider 300 fiber sections ($K = 300$) with $\sigma_{x,y} = 7\%a_1$ and 100km fiber length. The uncoded system has SNR penalty equal to 3dB with $CDL = 8$ dB at $BER = 10^{-4}$. We observe that the CDL is completely mitigated using the ML decoder since the performance is the same as the Gaussian channel ($CDL = zero$). On the other side, we notice that the ZF decoder performs worse than the ML decoder. It mainly comes from the orthogonality between the nearest neighbor in the TAST codewords, as explained in Eq. 6.32.

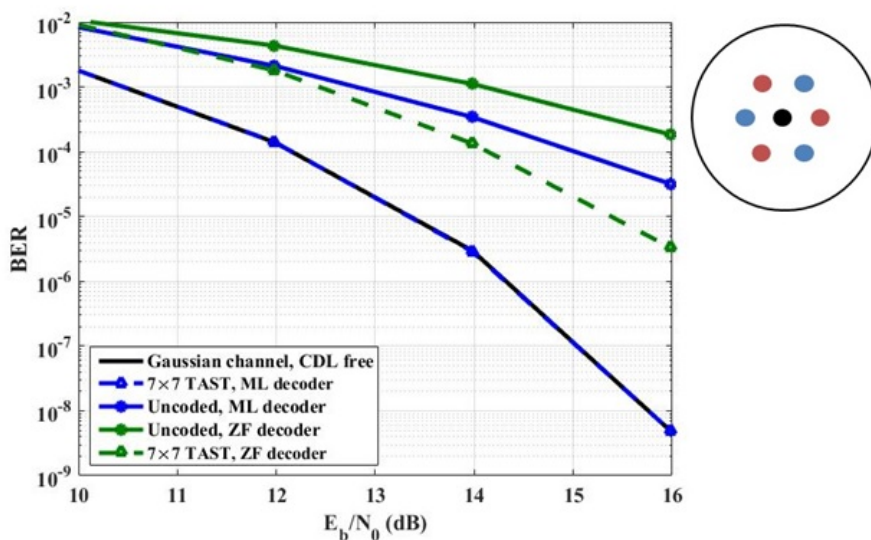


Figure 6.3: 7×7 TAST code performance for 7-core Hetero-MCF, misalignment level ($\sigma_{x,y}=7\%r_c$) corresponding to $CDL = 8$ dB

Regarding the TAST code performance efficiency by mitigating the CDL completely, the decoding complexity of the ML decoder is high compared to the ZF decoder. In Table 6.2, we illustrate the complexity of the ML and ZF decoders for $M \times M$ MIMO systems as shown in [45] and in particular the numerical application for the 7-core MCF. In the case of the ML decoder, we consider the complexity estimation of exhaustive search ML decoder. Noticeably, implementing the ML decoder for full rate TAST codes in MCF systems with a large number of cores will become very costly and require very high computational effort. Therefore, for the next section, we propose a solution where we can apply the ZF decoder at the receiver side and achieve performance close to the ML decoder and the AWGN channel.

6. SPACE-TIME CODING FOR MULTI-CORE FIBER

Table 6.2: Comparison of the complexities using ML and ZF decoders

	ZF	ML exhaustive search
$M \times M$ MIMO	$\frac{M^3+3M^2-M}{M}$	$\approx q^M$
7×7 TAST($M = 49$)	2547	2.7×10^8

6.2.2 Combination of TAST code and core scrambling

In the previous subsection, we observe the perfect CDL mitigation brought by the ST codes and ML detection. However, the remaining issue is the computational complexity of the optimal decoders, especially for a large number of cores. In chapter. 3, the scrambling is proposed to enhance the system performance of the MCFs by reducing the CDL value. In the 7-core Hetero-MCF case, we apply one deterministic scrambling strategy: the Snail scrambler. In this part, we investigate the TAST code's performance in combination with the core scrambling aiming to reduce the decoding complexity. The received signal have been illustrated in (Eq. 4.1, chapter. 4) as:

$$\mathbf{Y}_{C \times T} = \sqrt{\ell} \prod_{k=1}^K (\mathbf{T}_k (\mathbf{H}_{\mathbf{X}\mathbf{T}})_k \mathbf{M}_k \mathbf{P}_k) \mathbf{X}_{C \times T} + \mathbf{N}_{C \times T} \quad (6.34)$$

In order to investigate the performance of the TAST code with the scrambling, we simulate the 7×7 TAST code after installing the Snail scrambling for 7-core Hetero-MCF transmission system as shown in Fig. 6.4. In this scheme, we set the transverse offset to be equal to $7\%r_c$ with $K = 300$ and installing 6 scramblers in the fiber link. Then, we apply the sub-optimal ZF decoder at the receiver side. In Fig. 6.5, we plot the BER performance versus SNR, we notice the coding gain provided by the TAST code combined with the Snail scrambling while applying the sub-optimal ZF decoder (Dashed line), the system performance with TAST code and core scrambling is enhanced by 1.2dB compared to the uncoded system with the scrambling and ML decoder. In addition, the system performance has only SNR penalty equal to 0.1dB compared to the Gaussian channel and the optimal solution (7×7 TAST with ML decoder) at $\text{BER} = 10^{-4}$.

To explain the previous observation, we need to return to the upper bound error

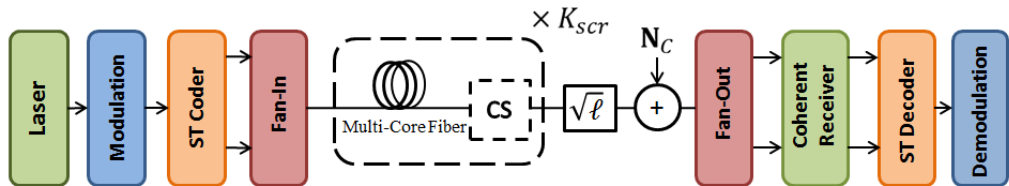


Figure 6.4: Space-Time coded MCF transmission system including core scrambling

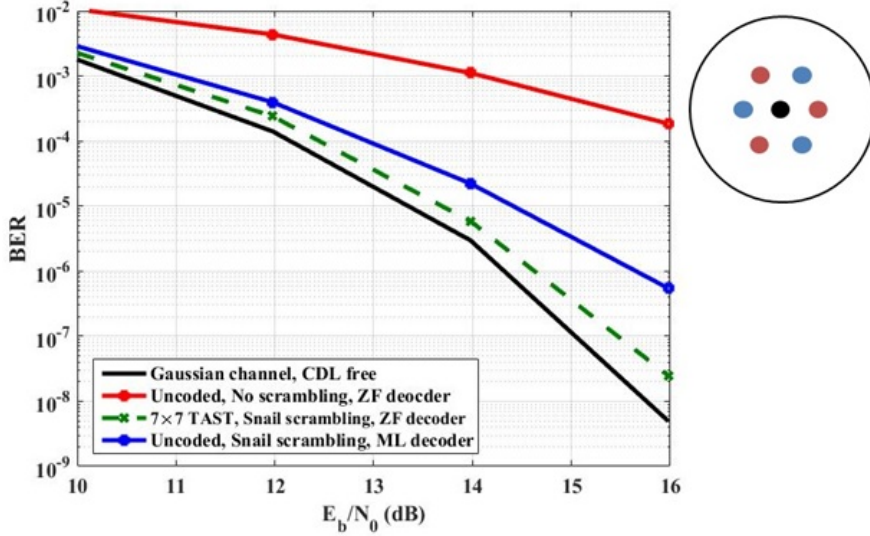


Figure 6.5: BER performance of 7-core Hetero-MCF with 7×7 TAST code and Snail scrambling, with misalignment level $\sigma_{x,y} = 7\%r_c$ corresponding to CDL = 1.8dB

probability expression obtained for the ZF decoder in Eq. 6.32. We proved that the ZF error probability is a function of the ODF, where in the case of equality the channel model is orthogonal and the ZF performs optimally. Thus, Fig. 6.6 shows the CDF of the ODF (δ) for the 7-core Hetero-MCF channel model with and without core scrambling. We observe that the system without core scrambling has an orthogonal defect factor in 70% of the time is equal to 4. In contrast, the MCF system with core scrambling has an ODF with less than 1.5 during 70% of the time which makes the ZF near the optimal performance so close to the ML decoder and AWGN channel.

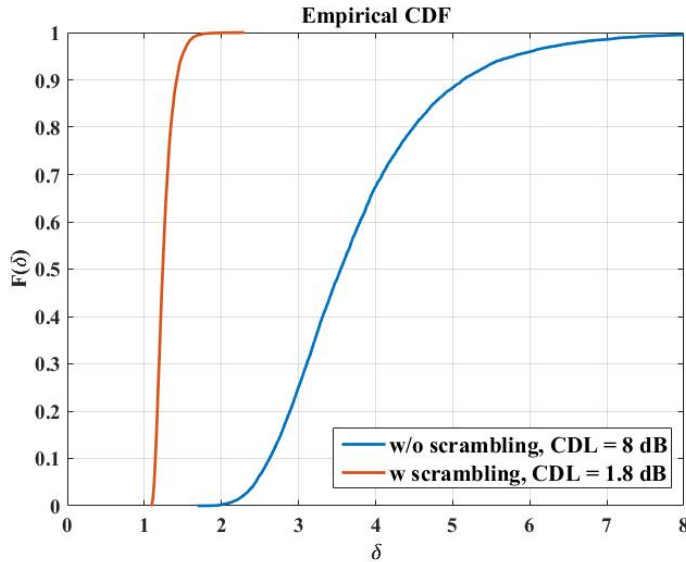


Figure 6.6: CDF of the ODF for 7×7 TAST with and without core scrambling

Summary

This chapter aims to introduce the ST coding technique to the MCF transmission system as a digital solution in order to mitigate the CDL completely. We presented some ST codes based on the STBC family by giving the properties of the each codes and rate limitations. We ended up by implementing the TAST code for the MCF transmission system caused by the scalability proprieties provided by the TAST codes. We showed that the TAST codes completely mitigate the CDL at the cost of the decoder complexity. Therefore, we introduced a combined solution between the TAST codes and the core scrambling, this solution provides performance close to the optimal decoder. Finally, the observed results have been proved mathematically by driving an upper bound error probability for each transmission system.

Chapter 7

Introduction to Massive SDM Transmission Systems

The thesis contribution and goals are mainly studying the MCF transmission system impaired by the non-unitary effect given by the CDL. In the meanwhile, we proposed optical and digital solutions in order to enhance the transmission performance. However, the potential of the SDM is not just limited by cores or modes multiplexing alone. This can be extended to further multiplexing techniques which includes combining the MCF and MMF at the same time (see Fig. 1.17). The massive SDM systems will allow capacity increasing in order to continue answering the traffic capacity demands.

This chapter paves the road to study the SDM based on FMFs and MCFs together. However, we do not provide performance analysis and investigation, the goal is to introduce the necessary knowledge as the first step towards understanding the fiber design concept and the system performance. We start by illustrating the design difference between the MCF and massive SDM systems. Then, we explain the propagation impairment that affects the spatial channels. After, we introduce the channel model of the space division multiplexing. Finally, we discuss some perspectives for further evaluation in the future works.

7.1 The Future of Massive SDM

The MCFs have more potential to be commercialized due to its lower complexity compared to the MMFs. However, the spatial degree of freedom is not concerning using just a multi-core (MCF) or a few-mode (FMF). Even if MCF seems sufficient to answer a required capacity for the next 20 years, it is more suitable to have more degrees of freedom available for the next fiber generations. In order to fully exploit the spatial dimension in the

7. INTRODUCTION TO MASSIVE SDM TRANSMISSION SYSTEMS

SDM system, integration between the few-mode and multi-core should be investigated, as shown in Fig. 7.1. In the literature [53][113], the few-mode MCFs are referred to as Dense SDM (DSDM) or a few-mode multi-core (FM-MCF), in our work, we call it Massive SDM inspired by Massive MIMO in wireless communication. Massive SDM indicates the unprecedented capacities (beyond petabits/s) that can be achieved by neither the MCFs nor the FMFs alone.

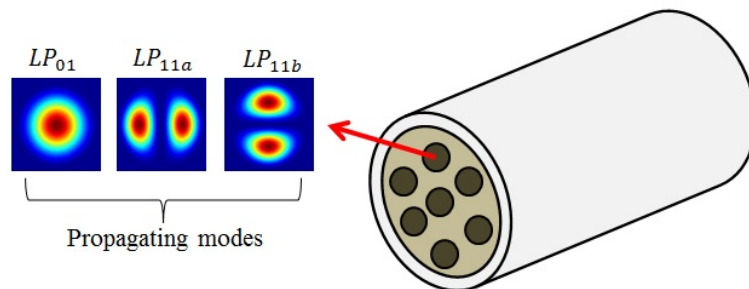


Figure 7.1: Massive SDM fiber with three modes propagating $\{LP_{01}, LP_{11a}$ and $LP_{11b}\}$

7.1.1 Massive SDM Achievements

Experimentally, several contributions have been done to address the SDM scalability by implementing the Massive SDM transmission system, as shown in Table.7.1. In [114], the authors demonstrate 12-core and 3-mode transmission with 61.97 Tbits/s capacity and 40.4 km distance. For higher spatial efficiency, a 19-core and 6-mode were achieved but with transmission reach 9.8 km [115]. In [116], the authors demonstrate longer transmission distance experiments equal to 527 km with the help of FM-EDFAs for 12-core and 3-mode SDM. Lastly, 2.05 Pbits/s can be achieved using 19-core and 6-mode SDM as it has been done in [117].

Table 7.1: Recently Achievement reported for Massive SDM transmission

Reference	Spatial channels	distance (km)	Capacity (Tbit/s)
Van Uden [118]	7-core \times 3-mode	1	200
Mizuno [114]	12-core \times 3-mode	40.4	61.97
Shibahara [115]	12-core \times 3-mode	527	23.58
Igarashi [116]	19-core \times 3-mode	9.8	30.3
Soma [117]	19-core \times 3-mode	9.8	2050

7.1.2 Massive SDM impairment

The propagation impairments that impact the Massive SDM transmission performance is the combination of both the MCFs and the FMFs impairments. Most of them are common problems represented in the crosstalk and the differential group velocity delay between the cores or modes. Despite, the DGVD has more impact on the FMFs than the MCFs. In this section, the crosstalk between the cores, regardless of the propagating LP mode, is referred to as the inter-core crosstalk (IC-XT) and the crosstalk between the modes; regardless the core; is referred as the inter-mode crosstalk (IM-XT). Moreover, in MCFs, the crosstalk occurs between the fundamental mode LP_{01} (IC-XT $_{01-01}$), for Massive SDM, we should take into account the IC-XT between the higher order modes such as the LP_{11} (IC-XT $_{11,11}$) also between the different modes such as LP_{01} and LP_{11} (IC-XT $_{01,11}$) as shown in Fig. 7.2.

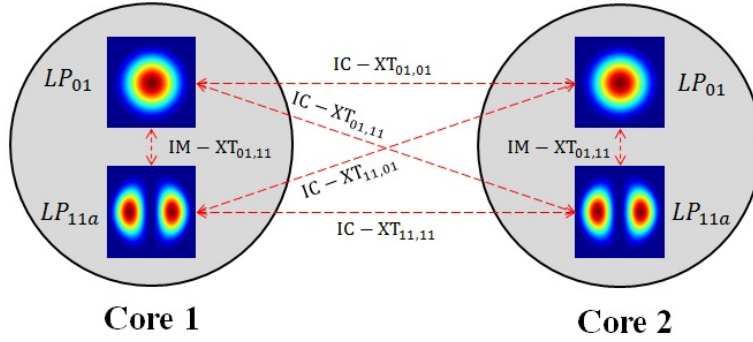


Figure 7.2: Illustration drawing of the crosstalk relation between two cores each propagates two modes $\{LP_{01}$ and $LP_{11a}\}$

Based on the coupled power theory (CPT) presented in Chapter. 2, the IC-XT between different modes can be determined. In Fig. 7.3, we plot the IC-XT between two homogeneous cores while each core allows propagating two LP-modes (LP_{01} and LP_{11}) for transmission distance equal to $100km$ and different core pitch. We notice that the crosstalk level for higher order mode (IC-XT $_{11}$) is larger than the fundamental mode IC-XT $_{01}$ with 18 dB difference, this observation is due to the effective area of LP_{11} which is higher than the LP_{01} mode and also because the mode confinement of LP_{11} is weaker than LP_{01} . In addition, the crosstalk value between different modes is weak due to the large difference in the effective indices [119]. Consequently, we can conclude that the higher modes dominate the crosstalk in Massive SDM system.

The IM-XT occurs at the splice point and it is computed using the overlap integral of the propagating modes electrical fields in [120] as:

$$c_{i,j} = \iint_A E_i^{(k-1)}(x,y) E_j^{(k)} * (x + \Delta x, y + \Delta y) dA \quad (7.1)$$

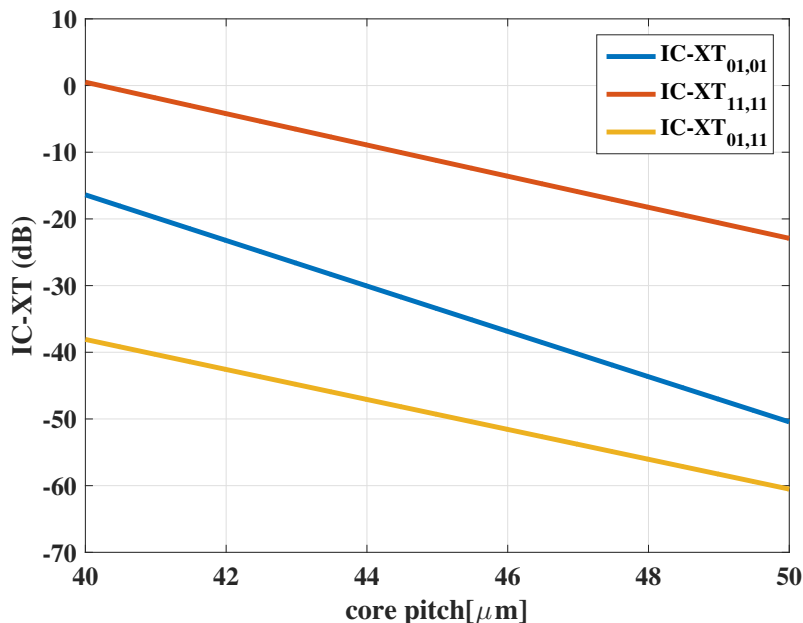


Figure 7.3: IC-XT function of the core pitch after 100 km propagating

$E_i^{(k-1)}$ and $E_j^{(k)} * (x + \Delta x, y + \Delta y)$ are the normalized complex amplitudes of the i^{th} mode before and after the splice. Δx and Δy are the fiber displacement in the x and y directions with zero mean and standard deviation $\sigma_{x,y}$. Finally, the misalignment loss in the same core varies from mode to another due to the mode field radius difference, as shown in Eq. 3.2. Thus, in our design, we should consider the fluctuation in the core position and the losses of higher order modes.

7.2 Massive SDM Channel Model

The impact of combining different DoFs on optical communication systems has been reported in many studies [121][122]. In [121], a channel model for MDM transmission systems supporting the two orthogonal polarizations in addition to the mode multiplexing has been proposed. Moreover, the effects of both PDL and MDL have been investigated by EL-Mehdi *et al.* in [122]. In our work, we introduce the Massive SDM channel model aiming to study the MDL and CDL effects. Fig. 7.4 illustrates the transmission scheme of the Massive SDM. We consider the Massive SDM system based on C cores where M modes propagate in each core. We do not consider the nonlinearity and the dispersive effects since it does not reduce the system capacity. The Massive SDM channel model with dimension $S = C \times M$ can be described as:

$$\mathbf{Y}_{S \times 1} = \mathbf{H}_{S \times S} \mathbf{X} + N_{S \times 1} = \prod_{k=1}^K (\mathbf{H}_{SDM})_k \mathbf{M}_k \mathbf{X} + \mathbf{N} \quad (7.2)$$

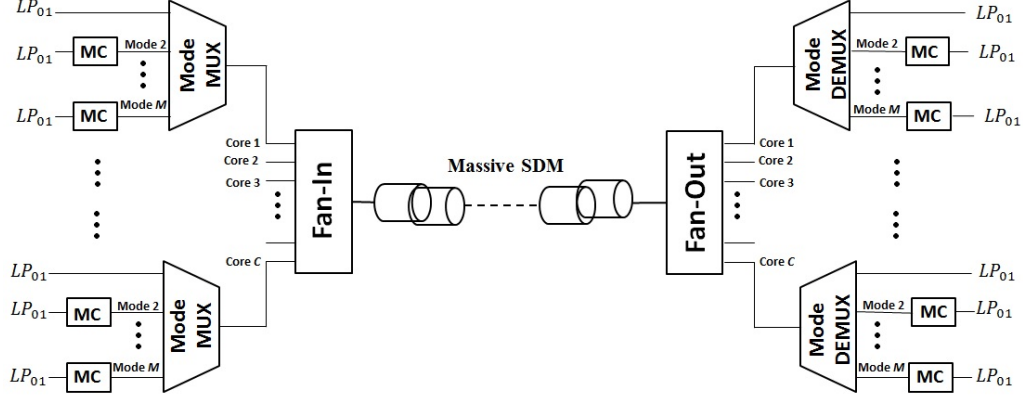


Figure 7.4: Massive space division multiplexing transmission system. MC: mode converter.

where $\mathbf{X} = [x_1, \dots, x_S]^T$ and $\mathbf{Y} = [y_1, \dots, y_S]^T$ are the emitted and received symbol vector. \mathbf{N} is AWGN with zero mean and std is equal to $\%a_1$. The Massive SDM channel model is represented by $S \times S$ block matrix \mathbf{H}_{SDM} as:

$$\mathbf{H}_{SDM} = \begin{pmatrix} [(\mathbf{I} - \mathbf{\Sigma}) \cdot \mathbf{H}_{MDM}]_1 & \mathbf{X}\mathbf{T}_{1,2} & \dots & \mathbf{X}\mathbf{T}_{1,C} \\ \mathbf{X}\mathbf{T}_{2,1} & [(\mathbf{I} - \mathbf{\Sigma}) \cdot \mathbf{H}_{MDM}]_2 & \dots & \mathbf{X}\mathbf{T}_{2,C} \\ \vdots & \vdots & \ddots & \vdots \\ \mathbf{X}\mathbf{T}_{C,1} & \mathbf{X}\mathbf{T}_{C,2} & \dots & [(\mathbf{I} - \mathbf{\Sigma}) \cdot \mathbf{H}_{MDM}]_C \end{pmatrix} \quad (7.3)$$

the block $(\mathbf{I} - \mathbf{\Sigma})$ represents the loss of the SDM transmission system, where \mathbf{I} is the identity matrix with dimension \mathbf{M} and $\mathbf{\Sigma}$ is a diagonal matrix contains the sum of the IC-XT for all the excited modes. The following is an example of $\mathbf{\Sigma}$ for Massive SDM with two modes $\{LP_{01}$ and $LP_{11}\}$:

$$\mathbf{\Sigma} = \begin{bmatrix} \text{IC-XT}_{01,01} + \text{IC} - \text{XT}_{01,11} & 0 \\ 0 & \text{IC-XT}_{11,11} + \text{IC} - \text{XT}_{11,01} \end{bmatrix} \quad (7.4)$$

$\mathbf{X}\mathbf{T}_{n,m}$ is square matrix illustrates the IC-XT level between core n and m , it can be seen as a generalization of the \mathbf{H}_{XT} where only the fundamental mode was considered. To continue the example provided in Eq. 7.4, the $\mathbf{X}\mathbf{T}_{n,m}$ of Massive SDM for two modes $\{LP_{01}$ and $LP_{11}\}$ is represented as:

$$\mathbf{X}\mathbf{T}_{n,m} = \begin{bmatrix} \text{IC-XT}_{01,01} & \text{IC-XT}_{01,11} \\ \text{IC-XT}_{11,11} & \text{IC-XT}_{11,01} \end{bmatrix} \quad (7.5)$$

\mathbf{H}_{MDM} represents the channel model of the multi-mode impaired by the MDL. In our work, we adopt the same channel model construction in [3]. The MDL is given by $M \times M$ matrix as:

$$\mathbf{H}_{MMF} = \prod_{k=1}^K (T_k C_k) \quad (7.6)$$

where \mathbf{H}_{MMF} is concatenation of K fiber sections, T_k is a diagonal matrix of random phase entities ($\exp(i\phi_m)$, where $\phi_m \in [0, 2\pi]$). C_k is the channel matrix of the non-unitary modal coupling in Eq. 7.1, in our content, it represents the IM-XT. Finally, \mathbf{M}_k is the misalignment channel model of the Massive SDM where it is introduced as a diagonal matrix of the losses for each mode in each core as follows:

$$\mathbf{M}_k = \begin{pmatrix} \alpha_1 & & 0 \\ & \ddots & \\ 0 & & \alpha_C \end{pmatrix} \quad \text{where} \quad \alpha_k = \begin{pmatrix} \epsilon_1 & & 0 \\ & \ddots & \\ 0 & & \epsilon_M \end{pmatrix} \quad (7.7)$$

ϵ_k is the loss of each mode in the same core i , $k \in [1, \dots, M]$.

7.2.1 Future Validations

In the previous subsection, we propose a channel model of the Massive SDM transmission system. The proposed crosstalk matrix considers the coupling between the cores and the modes that need to be validated in future work. Notably, the manufacturing process will require considering different parameters depend on the MCF and FMF design limitations. The fiber design characterization centered around determining the core pitch, the type of cores (Homogeneous or Heterogeneous core), the system DMGD level and the coupled level between the modes and the cores at the same time. Moreover, The massive systems will require designing large MIMO DSP to operate. Thus, the complexity of the Massive SDM system will be one of the significant challenges that need to be addressed. Consequently, low complex coding and decoding techniques should be proposed in order to enhance system performance.

Defining a new parameter that we can call it spatial dependent loss (SDL) will be necessary to evaluate the Massive SDM transmission system performance. In [122], the authors showed that the global non-unitary effect is approximately equal to the sum of the PDL and MDL over the FMFs system combined with PolMux. Therefore, the contribution of the CDL and MDL on the SDL system can also be observed in the case of Massive SDM systems.

After the validation of the proposed Massive SDM system, we can move forward to introduce a mathematical channel model as has been done in this thesis for MCF systems. As a first thought, the mathematical Massive SDM model can be a combination of the MCF and FMF channel models. Then, we can observe the distribution of SDL. Consequently, deriving an upper bound error probability for the Massive SDM transmission systems.

Finally, the proposed Massive SDM system can be combined with PolMux for a further degree of freedom and higher capacity. The new channel model can be based on a block matrix, as shown in this chapter. Also, the transmission system will be affected by the PDL rises between the two polarizations.

Summary

In this chapter, we put the first step towards exploring the Massive SDM systems. We reviewed some experimental demonstrations of the Massive SDM transmission. After, we explained the impairments that impact the system performance. Lastly, We proposed channel mode for the Massive SDM systems. Future work, this model can be the base to build the upcoming evaluation on the Massive SDM transmission.

Conclusions & Perspectives

Conclusions

The bandwidth demands in the network increase rapidly in the last decades due to the high number of users and machines connected to the internet. Significant technology changes and strategies are currently implementing to handle the future capacity demands in the optical systems starting from the year 2020. In the past decades, several key technologies have been introduced to the optical communication systems that help carry the data traffic in the optical network. Starting from introducing the EDFA amplifiers until developing the coherent PDM systems to operate at 100 Gb/s. Higher modulation formats and Dense WDM systems with channel spacing less than 50 GHz can reach transmission capacity equal to 100 Tb/s and still delivering the required capacity. The conventional SMF almost reached the capacity crunch and cannot address the data traffic demands from the internet networks. Therefore, laboratories started conducting an intensive investigation in the spatial degree of freedom. In general, the SDM systems are affected by different impairments. In this thesis, we were interested in the SDM based on the multi-core fibers approach impaired by the CDL.

Since the MCFs have several structures proposals, we focused on the most commonly implemented layouts in the literature in our study. The MCFs are built either by homogeneous cores or heterogeneous with and without trench assistance. Besides, MCFs are categorized into coupled and uncoupled systems impacted by different CDL levels, resulting in a variation in the transmission performance. Thus, the first step in our study was developing a valid channel model for all system designs. The physical description of the transmission system helped investigate each MCF structure's performance based on the crosstalk and misalignment level. We noticed that the crosstalk and the misalignment directly impact the CDL value, which depends on the fiber structure. Therefore, the second direction was to propose a theoretical MCF channel model in order to estimate the performance of the MCF transmission function of the crosstalk and misalignment. The theoretical model proved that each core has lognormal distribution resulting in Gaussian behavior for the CDL. In order to finalize the performance evaluation, we derived an upper bound on error probability for the optimal ML decoder and sub-optimal ZF decoder

scheme.

The optical technique was our first approach to mitigate CDL value. We introduced the core scrambling strategy to average the losses over all the cores which reduces the core dependent loss. The drawback is the number of the installed scramblers in the link to achieve a sufficient CDL value. For that reason, we proposed three deterministic techniques based on the MCF structure, the Snail, the Circular and the Snake scrambling. Each technique proved the ability to efficiently reduce the CDL in the system by installing a small number of scramblers compared to the random core scrambling. After, the theoretical channel model helped to obtain the optimal number of deterministic scrambling that can be installed to decrease the CDL value optimally. We showed that the ZF decoder has the same performance as the ML decoder by applying the core scrambling. That helps to reduce the decoding complexity.

After that, we proposed two digital techniques to mitigate the CDL and enhance system performance. First, the ZF pre-compensation technique achieves the same performance as the optimal deterministic core scrambling with a very low complex transmission scheme, consequently a more cost-efficient solution. In order to obtain further SNR improvement, the second digital solution was applying the ST coding over MCF systems. We showed analytically that the TAST codes mitigate completely the CDL combined with the ML decoder. Also, we derived an upper bound error probability of the coded system while applying the ZF decoder. We observed that the error probability is a function of the orthogonal defect function. From this point, we proposed a combination between the TAST code and core scrambling that provided more SNR gain with low-complexity and performance close to the Gaussian channel.

Lastly, we introduced the Massive SDM system where the MMFs and MCFs are combined. The aim was to provide all the knowledge and tools in order to be able to evaluate and investigate the fiber design concept and system performance. We start by explaining the propagation impairments that affect the spatial channels. After, we introduced the channel model of the space division multiplexing. We showed that to design a massive SDM system; we should consider the higher order modes since it dominates the fiber impairment, unlike the conventional MCFs, where just the fundamental mode is propagating.

Perspectives

The previous conclusions open the door to two tracks for further research studies. The two tracks are shared between the MCFs system and the Massive SDM systems as follows:

- We look forward to conducting experiments to validate the works on the MCF systems presented in this thesis. Starting from the theoretical channel model until the

optical and digital techniques proposed to mitigate CDL. The experiments' success is the best way to push the deployment of the MCF transmission systems in the industry. The introduced strategies showed low complex detection processing at the receiver side, which is one of the issues that limit the SDM implementation.

- Applying the forward error correction (FEC) codes combined with the ST codes can add more enhancement gain to the MCF system. Besides, the amplification stage can be installed in the transmission link, which adds another term called the core dependent gain. As preliminary thought, We can deal with core gain as the losses by applying the same strategies in this thesis.
- The last part of the thesis established the channel model of the Massive SDM transmission system. The second step is to evaluate the performance of Massive SDM and investigate techniques to enhance system performance. Moreover, extension of our study to fully exploit the Massive SDM transmission system after the integration with the PDM and WDM systems. The new generation optical system will be affected by all the previously studied non-unitary effects (PDL, MDL, and CDL), which require a new design for the massive MIMO DSP. In this case, the DSP processing complexity will be the challenge in order to be able to operate.

Appendix A

Matrix and Distribution Operations

A.1 QR Decomposition

The QR decomposition also called QR factorization of a real square $N \times N$ matrix \mathbf{H} is a decomposition of \mathbf{H} into an orthogonal matrix \mathbf{Q} and an upper triangular matrix \mathbf{R} such as:

$$\mathbf{H} = \mathbf{QR} \quad (\text{A.1})$$

If \mathbf{H} is non-singular, the factorization is unique. There are several methods for computing the QR decomposition, the popular one is the Gram-Schmidt process. Consider the columns $h_i, \{i:1 \rightarrow N\}$ of \mathbf{H} . The Gram-Schmidt orthonormalization consists of:

$$u_1 = h_1, e_1 = \frac{u_1}{\|u_1\|}, \quad (\text{A.2})$$

$$u_2 = a_2 - \langle a_1, e_1 \rangle e_1, e_2 = \frac{u_2}{\|u_2\|}, \quad (\text{A.3})$$

$$\begin{aligned} u_{k+1} &= a_{k+1} - \langle a_{k-1}, e_1 \rangle e_1 - \dots - \langle a_{k-1}, e_k \rangle e_k, \\ e_{k+1} &= \frac{u_{k+1}}{\|u_{k+1}\|}, \end{aligned} \quad (\text{A.4})$$

where $\|\cdot\|$ is the Euclidean norm and $\langle a, b \rangle = a^T b$ is the scalar product of two column vectors. The resulting QR factorization yields:

$$\mathbf{H} = \mathbf{QR} = \mathbf{Q} \begin{bmatrix} \langle a_{k-1}, e_1 \rangle & \langle a_{k-1}, e_N \rangle & \dots & \langle a_2, e_N \rangle \\ 0 & \langle a_{k-1}, e_1 \rangle & & \vdots \\ \vdots & & \ddots & \\ 0 & \dots & \dots & \langle a_{k-1}, e_1 \rangle \end{bmatrix}$$

A.2 The PDF of the maximum and minimum of normal distribution

We derive the PDF of $U = \max\{X\}$ and $V = \min\{X\}$ where X is normal distribution with mean μ and standard deviation σ .

The normal distribution has CDF as:

$$F(x) = \frac{1}{2} \left[1 + \operatorname{erf} \left(\frac{x - \mu}{\sigma\sqrt{2}} \right) \right] \quad (\text{A.5})$$

assuming $G_U(x)$ is the CDF of U which is equal to $(F(x))^n$, where n is the number of sample of independent and identically distributed random variables. Also, $G_V(x)$ is the CDF of V which is equal to $1 - (1 - F(x))^n$.

The PDF is obtained by taking the derivative of the CDF. In this case, the PDF of $G_U(x) = n F(x)^{n-1} f(x)$, which is given as:

$$f_U(x) = \frac{n}{2^{n-2}\sigma\sqrt{2\pi}} \left[1 + \operatorname{erf} \left(\frac{x - \mu}{\sigma\sqrt{2\pi}} \right) \right]^{n-1} e^{-\left(\frac{x - \mu}{\sigma\sqrt{2\pi}}\right)^2} \quad (\text{A.6})$$

and the PDF of $G_V(x) = n(1 - F(x))^{n-1} f(x)$, knowing that $\operatorname{erfc}(x) = 1 - \operatorname{erf}(x)$:

$$f_V(x) = \frac{n}{\sigma\sqrt{2\pi}} \left[\operatorname{erfc} \left(\frac{x - \mu}{\sigma\sqrt{2\pi}} \right) \right]^{n-1} e^{-\left(\frac{x - \mu}{\sigma\sqrt{2\pi}}\right)^2} \quad (\text{A.7})$$

A.3 SVD decomposition

In linear algebra, the singular value decomposition (SVD) is a factorization of a real or complex of $m \times n$ matrix in the form of:

$$H = U\Sigma V^H \quad (\text{A.8})$$

where U and V are unitary matrices and Σ is a diagonal matrix contains and non-negative real numbers. The SVD is related to the eigenvalue decomposition which can be computed by using the characteristic polynomial:

$$p(\lambda) = \det(\mathbf{H} - \lambda\mathbf{I}) = 0 \quad (\text{A.9})$$

where $\det(\cdot)$ is the determinant of the matrix. The left singular vectors of \mathbf{H} are the eigenvectors of $\mathbf{H}\mathbf{H}^H$, The right singular vectors of \mathbf{H} are the eigenvectors of $\mathbf{H}^H\mathbf{H}$ and the non-zero singular values of \mathbf{H} are the square roots of the non-zero eigenvalues of $\mathbf{H}\mathbf{H}^H$.

Bibliography

- [1] Haoshuo Chen and AMJ Ton Koonen. Spatial division multiplexing. In *Fibre Optic Communication*, pages 1–48. Springer, 2017. Cited pages [xv](#), [19](#), [20](#), [22](#), [40](#), and [43](#)
- [2] Masanori Koshihara, Kunimasa Saitoh, Katsuhiro Takenaga, and Shoichiro Matsuo. Analytical expression of average power-coupling coefficients for estimating intercore crosstalk in multicore fibers. *IEEE Photonics Journal*, 4(5):1987–1995, 2012. Cited pages [xv](#), [26](#), [27](#), and [28](#)
- [3] El-mehdi Amhoud. *Coding Techniques for Space-Division Multiplexed Optical Fiber Systems*. PhD thesis, 2017. Cited pages [xix](#), [2](#), [22](#), [24](#), [43](#), [64](#), [81](#), [92](#), and [109](#)
- [4] Tingye Li. Optical fiber communication-the state of the art. *IEEE Transactions on Communications*, 26(7):946–955, 1978. Cited pages [1](#) and [5](#)
- [5] Cisco visual networking index: Forecast and trends, 2017–2022. *Cisco Systems*, 2019. Cited page [1](#)
- [6] Qiu Winston. Dunant cable system implements space-division multiplexing (SDM) technology, 2019. Cited page [2](#)
- [7] D. Francois Michael, George Chris, and Stowell Jayne. Introducing equiano, a subsea cable from portugal to south africa, 2019. Cited page [2](#)
- [8] S Fujita, M Kitamura, T Torikai, N Henmi, H Yamada, T Suzuki, I Takano, and M Shikada. 10 Gbit/s, 100 km optical fibre transmission experiment using high-speed MQW DFB-LD and back-illuminated gainas apd. *Electronics Letters*, 25(11):702–703, 1989. Cited page [6](#)
- [9] Tingye Li. The impact of optical amplifiers on long-distance lightwave telecommunications. *Proceedings of the IEEE*, 81(11):1568–1579, 1993. Cited page [6](#)
- [10] Herwig Kogelnik. High-capacity optical communications: personal recollections. *IEEE Journal of Selected Topics in Quantum Electronics*, 6(6):1279–1286, 2000. Cited page [6](#)
- [11] Dayou Qian, Ming-Fang Huang, Ezra Ip, Yue-Kai Huang, Yin Shao, Junqiang Hu, and Ting Wang. 101.7-Tb/s (370× 294-Gb/s) PDM-128QAM-OFDM transmission over 3× 55-km SSMF using pilot-based phase noise mitigation. In *National Fiber Optic Engineers Conference*, page PDPB5. Optical Society of America, 2011. Cited page [6](#)
- [12] Charles Cox, Edward Ackerman, Roger Helkey, and Gary E Betts. Direct-detection analog optical links. volume 45, pages 1375–1383. IEEE, 1997. Cited page [7](#)
- [13] Hamutal Shalom, Avi Zadok, Moshe Tur, Peter J Legg, WD Cornwell, and Ivan Andonovic. On the various time constants of wavelength changes of a DFB laser under direct modulation. *IEEE Journal of Quantum Electronics*, 34(10):1816–1822, 1998. Cited page [7](#)

BIBLIOGRAPHY

- [14] Kiyoshi Nosu. Advanced coherent lightwave technologies. *IEEE Communications Magazine*, 26(2):15–21, 1988. Cited page [11](#)
- [15] Kazuro Kikuchi. Coherent optical communication systems. In *Optical Fiber Telecommunications VB*, pages 95–129. Elsevier, 2008. Cited page [11](#)
- [16] Gabriel Charlet. Coherent detection associated with digital signal processing for fiber optics communication. *Comptes Rendus Physique*, 9(9-10):1012–1030, 2008. Cited page [11](#)
- [17] H-G Unger. Planar optical waveguides. In *Fiber and Integrated Optics*, pages 183–221. Springer, 1979. Cited page [12](#)
- [18] Govind P Agrawal. Nonlinear fiber optics. In *Nonlinear Science at the Dawn of the 21st Century*, pages 195–211. Springer, 2000. Cited pages [12](#), [13](#), and [15](#)
- [19] SV Chernikov and JR Taylor. Measurement of normalization factor of n^2 for random polarization in optical fibers. *Optics letters*, 21(19):1559–1561, 1996. Cited page [15](#)
- [20] Philippe M Becker, Anders A Olsson, and Jay R Simpson. *Erbium-doped fiber amplifiers: fundamentals and technology*. Elsevier, 1999. Cited page [15](#)
- [21] LE Nelson and RM Jopson. Introduction to polarization mode dispersion in optical systems. In *Polarization mode dispersion*, pages 1–33. Springer, 2004. Cited page [17](#)
- [22] RM Jopson, LE Nelson, GJ Pendock, and AH Gnauck. Polarization-mode dispersion impairment in return-to-zero and nonreturn-to-zero systems. In *Optical Fiber Communication Conference*, page WE3. Optical Society of America, 1999. Cited page [17](#)
- [23] Hong Jiang, Ross Saunders, and Stephen Colaco. SiGe equalizer IC for PMD mitigation and signal optimization of 40 Gbits/s transmission. In *OFC/NFOEC Technical Digest. Optical Fiber Communication Conference*, volume 3, pages 3–pp. IEEE, 2005. Cited page [17](#)
- [24] Sander L Jansen, Itsuro Morita, Tim C Schenk, and Hideaki Tanaka. Long-haul transmission of 16×52.5 gbits/s polarization-division-multiplexed OFDM enabled by mimo processing. *Journal of Optical Networking*, 7(2):173–182, 2008. Cited page [17](#)
- [25] M. A. Bhatti and A. S. Siddiqui. measurement of polarization dependent loss in optical fiber and bulk optical devices. *Optical Fiber Measurement Conference*, pages 25–26, 1995. Cited page [17](#)
- [26] L. Ducos, R. Clin, P. Blanchard, and F. Gautier. polarization dependent loss of passive optical components. *Optical Fiber Measurement Conference*, pages 25–26, 1995. Cited page [17](#)
- [27] N. Gisin. statistics of polarization dependent losses. *Optics Communications*, pages 399–405, 1995. Cited page [17](#)
- [28] Antonio Mecozzi and Mark Shtaif. The statistics of polarization-dependent loss in optical communication systems. *Photonics Technology Letters*, 14(3):313–315, 2002. Cited page [17](#)
- [29] Chen Zhu, Binhuang Song, Leimeng Zhuang, Bill Corcoran, and Arthur J Lowery. Pairwise coding to mitigate polarization dependent loss. In *Optical Fiber Communications Conference and Exhibition (OFC)*, pages 1–3. IEEE, 2015. Cited page [18](#)
- [30] Elie Awwad, Yves Jaouën, and Ghaya Rekaya-Ben Othman. Polarization-time coding for PDL mitigation in long-haul PolMux OFDM systems. *Optics express*, 21(19):22773–22790, 2013. Cited pages [18](#) and [89](#)

-
- [31] Fabrizio Forghieri, RW Tkach, Andrew R Chraplyvy, and Dietrich Marcuse. Reduction of four-wave mixing crosstalk in WDM systems using unequally spaced channels. *IEEE Photonics Technology Letters*, 6(6):754–756, 1994. Cited page [18](#)
- [32] AR Chraplyvy, AH Gnauck, RW Tkach, and RM Derosier. 8* 10 Gb/s transmission through 280 km of dispersion-managed fiber. *IEEE photonics technology letters*, 5(10):1233–1235, 1993. Cited page [18](#)
- [33] S Iano, T Sato, S Sentsui, T Kuroha, and Y Nishimura. Multicore optical fiber. In *Optical Fiber Communication Conference*, page WB1. Optical Society of America, 1979. Cited page [19](#)
- [34] S Berdagué and P Facq. Mode division multiplexing in optical fibers. *Applied optics*, 21(11):1950–1955, 1982. Cited page [19](#)
- [35] Peter J Winzer. Making spatial multiplexing a reality. *Nature Photonics*, 8(5):345, 2014. Cited page [19](#)
- [36] Peter J Winzer. Energy-efficient optical transport capacity scaling through spatial multiplexing. *IEEE Photonics Technology Letters*, 23(13):851–853, 2011. Cited page [19](#)
- [37] Haoshuo Chen, Vincent Sleiffer, Frans Huijskens, Roy van Uden, Chigo Okonkwo, Paolo Leoni, Maxim Kuschnerov, Lars Grüner-Nielsen, Yi Sun, Huug de Waardt, et al. Employing prism-based three-spot mode couplers for high capacity MDM/WDM transmission. *IEEE Photonics Technology Letters*, 25(24):2474–2477, 2013. Cited page [20](#)
- [38] Clemens Koebele, Massimiliano Salsi, Laurent Milord, Roland Ryf, Cristian Bolle, Pierre Sillard, Sébastien Bigo, and Gabriel Charlet. 40km transmission of five mode division multiplexed data streams at 100Gb/s with low MIMO-DSP complexity. In *European Conference and Exposition on Optical Communications*, pages Th–13. Optical Society of America, 2011. Cited page [20](#)
- [39] Kengo Watanabe, Tsunetoshi Saito, Yukihiro Tsuchida, Koichi Maeda, and Masato Shiino. Fiber bundle type fan-out for multicore er doped fiber amplifier. In *18th OptoElectronics and Communications Conference held jointly with 2013 International Conference on Photonics in Switching (OECC/PS)*, pages 1–2. IEEE, 2013. Cited page [20](#)
- [40] Ali A Said, Mark Dugan, Philippe Bado, Yves Bellouard, Andrew Scott, and Jose R Mabesa Jr. Manufacturing by laser direct-write of three-dimensional devices containing optical and microfluidic networks. In *Photon Processing in Microelectronics and Photonics III*, volume 5339, pages 194–204. International Society for Optics and Photonics, 2004. Cited page [20](#)
- [41] KS Abedin, TF Taunay, M Fishteyn, MF Yan, B Zhu, JM Fini, EM Monberg, FV Dimarcello, and PW Wisk. Amplification and noise properties of an erbium-doped multicore fiber amplifier. *Optics express*, 19(17):16715–16721, 2011. Cited page [21](#)
- [42] Cen Xia, Neng Bai, Ibrahim Ozdur, Xiang Zhou, and Guifang Li. Supermodes for optical transmission. *Optics express*, 19(17):16653–16664, 2011. Cited pages [21](#) and [23](#)
- [43] Melin Gilles, Kerampran Romain, Monteville Achille, Bordais Sylvain, Robin Thierry, Landais David, Lebreton Aurelien, Jaouën Yves, and Taunay Thierry. Power efficient all-fiberized 12-core erbium/ytterbium doped optical amplifier. *Optical Fiber Communication Conference*, 2020. Cited page [21](#)
- [44] Sercan Ö Arık and Joseph M Kahn. Coupled-core multi-core fibers for spatial multiplexing. *IEEE Photonics Technology Letters*, 25(21):2054–2057, 2013. Cited page [23](#)
-

BIBLIOGRAPHY

- [45] Elie Awwad. *Emerging space-time coding techniques for optical fiber transmission systems*. PhD thesis, 2015. Cited pages [24](#), [43](#), and [99](#)
- [46] Masanori Koshihara, Kunimasa Saitoh, Katsuhiro Takenaga, and Shoichiro Matsuo. Multi-core fiber design and analysis: coupled-mode theory and coupled-power theory. *Opt. Express*, 19(26):B102–B111, Dec 2011. Cited page [26](#)
- [47] Guifang Li, Neng Bai, Ningbo Zhao, and Cen Xia. Space-division multiplexing: the next frontier in optical communication. *Advances in Optics and Photonics*, 6(4):413–487, 2014. Cited pages [27](#) and [28](#)
- [48] Lin Gan, Ming Tang, Li Shen, Chen Xing, Changjian Ke, Chen Yang, Weijun Tong, Songnian Fu, and Deming Liu. Realistic model for frequency-dependent crosstalk in weakly-coupled multicore fiber. In *Optical Fiber Communication Conference*, pages Tu3B–6. Optical Society of America, 2018. Cited page [29](#)
- [49] Lin Gan, Li Shen, Ming Tang, Chen Xing, Yanpeng Li, Changjian Ke, Weijun Tong, Borui Li, Songnian Fu, and Deming Liu. Investigation of channel model for weakly coupled multicore fiber. *Optics express*, 26(5):5182–5199, 2018. Cited page [29](#)
- [50] Feihong Ye, Jiajing Tu, Kunimasa Saitoh, and Toshio Morioka. Simple analytical expression for crosstalk estimation in homogeneous trench-assisted multi-core fibers. *Optics express*, 22(19):23007–23018, 2014. Cited pages [29](#) and [30](#)
- [51] Yusuke Sasaki, Yoshimichi Amma, Katsuhiro Takenaga, Shoichiro Matsuo, Kunimasa Saitoh, and Masanori Koshihara. Investigation of crosstalk dependencies on bending radius of heterogeneous multi-core fiber. In *Optical Fiber Communication Conference*, pages OTh3K–3. Optical Society of America, 2013. Cited pages [30](#), [32](#), [34](#), and [35](#)
- [52] Masanori Koshihara, Kunimasa Saitoh, and Yasuo Kokubun. Heterogeneous multi-core fibers: Proposal and design principle. *Electronic Express*, 6:98–103, 2009. Cited pages [30](#) and [35](#)
- [53] Takayuki Mizuno, Kohki Shibahara, Feihong Ye, Yusuke Sasaki, Yoshimichi Amma, Katsuhiro Takenaga, Yongmin Jung, Klaus Pulverer, Hirotaka Ono, Yoshiteru Abe, et al. Long-haul dense space-division multiplexed transmission over low-crosstalk heterogeneous 32-core transmission line using a partial recirculating loop system. *Journal of Lightwave Technology*, 35(3):488–498, 2017. Cited pages [30](#), [35](#), and [106](#)
- [54] Kunimasa Saitoh and Shoichiro Matsuo. Multicore fiber technology. *Journal of Lightwave Technology*, 34(1):55–66, 2016. Cited pages [30](#), [31](#), and [44](#)
- [55] Kunimasa Saitoh, Takashi Matsui, Taiji Sakamoto, Masanori Koshihara, and Shigeru Tomita. Multi-core hole-assisted fibers for high core density space division multiplexing. In *OECC 2010 Technical Digest*, pages 164–165. IEEE, 2010. Cited page [31](#)
- [56] Yoshimichi Amma, Yusuke Sasaki, Katsuhiro Takenaga, Shoichiro Matsuo, Jiajing Tu, Kunimasa Saitoh, Masanori Koshihara, Toshio Morioka, and Yutaka Miyamoto. High-density multicore fiber with heterogeneous core arrangement. In *Optical Fiber Communication Conference*, pages Th4C–4. Optical Society of America, 2015. Cited pages [32](#), [34](#), and [35](#)
- [57] Jiajing Tu, Kunimasa Saitoh, Masanori Koshihara, Katsuhiro Takenaga, and Shoichiro Matsuo. Design and analysis of large-effective-area heterogeneous trench-assisted multi-core fiber. *Optics express*, 20(14):15157–15170, 2012. Cited page [32](#)

-
- [58] André Filipe Simões da Silva Marques. *Transmission of 5G signals in multicore fibers impaired by inter-core crosstalk*. PhD thesis, 2018. Cited pages [34](#) and [35](#)
- [59] Tetsuya Hayashi, Tetsuya Nakanishi, Kaoru Hirashima, Osamu Shimakawa, Fumiaki Sato, Koichi Koyama, Akira Furuya, Yasunori Murakami, and Takashi Sasaki. 125- μm -cladding eight-core multi-core fiber realizing ultra-high-density cable suitable for o-band short-reach optical interconnects. *Journal of Lightwave Technology*, 34(1):85–92, 2016. Cited pages [34](#) and [35](#)
- [60] J. Sakaguchi, Y. Awaji, N. Wada, A. Kanno, T. Kawanishi, T. Hayashi, T. Taru, T. Kobayashi, and M. Watanabe. 109-Tb/s ($7 \times 97 \times 172$ -gb/s SDM/WDM/PDM) QPSK transmission through 16.8-km homogeneous multi-core fiber. pages 1–3, March 2011. Cited pages [34](#) and [35](#)
- [61] B Zhu, TF Taunay, M Fishteyn, X Liu, S Chandrasekhar, MF Yan, JM Fini, EM Monberg, and FV Dimarcello. 112-Tb/s space-division multiplexed DWDM transmission with 14-b/s/hz aggregate spectral efficiency over a 76.8-km seven-core fiber. *Optics Express*, 19(17):16665–16671, 2011. Cited pages [34](#) and [35](#)
- [62] Koki Takeshima, Takehiro Tsuritani, Yukihiro Tsuchida, Koichi Maeda, Tsunetoshi Saito, Kengo Watanabe, Toru Sasa, Katsunori Imamura, Ryuichi Sugizaki, Koji Igarashi, et al. 51.1-tbit/s mcf transmission over 2,520 km using cladding pumped 7-core EDFAs. In *Optical Fiber Communication Conference*, pages W3G–1. Optical Society of America, 2015. Cited pages [34](#) and [35](#)
- [63] Jiajing Tu, Kunimasa Saitoh, Masanori Koshihara, Katsuhiko Takenaga, and Shoichiro Matsuo. Optimized design method for bend-insensitive heterogeneous trench-assisted multi-core fiber with ultra-low crosstalk and high core density. *IEEE Journal of Lightwave Technology*, 31(15):2590–2598, 2013. Cited pages [34](#) and [35](#)
- [64] T. Mizuno, T. Kobayashi, H. Takara, A. Sano, H. Kawakami, T. Nakagawa, Y. Miyamoto, Y. Abe, T. Goh, M. Oguma, T. Sakamoto, Y. Sasaki, I. Ishida, K. Takenaga, S. Matsuo, K. Saitoh, and T. Morioka. 12-core \times 3-mode dense space division multiplexed transmission over 40 km employing multi-carrier signals with parallel mimo equalization. In *Optical Fiber Communication Conference: Postdeadline Papers*, page Th5B.2. Optical Society of America, 2014. Cited pages [34](#) and [35](#)
- [65] Jun Sakaguchi, Benjamin J Puttnam, Werner Klaus, Yoshinari Awaji, Naoya Wada, Atsushi Kanno, Tetsuya Kawanishi, Katsunori Imamura, Harumi Inaba, Kazunori Mukasa, et al. 19-core fiber transmission of $19 \times 100 \times 172$ -Gb/s SDM-WDM-PDM-QPSK signals at 305Tb/s. In *Optical Fiber Communication Conference*, pages PDP5C–1. Optical Society of America, 2012. Cited pages [34](#) and [35](#)
- [66] Takayuki Mizuno, Kohki Shibahara, Hirotaka Ono, Yoshiteru Abe, Y Miyamoto, Feihong Ye, Toshio Morioka, Y Sasaki, Yoshimichi Amma, K Takenaga, et al. 32-core dense SDM unidirectional transmission of PDM-16QAM signals over 1600 km using crosstalk-managed single-mode heterogeneous multicore transmission line. In *IEEE Optical Fiber Communications Conference and Exhibition*, pages 1–3, 2016. Cited pages [34](#) and [35](#)
- [67] Benjamin J. Puttnam, R.S. Luís, W Klaus, J Sakaguchi, J-M Delgado Mendinueta, Y Awaji, N Wada, Yoshiaki Tamura, Tetsuya Hayashi, Masaaki Hirano, et al. 2.15 Pb/s transmission using a 22 core homogeneous single-mode multi-core fiber and wideband optical comb. In *European Conference on Optical Communication (ECOC)*, pages 1–3. IEEE, 2015. Cited page [35](#)
- [68] Dablu Kumar and Rakesh Ranjan. Estimation of crosstalk in homogeneous multicore fiber for high core count under limited cladding diameter. In *IEEE Information and Communication Technology*, pages 1–4, 2017. Cited pages [35](#) and [48](#)
-

BIBLIOGRAPHY

- [69] Ruben S Luis, Benjamin J Puttnam, Georg Rademacher, Yoshinari Awaji, and Naoya Wada. On the use of high-order MIMO for long-distance homogeneous single-mode multicore fiber transmission. In *European Conference on Optical Communication (ECOC)*, pages 1–3. IEEE, 2017. Cited pages [38](#) and [48](#)
- [70] R-J Essiambre, R Ryf, NK Fontaine, and S Randel. Breakthroughs in photonics 2012: Space-division multiplexing in multimode and multicore fibers for high-capacity optical communication. *IEEE Photonics Journal*, 5(2):0701307–0701307, 2013. Cited page [38](#)
- [71] Jiwen Cui, Shengqi Zhu, Kunpeng Feng, Dang Hong, Junying Li, and Jiubin Tan. Fan-out device for multicore fiber coupling application based on capillary bridge self-assembly fabrication method. *Optical Fiber Technology*, 26:234–242, 2015. Cited pages [39](#) and [40](#)
- [72] Dietrich Marcuse. Loss analysis of single-mode fiber splices. *Bell System Technical Journal*, 56(5):703–718, 1977. Cited pages [39](#) and [45](#)
- [73] AI Filipenko and OV Sychova. Research of misalignments and cross-sectional structure influence on optical loss in photonic crystal fibers connections. In *IEEE International Conference on Advanced Optoelectronics and Lasers*, pages 85–87, 2013. Cited pages [40](#) and [45](#)
- [74] Pierre Sillard, Marianne Bigot-Astruc, and Denis Molin. Few-mode fibers for mode-division-multiplexed systems. *Journal of Lightwave Technology*, 32(16):2824–2829, 2014. Cited page [40](#)
- [75] Filipe Ferreira, Stylianos Sygletos, and Andrew Ellis. Impact of linear mode coupling on the group delay spread in few-mode fibers. In *Optical Fiber Communication Conference*, pages Tu2D–1. Optical Society of America, 2015. Cited page [40](#)
- [76] Adolfo VT Cartaxo, Ruben S Luís, Benjamin J Puttnam, Tetsuya Hayashi, Yoshinari Awaji, and Naoya Wada. Dispersion impact on the crosstalk amplitude response of homogeneous multi-core fibers. *IEEE Photonics Technology Letters*, 28(17):1858–1861, 2016. Cited page [40](#)
- [77] Sercan Ö Arık, Daulet Askarov, and Joseph M Kahn. Effect of mode coupling on signal processing complexity in mode-division multiplexing. *Journal of Lightwave Technology*, 31(3):423–431, 2013. Cited pages [40](#) and [43](#)
- [78] Md Saifuddin Faruk and Kazuro Kikuchi. Adaptive frequency-domain equalization in digital coherent optical receivers. *Optics Express*, 19(13):12789–12798, 2011. Cited page [40](#)
- [79] Peter J Winzer and Gerard J Foschini. MIMO capacities and outage probabilities in spatially multiplexed optical transport systems. *Optics Express*, 19(17):16680–16696, 2011. Cited page [41](#)
- [80] Keang-Po Ho and Joseph M Kahn. Mode-dependent loss and gain: statistics and effect on mode-division multiplexing. *Optics express*, 19(17):16612–16635, 2011. Cited pages [41](#) and [48](#)
- [81] Adriana Lobato, Filipe Ferreira, Beril Inan, Susmita Adhikari, Maxim Kuschnerov, Antonio Napoli, Bernhard Spinnler, and Berthold Lankl. Maximum-likelihood detection in few-mode fiber transmission with mode-dependent loss. *IEEE Photonics Technology Letters*, 25(12):1095–1098, 2013. Cited page [41](#)
- [82] Kengo Watanabe and Tsunetoshi Saito. Compact fan-out for 19-core multicore fiber, with high manufacturability and good optical properties. In *IEEE Opto-Electronics and Communications Conference*, pages 1–3, 2015. Cited page [45](#)
- [83] Emanuele Viterbo and Joseph Boutros. A universal lattice code decoder for fading channels. *IEEE Transactions on Information theory*, 45(5):1639–1642, 1999. Cited pages [48](#) and [94](#)

-
- [84] Adriana Lobato, Johannes Rabe, Filipe Ferreira, Maxim Kuschnerov, Bernhard Spinnler, and Berthold Lankl. Near-ML detection for MDL-impaired few-mode fiber transmission. *Optics express*, 23(8):9589–9601, 2015. Cited page [48](#)
- [85] Kyle Guan, Peter J Winzer, and Mark Shtaif. BER performance of MDL-impaired MIMO-SDM systems with finite constellation inputs. *IEEE Photonics Technology Letters*, 26(12):1223–1226, 2014. Cited page [48](#)
- [86] Charles R Schwarz. Statistics of range of a set of normally distributed numbers. *Journal of surveying engineering*, 132(4):155–159, 2006. Cited pages [52](#) and [53](#)
- [87] Daniel Polani. *Kullback-Leibler Divergence*, pages 1087–1088. Springer New York, New York, NY, 2013. Cited page [54](#)
- [88] John G. Proakis. *Digital communication*. Fifth edition, Hill international edition, 2008. Cited pages [55](#), [60](#), [90](#), and [98](#)
- [89] Neelesh B Mehta, Jingxian Wu, Andreas F Molisch, and Jin Zhang. Approximating a sum of random variables with a lognormal. *IEEE Transactions on Wireless Communications*, 6(7), 2007. Cited page [58](#)
- [90] R Xu and FCM Lau. Performance analysis for MIMO systems using zero forcing detector over fading channels. *IEEE Proceedings-Communications*, 153(1):74–80, 2006. Cited page [59](#)
- [91] R Xu and FCM Lau. Performance analysis for MIMO systems using Zero Forcing detector over fading channels. *IEEE Proceedings-Communications*, 153(1):74–80, 2006. Cited pages [60](#) and [98](#)
- [92] WF Love. Novel mode scrambler for use in optical-fiber bandwidth measurements. In *Optical Fiber Communication Conference*, page ThG2. Optical Society of America, 1979. Cited page [64](#)
- [93] Stefan Warm and Klaus Petermann. Capacity increase in spliced mode-multiplexed transmission systems by using mode mixers. In *IEEE Photonics Society Summer Topical Meeting Series*, pages 201–202. IEEE, 2012. Cited page [64](#)
- [94] Claude Elwood Shannon. A mathematical theory of communication. *Bell system technical journal*, 27(3):379–423, 1948. Cited page [78](#)
- [95] Claude Elwood Shannon. Communication in the presence of noise. *Proceedings of the IRE*, 37(1):10–21, 1949. Cited page [79](#)
- [96] Emre Telatar. Capacity of multi-antenna gaussian channels. *European transactions on telecommunications*, 10(6):585–595, 1999. Cited page [79](#)
- [97] Yang Wen Liang and B Columbia. Ergodic and outage capacity of narrowband mimo gaussian channels. *Dept. of Electrical and computer Engg. University of British Columbia, Vancouver, British Columbia*, 2005. Cited page [80](#)
- [98] A Tulino, Angel Lozano, and Sergio Verdú. MIMO capacity with channel state information at the transmitter. In *Eighth IEEE International Symposium on Spread Spectrum Techniques and Applications-Programme and Book of Abstracts (IEEE Cat. No. 04TH8738)*, pages 22–26. IEEE, 2004. Cited page [81](#)
- [99] Giuseppe Caire and Shlomo Shamai. On the capacity of some channels with channel state information. In *Proceedings. 1998 IEEE International Symposium on Information Theory (Cat. No. 98CH36252)*, page 42. IEEE, 1998. Cited page [81](#)
-

BIBLIOGRAPHY

- [100] R Xu and FCM Lau. Performance analysis for mimo systems using zero forcing detector over fading channels. *IEEE Proceedings-Communications*, 153(1):74–80, 2006. Cited page [81](#)
- [101] Peter J Winzer and Gerard J Foschini. MIMO capacities and outage probabilities in spatially multiplexed optical transport systems. *Optics express*, 19(17):16680–16696, 2011. Cited pages [84](#) and [85](#)
- [102] C Koebele, M Salsi, G Charlet, and S Bigo. Nonlinear effects in long-haul transmission over bimodal optical fibre. In *36th European Conference and Exhibition on Optical Communication*, pages 1–3. IEEE, 2010. Cited pages [84](#) and [85](#)
- [103] Elie Awwad, Ghaya Rekaya-Ben Othman, and Yves Jaouën. Space-time coding schemes for MDL-impaired mode-multiplexed fiber transmission systems. *Journal of Lightwave Technology*, 33(24):5084–5094, 2015. Cited page [89](#)
- [104] El-Mehdi Amhoud, Ghaya Rekaya-Ben Othman, Laurent Bigot, Mengdi Song, Esben Ravn Andresen, Guillaume Labroille, Marianne Bigot-Astruc, and Yves Jaouen. Experimental demonstration of space-time coding for mdl mitigation in few-mode fiber transmission systems. In *European Conference on Optical Communication (ECOC)*, pages 1–3. IEEE, 2017. Cited page [89](#)
- [105] Yves Jaouën, Sami Mumtaz, Elie Awwad, and Ghaya Rekaya-Ben Othman. Space-time codes for fiber communications: Coding gain and experimental validation. In *8th International Symposium on Communication Systems, Networks & Digital Signal Processing (CSNDSP)*, pages 1–5. IEEE, 2012. Cited page [89](#)
- [106] Vahid Tarokh, Nambi Seshadri, and A Robert Calderbank. Space-time codes for high data rate wireless communication: Performance criterion and code construction. *IEEE transactions on information theory*, 44(2):744–765, 1998. Cited page [90](#)
- [107] Siavash M Alamouti. A simple transmit diversity technique for wireless communications. *1998*, 1998. Cited page [92](#)
- [108] Vahid Tarokh, Hamid Jafarkhani, and A Robert Calderbank. Space-time block codes from orthogonal designs. *IEEE Transactions on Information theory*, 45(5):1456–1467, 1999. Cited page [92](#)
- [109] J-C Belfiore, Ghaya Rekaya, and Emanuele Viterbo. The golden code: a 2/spl times/2 full-rate space-time code with nonvanishing determinants. *IEEE Transactions on information theory*, 51(4):1432–1436, 2005. Cited page [92](#)
- [110] Ezio Biglieri, Yi Hong, and Emanuele Viterbo. On fast-decodable space-time block codes. *arXiv preprint arXiv:0708.2804*, 2007. Cited page [92](#)
- [111] Hesham El Gamal and Mohamed Oussama Damen. Universal space-time coding. *IEEE Transactions on Information Theory*, 49(5):1097–1119, 2003. Cited page [93](#)
- [112] O. Damen and G. Rekaya-Ben Othman. On the performance of spatial modulations over multimode optical fiber transmission channels. *IEEE Transactions on Communications*, 67(5):3470–3481, May 2019. Cited pages [96](#), [97](#), and [98](#)
- [113] Taiji Sakamoto, Kunimasa Saitoh, Shota Saitoh, Kohki Shibahara, Masaki Wada, Yoshiteru Abe, Azusa Urushibara, Katsuhiko Takenaga, Takayuki Mizuno, Takashi Matsui, et al. Six-mode seven-core fiber for repeated dense space-division multiplexing transmission. *Journal of Lightwave Technology*, 36(5):1226–1232, 2018. Cited page [106](#)

- [114] T Mizuno, T Kobayashi, H Takara, A Sano, H Kawakami, T Nakagawa, Y Miyamoto, Y Abe, T Goh, M Oguma, et al. 12-core \times 3-mode dense space division multiplexed transmission over 40 km employing multi-carrier signals with parallel MIMO equalization. In *Optical Fiber Communication Conference*, pages Th5B–2. Optical Society of America, 2014. Cited page [106](#)
- [115] Kohki Shibahara, Doohwan Lee, Takayuki Kobayashi, Takayuki Mizuno, Hidehiko Takara, Akihide Sano, Hiroto Kawakami, Yutaka Miyamoto, Hirotaka Ono, Manabu Oguma, et al. Dense SDM (12-core \times 3-mode) transmission over 527 km with 33.2-ns mode-dispersion employing low-complexity parallel MIMO frequency-domain equalization. *Journal of Lightwave Technology*, 34(1):196–204, 2016. Cited page [106](#)
- [116] Koji Igarashi, Daiki Souma, Yuta Wakayama, Koki Takeshima, Yu Kawaguchi, Takehiro Tsuritani, Itsuro Morita, and Masatoshi Suzuki. 114 space-division-multiplexed transmission over 9.8-km weakly-coupled-6-mode uncoupled-19-core fibers. In *Optical Fiber Communication Conference*, pages Th5C–4. Optical Society of America, 2015. Cited page [106](#)
- [117] D Soma, K Igarashi, Y Wakayama, K Takeshima, Y Kawaguchi, N Yoshikane, T Tsuritani, I Morita, and M Suzuki. 2.05 peta-bit/s super-nyquist-WDM SDM transmission using 9.8-km 6-mode 19-core fiber in full C band. In *2015 European Conference on Optical Communication (ECOC)*, pages 1–3. IEEE. Cited page [106](#)
- [118] RGH van Uden, R Amezcua Correa, E Antonio-Lopez, FM Huijskens, Guifang Li, A Schulzgen, H de Waardt, AMJ Koonen, and CM Okonkwo. 1 km hole-assisted few-mode multi-core fiber 32QAM WDM transmission. In *The European Conference on Optical Communication (ECOC)*, pages 1–3. IEEE, 2014. Cited page [106](#)
- [119] Yusuke Sasaki, Katsuhiro Takenaga, Shoichiro Matsuo, Kazuhiko Aikawa, and Kunimasa Saitoh. Few-mode multicore fibers for long-haul transmission line. *Optical Fiber Technology*, 35:19–27, 2017. Cited page [107](#)
- [120] Stefan Warm and Klaus Petermann. Splice loss requirements in multi-mode fiber mode-division-multiplex transmission links. *Optics Express*, 21(1):519–532, 2013. Cited page [107](#)
- [121] Mahdiah B Shemirani, Wei Mao, Rahul Alex Panicker, and Joseph M Kahn. Principal modes in graded-index multimode fiber in presence of spatial-and polarization-mode coupling. *Journal of lightwave technology*, 27(10):1248–1261, 2009. Cited page [108](#)
- [122] El Mehdi Amhoud, Ghaya Rekaya Ben-Othman, and Yves Jaouën. Combined polarization-and mode-dependent loss effects on few-mode fibers systems. In *Signal Processing in Photonic Communications*, pages SpM4F–3. Optical Society of America, 2017. Cited pages [108](#) and [110](#)

Publications

Journal Paper

- Akram Abouseif, Ghaya Rekaya-Ben Othman and Oussama Damen, “Performance Analysis of CDL-impaired Multi-Core Fiber Transmission”, submitted to IEEE Transaction on Communication, April 2020.
- Akram Abouseif, Ghaya Rekaya-Ben Othman and Yves Jaouën, “Channel Model and Optimal Core Scrambling for Multi-Core Fiber Transmission System”, Optics Communications, August 2019.

Conference proceedings

- Akram Abouseif, Ghaya Rekaya-Ben Othman and Yves Jaouën, “Space-Time Coding Performance Analysis for CDL-impaired Multi-Core Fiber Transmission”, ICT, Bali, Indonesia, October 2020.
- Akram Abouseif, Ghaya Rekaya-Ben Othman and Yves Jaouën, “Space-Time Coding and Core Scrambling for Low Complexity MIMO Detection in Multi-Core Fiber Transmission”, SPPcom, Montreal, Canada, July 2020.
- Akram Abouseif, Ghaya Rekaya-Ben Othman and Yves Jaouën, “Performance Enhancement Techniques Based on CDL-impaired Multi-core Fiber Channel Model”, ACP, Sichuan, China, November 2019.
- Akram Abouseif, Ghaya Rekaya-Ben Othman and Yves Jaouën, “Zero Forcing Pre-Compensation Technique for Multi-Core Fiber Transmission System”, SPPcom, California, USA, August 2019.
- Akram Abouseif, Ghaya Rekaya-Ben Othman and Yves Jaouën, “Deterministic Core Scrambling for Multi-Core Fiber Transmission”, OECC, Jeju Island, Korea, July 2018.
- Akram Abouseif, Ghaya Rekaya-Ben Othman and Yves Jaouën, “Multi-core Fiber Channel Model and Core Dependent Loss Estimation”, SPPcom, Lausanne, Switzerland, July 2018.

Publications

- Akram Abouseif, Ghaya Rekaya-Ben Othman and Yves Jaouën, “Core Mode scramblers for ML-detection based multi-cores fibers transmission”, ACP, China, November 2017.

Patents

- Akram Abouseif and Ghaya Rekaya-Ben Othman , “METHODS AND DEVICES FOR MULTI-CORE FIBER DATA TRANSMISSION USING DATA PRECODING”, European Application July 2019, *n*° EP 19290058.7
- Akram Abouseif, Ghaya Rekaya-Ben Othman and Yves Jaouën, “DEVICES AND METHODS FOR ADAPTIVE DECODING AND CORE SCRAMBLING IN MULTI-CORE FIBER TRANSMISSION SYSTEMS“, European Application September 2018, *n*° EP 18306214.0.
- Akram Abouseif, Ghaya Rekaya-Ben Othman and Yves Jaouën, “OPTICAL TRANSMISSION SYSTEM AND METHOD FOR CORE SCRAMBLING FOR MULTI-CORE OPTICAL FIBERS”, European Application April 2018, *n*° EP 18305533.4. extension WO2019206631(A1).
- Akram Abouseif, Ghaya Rekaya-Ben Othman and Yves Jaouën, “METHODS AND DEVICES FOR THE DETERMINATION OF CORE DEPENDENT LOSS IN MULTI-CORE FIBER TRANSMISSION SYSTEMS”, European Application April 2018, *n*° EP 18305535.9. extension WO2019206634(A1).
- Akram Abouseif, Ghaya Rekaya-Ben Othman and Yves Jaouën, “METHODS AND DEVICES FOR THE DETERMINATION OF CORE DEPENDENT LOSS IN MULTI-CORE FIBER TRANSMISSION SYSTEMS USING CORE SCRAMBLING, European Application April 2018, *n*° EP 18305538.3, extension WO2019206639(A1).
- Akram Abouseif, Ghaya Rekaya-Ben Othman and Yves Jaouën, “OPTICAL TRANSMISSION SYSTEM AND METHOD FOR CORE SELECTION IN MULTI-CORE FIBERS”, European Application April 2018, *n*° EP 18305539.1, WO2019206640(A1).

Titre: Techniques DSP émergentes pour les systèmes de transmission à fibres optiques multicœurs

Mots clés: Communications optiques, fibre multicœur, entrées multiples et sorties multiples (MIMO), conception de fibre, modèle de canal et codage Espace-Temps

Résumé: Les systèmes de communication optique ont connu plusieurs phases de développement au cours des dernières décennies. Ils approchent aujourd'hui les limites de capacité du canal non-linéaire. L'espace est aujourd'hui le dernier degré de liberté à mettre en œuvre afin de continuer à répondre aux demandes de capacité à venir pour les prochaines années. Par conséquent, des recherches intensives sont menées pour explorer tous les aspects concernant le déploiement du système de multiplexage par division spatiale (SDM). Plusieurs dégradations ont un impact sur les systèmes SDM en raison de l'interaction des canaux spatiaux qui dégrade les performances du système. Dans cette thèse, nous nous concentrons sur les fibres multicœurs (MCF) comme l'approche la plus prometteuse pour être le premier représentant du système SDM. Nous présentons différentes solutions numériques et optiques pour atténuer l'effet non unitaire connu sous le nom de perte dépendante du cœur (CDL). La première partie est consacrée à l'étude des performances de la transmission MCF en tenant compte des dégradations de propagation qui impactent les systèmes MCF. Nous proposons un modèle de canal qui aide à identifier le système MCF. La deuxième partie est consacrée à la technique optique pour améliorer les performances de transmission avec une solution optimale pour la réduction des CDL. Ensuite, nous avons introduit des techniques numériques pour des améliorations supplémentaires, la pré-compensation Zero Forcing et le codage spatio-temporel pour une atténuation CDL supplémentaire. Tous les résultats de simulation sont validés analytiquement en dérivant les bornes supérieures de probabilité d'erreur.

Title: Emerging DSP Techniques for Multi-Core Fiber Transmission Systems

Keywords: Optical Communications, Multi-core Fiber, Multiple-Input-Multiple-Output (MIMO), Fiber Design, Channel Model and Space-Time Coding

Abstract: Optical communication systems have gone through several phases over the last few decades. As we know, optical systems are likely to reach the limits of their non-linear capability. At present, space is the last degree of freedom to continue to meet future capacity demands for the next few years. For this reason, intensive research is being conducted to explore all aspects of Space Division Multiplexing (SDM) deployment. Several impairments impact SDM systems due to the interaction of spatial channels, which degrades system performance. In this thesis, we focus on multicore fibers (MCFs) as the most promising approach to be the first representative of the SDM system. We present different digital and optical solutions to mitigate the non-unitary effect known as Core Dependent Loss (CDL). The first part is devoted to the study of the transmission performance of MCFs, taking into account the propagation impairments that affect MCF systems. We propose a channel model that helps to identify the MCF system. The second part is devoted to the optical technique to improve the transmission performance with an optimal solution. Then, we introduce digital techniques for further improvement, zero forcing pre-compensation and space-time coding for additional CDL mitigation. All simulation results are analytically validated by deriving the upper limits of the error probability.